The Impacts of Outdoor Air Conditions and Non-Uniform Exchanger Channels on a Run-Around Membrane Energy Exchanger

A Thesis Submitted to the College of

Graduate Studies and Research

In Partial Fulfillment of the Requirements

For the Degree of Master of Science

In the Department of Mechanical Engineering

University of Saskatchewan

Saskatoon

By

Howard Hemingson

Permission to Use

In presenting this thesis in partial fulfillment of the requirements for a Postgraduate degree from the University of Saskatchewan, I agree that the Libraries of this University may make it freely available for inspection. I further agree that permission for copying of this thesis in any manner, in whole or in part, for scholarly purposes may be granted by the professors who supervised my thesis work or, in their absence, by the Head of the Department or the Dean of the College in which my thesis work was done. It is understood that any copying or publication or use of this thesis or parts thereof for financial gain shall not be allowed without my written permission. It is also understood that due recognition shall be given to me and to the University of Saskatchewan in any scholarly use which may be made of any material in my thesis.

Requests for permission to copy or to make other use of material in this thesis in whole or part should be addressed to:

Head of the Department of Mechanical Engineering

University of Saskatchewan

Saskatoon, Saskatchewan (S7N 5A9)

ABSTRACT

This thesis contains the numerically investigations of the performance of a run-around membrane energy exchanger (RAMEE) at different outdoor air conditions and the effects of non-uniform exchanger channels. The RAMEE is a new type of building ventilation air energy recovery system that allows heat and moisture to be transferred between isolated supply and exhaust air streams. Two liquid-to-air membrane energy exchangers (LAMEEs) are placed in the supply and exhaust air ducts and transfer heat and moisture between air and a circulating liquid desiccant that couples the two LAMEEs together. The ability of the system to transfer heat and moisture between isolated supply and exhaust ducts makes it appropriate for numerous HVAC applications (e.g., hospitals and building energy retrofits).

The performance of the RAMEE at different outdoor air conditions is shown to be highly variable due to the coupling of the heat and moisture transfer by the desiccant. This coupling allows the humidity ratio between the indoor and outdoor air to influence the heat transfer and the moisture transfer is influenced by the difference between the indoor and outdoor air temperatures. The coupling produces some complex RAMEE performance characteristics at some outdoor air conditions where the effectiveness values (i.e., sensible, latent, and total) were shown to be less than 0% or greater than 100%. Effectiveness and operating correlations are developed to describe these complex behaviours because existing correlations do not account for the coupling effects. The correlations can serve as design and operation tools for the RAMEE which do not require the use of an iterative computational numerical model.

Non-uniform exchanger channels are present in the RAMEE because of pressure differences between the air and solution channels which deform the membrane into the air channel. The non-uniform channels are analytically shown to create maldistributed fluid flows and variable heat and mass transfer coefficients. The combined effects of these two changes lead to a reduction in the RAMEE effectiveness, which increases as the size of the membrane deformation increases. The reduction in total effectiveness for an exchanger where the membrane has a peak deflection of 10% of the nominal air channel thickness operating at a NTU of 12 was shown to be 12.5%. These results of non-uniform exchanger channels agree with previously conducted experimental results.

ACKNOWLEDGEMENTS

I wish to express my gratitude to my supervisors Professors Carey Simonson and Robert Besant for challenging and encouraging me during the process. Their enthusiasm towards the project was contagious and their guidance was invaluable. I look forward to future collaborations.

I would also like to thank the past and present graduate students in the RAMEE research group. I thank the past graduate students for establishing the background understanding that was essential to my project. I especially thank the current graduate students for all the collaborating work and the experiences we have shared together.

This research would not have been possible without the financial support from the University of Saskatchewan (Dean's Scholarship), the Department of Mechanical Engineering, the Natural Science and Engineering Research Council of Canada (NSERC), a Russell William Haid Memorial Scholarship, and Venmar CES Inc. Saskatoon. Thank you very much for your support.

DEDICATION

I dedicate this thesis to Lindsay, Brian, Cecile, Lorraine, Devin, Atticus, and to all my other friends and family. Your patience and unwavering support for me during this process was invaluable and I am eternally grateful for it.

TABLE OF CONTENTS

Page

LIST OF TABLES

LIST OF FIGURES

Figure **Page**

NOMENCLATURE

Acronyms

AHRI	Air-Conditioning, Heating and Refrigeration Institute
CFD	computational fluid dynamics
CRD	collaborative research and development
HVAC	heating, ventilation and air-conditioning
LAMEE	liquid-to-air membrane energy exchanger
NSERC	Natural Sciences and Engineering Research Council of Canada
RAMEE	run-around membrane energy exchanger
RH	relative humidity

English Symbols

A	membrane surface area, [m^2]
C	heat capacity rate, [W/K]
C_p	specific heat capacity, [kJ/kg]
Cr*	heat capacity ratio
D_h	hydraulic diameter, [m]
$\frac{dP}{dx}$	pressure gradient, [Pa/m]
H	specific enthalpy, [kJ/kg]
H*	operating condition factor
h	convective heat transfer coefficient, [$W/(m^2 \cdot K)$]
h_{fg}	latent heat of vapourization, [J/kg]
h_m	convective mass transfer coefficient, [$kg/(m^2 \cdot s)$]

J	mass flux rate, [kg/(m^2·s)]
k	membrane thermal conductivity, [W/(m·K)]
k_m	membrane water vapour permeability, [kg/(m·s)]
Le	Lewis number
$\dot{m}''$	mass flux rate, [kg/(m^2·s)]
$\dot{m}$	mass flow rate, [kg/s]
NTU	number of thermal transfer units
NTU_m	number of mass transfer units
Nu	Nusselt number
q”	heat flux, [W/m^2]
T	temperature, [°C]
U	overall heat transfer coefficient, [W/(m^2·K)]
U_m'	overall mass transfer coefficient, [kg/(m^2·s)]
V	velocity, [m/s]
W	humidity ratio, [kg_{vapour}/kg_{air}]
X	solution mass fraction, [kg_{water}/kg_{salt}]

Greek Symbols

Δ	difference (change in)
δ	thickness, [mm]
ε	effectiveness
μ	dynamic viscosity, [kg/(m·s)]
ρ	density, [kg/m^3]

Subscript

Air	air stream

E	exhaust
In	exchanger inlet
Lat	latent
Mem	membrane
Out	exchanger outlet
S	supply
Sen	sensible
Sol	solution
Sol,Mem	membrane-solution interface
Tot	total
Var	channel thickness variation

Chapter 1

INTRODUCTION

1.1 Overview of Building Ventilation

Energy has become an important issue in today's society. The combination of an expanding world economy and a limited hydrocarbon reserve has led to a steady increase in energy prices over the years. Also, concerns about climate change and its causes have added another layer of complexity to energy issues. A significant amount of research is being conducted into alternative energy sources and energy conservation in a wide range of fields. Building science is one area of research where substantial gains can be achieved in energy conservation.

Energy consumption in buildings accounts for up to 40% of all the energy consumed and this value is expected to increase in the near future (D&R International 2009). Up to 50% of this energy is consumed by the energy demands of building ventilation (D&R International 2009). The purpose of ventilation is to provide fresh air into a building to reduce the level contaminates in the air that are produced by the occupants and the building materials. The aim is to create a work space with high air quality and worker productivity (Fang et al. 2000, Kosonen and Tan 2004) and prevent symptoms associated with sick-building syndrome (Norback et al. 1990). The recommended ventilation rate depends on the building's use and, in the case of an office building, this rate is 8.5 L/s (18 cfm) per person (ANSI/ASHRAE Std. 62.1 2004). This outdoor air is at a different temperature and humidity (moisture content) compared to the

indoor space and must be conditioned so it does not alter the indoor condition. The energy required for this conditioning accounts for a large fraction of the energy used in buildings. In addition to the supplied outdoor air, indoor air is exhausted from the building to prevent the building from becoming significantly pressurized. This exhausted air is at or near the desired indoor conditions (ANSI/ASHRAE Std. 55 2004) and thus there is potential to transfer energy between the exhaust and outdoor ventilation air to precondition the ventilation air.

1.2 Ventilation Energy Recovery Systems

Ventilation energy recovery systems consist of air-to-air exchangers that use the exhaust air leaving a building to pre-condition the supply air entering it. This allows some of the energy that was initially used to condition the exhaust air to be recovered. This significantly reduces the costs associated with conditioning the supply air because it reduces the amount of energy required to condition the supply air and sometimes allows smaller conditioning equipment to be used (Zhang and Niu, 2001, Zhou et al. 2007, EPA 2010). Energy recovery systems are capable of recovering heat (sensible energy) and sometimes moisture (latent energy) between air streams. A system that transfers both heat and moisture is ideal because it has the potential to transfer up to four times more energy compared to a system that only transfers sensible energy (ASHRAE 2000).

The performance of energy recovery systems is usually expressed in terms of effectiveness. Systems that only recover heat have a sensible effectiveness, while systems that recover both heat and moisture have sensible and latent effectiveness. The sensible (latent) effectiveness is generally defined by the temperature (moisture) change

in an air stream divided by the temperature (moisture) difference between the air streams. The effectiveness values of energy recovery systems are usually between 40-80%, but can sometimes exceed 100% or be less than 0% in particular systems under some operating conditions (Simonson and Besant 1999a, ASHRAE 2004).

A wide range of energy recovery systems exist, which provide cost effective solutions in a wide range of heating, ventilation, and air-conditioning (HVAC) designs. These systems can be categorized based on whether the system transfers moisture or not and whether the supply and exhaust air ducts have to be adjacent to each other. Examples of air-to-air energy exchangers for HVAC systems include energy wheels, flat plate exchangers, and run-around glycol loops.

1.2.1 Flat Plate Exchangers

Flat plate exchangers are a simple and effective energy recovery device for building ventilation air. The exchanger consists of a stack of flat plates constructed from either metal, plastic, or vapour permeable membranes. The plates are configured to create alternating supply and exhaust channels (Figure 1.1). This arrangement creates a large transfer surface area in a small volume. The supply and exhaust air streams usually flow in a cross-flow configuration, but some exchangers use a flow configuration that has cross and counter-flow components. Flat plate exchangers operate with the supply and exhaust air ducts adjacent to each other. They have no moving parts and only create a small pressure drop in the air stream (ASHRAE 2000). They also have the benefit of minimal cross leakage and tolerate moderate to large pressure differences between air streams.

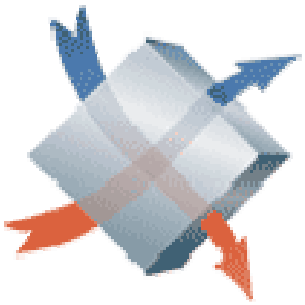

Figure 1.1: Flat plate exchanger (reprinted with permission from Venmar (2010))

Flat plate exchangers are very efficient in heat recovery and can achieve sensible effectiveness values of 50% to 80% in typical applications (ASHRAE 2000). Flat plate exchangers can also transfer moisture in addition to heat if they are constructed with vapour permeable membranes. These systems can achieve latent effectiveness values of 40% to 70% (Zhang et al. 2000) while maintaining the same sensible effectiveness as flat plate exchangers that only transfer heat. Correlations for the sensible (Incropera and DeWitt 2002) and latent (Zhang and Niu 2002) effectivenesses exist and are based on the overall heat/moisture transfer resistance, surface area of the exchanger, and the air stream flow rates. These correlations assume the heat and moisture transfers are independent of each other. The effectiveness of the exchanger is reduced by air channel thickness variations and flow maldistribution in the exchanger headers (Zhang 2009).

The flat plate exchanger's simple design and high performance in heat and moisture recovery makes it an economical solution in many applications. It is used in numerous commercial HVAC installations and is commonly used in residential ventilation units where the supply and exhaust air ducts are adjacent to each other.

1.2.2 Energy Wheels

Energy wheels are rotary air-to-air exchangers, which can transfer heat (heat wheel) or heat and moisture (enthalpy wheel). They consist of a cylinder with an air

permeable matrix that rotates between adjacent supply and exhaust air ducts (Figure 1.2). The matrix consists of numerous channels that pass through the thickness of the wheel which provides a large surface area for heat and moisture transfer. A variety of channel shapes exists, with a common one being corrugated pores. A small motor rotates the wheel which cycles the individual channels between the supply and exhaust air streams allowing for energy transfer between them. The wheel matrix is constructed from metal, plastic, or paper which is the heat transfer medium. In enthalpy wheels, the matrix is coated with a desiccant that allows for the moisture transfer. The energy wheel is able to operate with a minimal pressure drop, but cross leakage is more significant and can be up to 10% (ASHRAE 2000).

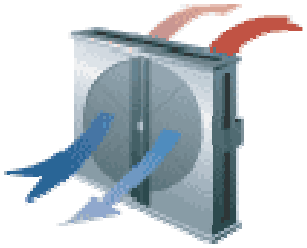

Figure 1.2: Energy wheel (reprinted with permission from Venmar (2010))

Energy wheels are some of the highest performing ventilation energy recovery systems and can achieve sensible and latent (in enthalpy wheels) effectivenesses of 50% to 80% (ASHRAE 2000). The higher effectivenesses are possible because the air streams move counter-flow to each other in the exchanger. Correlations exist to describe the effectiveness in heat wheels (Kays and London 1998) and in enthalpy wheels (Simonson and Besant 1999a) based on the wheel properties, air flow rates, and wheel rotational speed. These correlations show that in an enthalpy wheel, the sensible effectiveness is influenced by the moisture transfer, which is a unique characteristic of

enthalpy wheels. The performance of energy wheels can be reduced by variations in the channel sizes (Shang and Besant 2005).

Energy wheels generally provide the highest energy recovery amongst energy recovery systems (ASHRAE 2000). They are usually the preferred option for large air volume applications with adjacent supply and exhaust air ducts where a small amount of cross contamination between the air streams is permissible. They are commonly used in commercial applications.

1.2.3 Run-Around Coil Loop

A run-around coil loop consists of two finned tube liquid coils with one located in the supply and the other in exhaust air ducts (Figure 1.3). A coupling fluid, usually a water-glycol mixture, circulates between the coils and forms a loop. Energy is transferred between supply and exhaust air ducts that are located in different parts of the building. However, the run-around loop only transfers heat and no moisture. The run-around loop is suitable for retrofits of buildings with non-adjacent supply and exhaust ducts that do not have an energy recovery system. In buildings with non-adjacent supply and exhaust ducts it is often cost prohibitive to move the air ducts together and utilize a flat plate exchanger or energy wheel. The run-around coil loop eliminates cross leakage between the air streams and so is suitable in buildings where the exhaust air cannot contaminate the supply air, such as in hospitals and laboratories. The system requires a pump to circulate the fluid and there is a moderate air pressure drop across the coils.

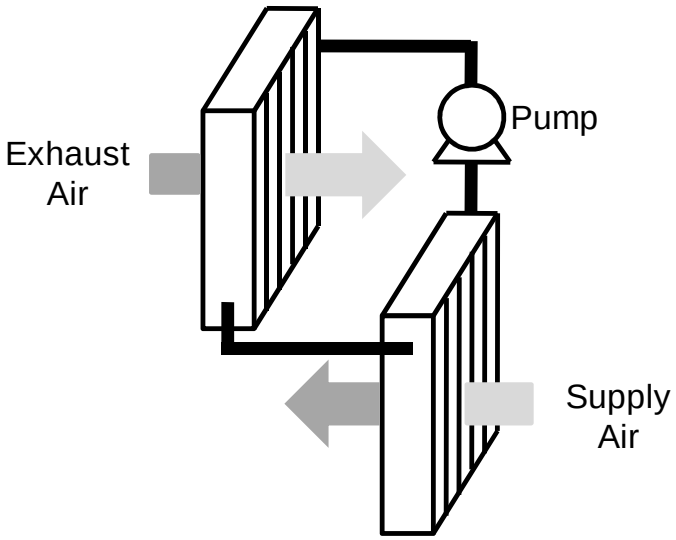

Figure 1.3: Run-around coil loop schematic.

The sensible effectiveness of a run-around loop ranges between 45% and 65%, which is somewhat lower than other systems (ASHRAE 2000). The system can be described by correlations that consider the size of the coils and the flow rates of the air streams and coupling fluid (London and Kays 1951). The effectiveness of the system can be changed by controlling the flow rate of the coupling fluid and a maximum effectiveness occurs when the coupling fluid and air streams' heat capacity rates are equal.

1.2.4 Twin Tower Enthalpy Loop

The twin tower enthalpy loop is a run-around system that is able to transfer heat and moisture between non-adjacent supply and exhaust air ducts (Figure 1.4). The system uses a liquid desiccant as a coupling fluid which is sprayed into the air stream at each exchanger. The flow arrangement between the desiccant and the air stream may be either cross or counter flow. The collected solution from the bottom of each exchanger is then pumped to the top of the other exchanger to complete the loop. The physical properties of the desiccant allow heat and moisture to be transferred between the air

streams. It is an open liquid loop system because the air and the liquid desiccant come into direct contact with each other in each exchanger. This allows the air stream to entrain desiccant in aerosol form. Woven mesh screens, known as demister pads, are used to remove these microscopic droplets, but some desiccant passes through and drifts downstream. These desiccant droplets corrode ducts and other HVAC equipment, such as fans and coils, which significantly increases maintenance costs. The system operates with a small pressure drop and requires pumps to circulate the liquid desiccant between the exchangers.

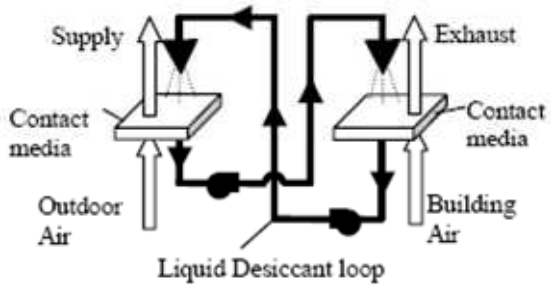

Figure 1.4: Twin-tower enthalpy loop schematic (Larson 2006)

The twin-tower enthalpy loop transfers heat and moisture with sensible and latent effectivenesses of 40% to 60% (ASHRAE 2000). The performance is not as high as a flat plate exchanger with vapour permeable membranes or an enthalpy wheel, but it is the only commercial system that transfers heat and moisture between non-adjacent ducts. No analytical solutions or correlations exist to describe its performance and there is no literature on the effects of controlling the desiccant solution flow rate.

Twin-tower enthalpy loops are commercially found in large air volume applications where humidity control is very important (Kathabar 2010). The energy savings in these applications are large enough to off-set the higher maintenance costs. Food and pharmaceutical processing plants are examples of buildings where this system has been used.

1.2.5 Run-Around Membrane Energy Exchanger

The run-around membrane energy exchanger (RAMEE) is another system that can transfer heat and moisture between non-adjacent air ducts. It is still in the development stage and is not yet commercialized, but has achieved sensible and latent effectivenesses of 55% and 40% respectively (Erb et al. 2010). The system is similar to the twin-tower enthalpy loop in that it transfers heat and moisture between two exchangers that are coupled together by a circulating liquid desiccant (Figure 1.5). The exchangers consist of alternating air and solution channels that are separated by vapour permeable membranes. The flow regimes used in these liquid-to-air membrane energy exchangers (LAMEE) are either cross flow, counter flow, or a combination of both. The membrane in the exchanger does not transmit liquid and therefore prevents the liquid desiccant and the air from coming into direct contact. This arrangement improves on the twin-tower enthalpy loop by preventing the desiccant from being aerosolized and corroding the downstream HVAC equipment. The run-around nature of the system also minimizes the risk of cross-contamination between air streams because the supply and exhaust air ducts are isolated from each other. Circulation pumps are used to move the desiccant solution between the exchangers.

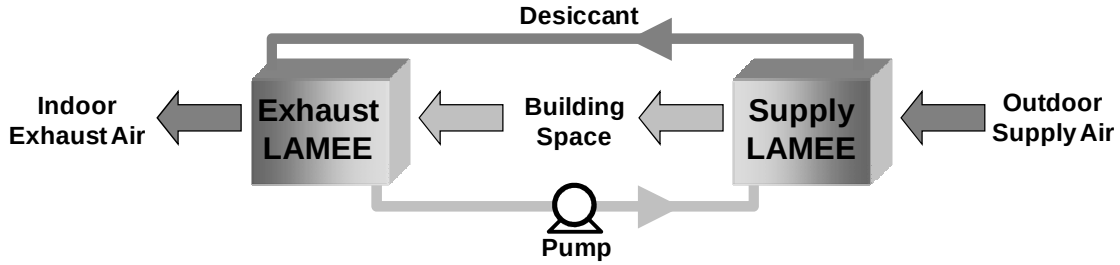

Figure 1.5: Run-around membrane energy exchanger schematic.

The RAMEE system is suitable for energy retrofits of older buildings with non-adjacent supply and exhaust air ducts and buildings where the exhaust air must not

contaminate the supply air. These are the same types of buildings where a run-around coil loop is appropriate, however the RAMEE system can transfer more energy than a run-around coil loop due to its moisture transfer capability.

1.3 Past RAMEE Research

The beginning of the RAMEE research dates back to 2002 when professors Besant and Simonson from the Department of Mechanical Engineering at the University of Saskatchewan partnered with Venmar CES Inc. and received a NSERC Collaborative Research and Development (CRD) grant which was renewed in 2008. The purposes of these grants are to research and develop the RAMEE system aiming towards a commercial product for Venmar CES and to provide training for graduate students. The development of the RAMEE and key findings are outlined in this section.

1.3.1 Primary Numerical Code

The first investigation on the RAMEE system was conducted through numerical simulations (Fan 2005, Fan et al. 2006). The code utilized a cross-flow configuration and demonstrated total effectiveness values up to 70%. Subsequent research revealed that the vapour permeability of the membrane used in the model was unrealistically high and that the narrow air and solution channels were impractical from a manufacturing point of view. Nonetheless, this model provided a solid foundation for later research.

1.3.2 RAMEE Prototype #1

The first RAMEE prototype was built based on the finding of the primary numerical model. It employed a cross-flow configuration and produced limited results because of unsatisfactory membrane deflections during operation. Nevertheless, the

prototype demonstrated heat and moisture transfer between two air streams (Hemingson 2005).

1.3.3 Investigation of Membrane Properties

The membrane limitations exhibited by the first prototype led to specific membrane investigations (Larson 2006). Larson investigated the vapour permeability and liquid resistance of several membranes and selected suitable ones to be used in the RAMEE. The deflection of the membrane was also addressed and methods of supporting it were proposed.

1.3.4 RAMEE Prototype #2

The second RAMEE prototype was constructed based on the findings of Larson (2006). This prototype used a superior membrane compared to Prototype #1 and a wire screen support structure to minimize membrane deflections. This prototype achieved a total effectiveness of 43%, which compared well with numerical simulations (Erb et al. 2010). However, the experimental results were different from numerical results and were attributed to small membrane deflections that were still present, heat loss and gains with the environment, and the transient response of the system.

1.3.5 Secondary Numerical Code

Additional numerical simulations was conducted to address the findings from the previous prototypes and to improve the understanding of the RAMEE system. A code to simulate the transient response of the system was created by Ahmadi (2008). This code also considered the heat loss and gains between the system and the environment. The simulations revealed the importance of the transient response and heat loss/gains which explained several of the observations from prototype #2 (Ahmadi et al. 2009a & 2009b).

Another code was created to study the effects of the solution flow-configuration (Vali 2009). This code was for a steady-state system and had the ability to model cross, counter, and a combination of cross and counter flow configurations. Investigations showed that the upper and lower effectiveness limits in the RAMEE system are achieved by counter and cross flow configurations, respectively, and that the combination of cross and counter flow configuration results in intermediate effectiveness values (Vali et al., 2009). Vali (2009) also investigated the RAMEE performance at summer and winter conditions (AHRI 2005) and showed different system performances at different conditions.

1.3.6 RAMEE Prototypes #3 and #4

The next generation of prototypes used the findings from the prior prototype (Erb et al. 2010) and numerical models (Ahmadi 2008, Vali 2009). Two prototypes were made which utilized a flow configurations that had cross and counter-flow portions (unlike the cross-flow in Prototype #2) and used different membranes and fabrication techniques (Beriault 2010, Mahmud et al. 2010).

Mahmud et al. (2010) fabricated a prototype that used Propore™ as its membrane. Propore™ was first recommended as a suitable membrane by Larson (2006) and was used in the prototype of Erb et. al. (2010). The maximum total effectiveness achieved by this prototype was 55% at an NTU of 12.

Prototype #4 was constructed by Beriault (2010) and was similar to Prototype #3 but it was constructed with improved techniques and utilized some different materials. Experimental results for non-standard outdoor air test conditions were obtained and were shown to be significantly different from standard test conditions.

1.4 Research Objectives

The general objective of this study is to expand on the understanding of the RAMEE system, which involves investigating some of the trends and discrepancies observed in previous studies. This study primarily focuses on the effects of outdoor air conditions and the effects of exchangers with non-uniform channels on the RAMEE performance. This is achieved through numerical modeling of the RAMEE, which, where available, is compared to experimental results for validation. The explicit objectives in this study are to:

1. Determine the effects of operating conditions (outdoor temperature and humidity ratio and solution flow rate) on system performance;
2. Develop correlations to describe the system performance at different outdoor air conditions and solution flow rates;
3. Determine the effects of non-uniform exchanger channels on the RAMEE performance.

1.5 Thesis Overview

The thesis contains the analysis and conclusions for the above objectives. Numerical data form the core of this thesis and the numerical model used to generate the data is presented in Chapter 2. The model was created by Vali (2009) and has undergone some modifications to more adequately describe the system. The model is described in general with attention to the modifications and the required additions to investigate non-uniform exchanger channels.

The effects of the outdoor air condition on the RAMEE performance (**Objective 1**) are covered in Chapter 3. This investigation focuses on the performance of the

system when it has maximum sensible, latent, and total energy transfers at a given outdoor air condition. The relationships between the outdoor air condition and the solution flow rate that causes these maximums are shown. Lastly, outdoor air conditions where heat and moisture are transferring in opposite directions to each other are described and compared to experimental results where applicable (Beriault 2010).

From the understanding of the relationship between the outdoor air conditions, solution flow rates, and system performance, correlations are developed to predict the sensible and latent effectiveness (**Objective 2**). This is contained in Chapter 4, which shows the development and validation of the correlations.

The investigation into the effects of exchangers with non-uniform channels on the RAMEE performance (**Objective 3**) is covered in Chapter 5. The results from the numerical analysis are compared to experimental results to estimate the actual impact of non-uniform channels on RAMEE performance.

The results of this thesis are summarized in Chapter 6 and the conclusions found throughout are explicitly stated. Recommendations for future investigation into the RAMEE are also made.

Chapter 2

NUMERICAL MODEL

2.1 Introduction

This chapter introduces the numerical model that is used to investigate the RAMEE system and achieve the objectives of this thesis. The model was created by Vali (2009) based on the model of Fan et al. (2006). During this thesis research, several modifications have been made to the model to better represent the RAMEE. This chapter contains a general description of the model and highlights the modifications made. This chapter also introduces design and operating parameters that are used to describe the RAMEE system, its operations and performance, and the outdoor air conditions.

2.2 RAMEE Numerical Model

This thesis relies extensively on numerical data because it allows a large number of outdoor air conditions and other parameters to be investigated quickly. The numerical model used was created by Vali (2009) and has been verified analytically for heat transfer (Vali et al. 2009) and validated with experimental results for heat and moisture transfer (Vali 2009). The numerical uncertainties are less that 2.5% for the heat transfer model and between 1-17% (total effectiveness) for the heat and moisture transfer model. The model has undergone slight modifications for this study to better

describe the system and allow the objectives of this study to be achieved. A description of the model and its important terms are contained in the following sections.

2.2.1 Assumptions

The numerical model is created based on several assumptions. These assumptions simplify the equations in the model and decrease its computational demands. The following assumptions are made in the numerical model:

RAMEE Assumptions

1. The geometry of each exchanger and flow channel is identical.
2. The mass flow rates of supply and exhaust air are equal.
3. The inlet air properties for each exchanger are uniform and steady.
4. Heat and moisture transfers between the system and the surroundings are negligible.

LAMEE Assumptions

5. The flow in each fluid channel is steady, laminar, and fully developed.
6. The heat and moisture transfer analysis mostly uses bulk mean fluid properties.
7. The heat and moisture transfers across the membrane are normal to its surface and the membrane properties are constant.
8. Heat conduction and moisture diffusion in the fluids in the flow direction are negligible compared to the advection of energy and moisture.
9. Phase change energy from the evaporation/condensation of water vapour at the liquid-membrane interface is all transferred from/to the liquid.

The first three assumptions for the RAMEE are for steady-state balanced operations at constant indoor and outdoor air conditions. Under normal operation (and adequate insulation), the heat and mass transfer in the system is significantly greater than what would occur with the environment and this justifies assumption 4 for such conditions.

The fluid flow in the LAMEEs is laminar with Reynolds numbers of ~1 for the liquid desiccant and 200-400 for the air flow. The entrance length effects as determined by the total effectiveness difference is less than 0.5% (@NTU = 5) compared to when they are neglected. Therefore, entrance length effects are neglected and fully developed flow is assumed.

Using the bulk fluid properties in assumption 6 simplifies the analysis to one dimension. The lateral gradients caused by the thermal and mass boundary layer resistances are accounted for in the overall transfer resistances. Moisture transfer in the solution is a little more complex and the boundary layer resistance to mass transfer is accounted for using the liquid-membrane interface vapour pressure difference with the bulk mean air flow value (see Section 2.2.3).

Heat and moisture transfer across the membrane is assumed to be normal to the membrane because it is very thin and its resistance is significantly greater than the convective coefficients of the fluids. The membrane's thermal and moisture transfer properties are independent of temperature and humidity (Larson et al. 2007).

Axial conduction is considered insignificant for Peclet numbers greater than 20 (Luo and Roetzel 1998). Assumption 8 is possible because under normal operating conditions the heat and mass Peclet numbers are very large (500-20,000) for both fluids.

The moisture phase change occurs at the interface between the solution and membrane. The solution absorbs/releases this phase change energy because the convective heat transfer coefficient of the solution (700 W/(m^2·K)) is more than an order of magnitude higher than the combined heat transfer coefficient of the air and membrane (27 W/(m^2·K))

2.2.2 Desiccant Solution

The RAMEE system uses a liquid desiccant as the coupling fluid between the two LAMEEs in order to enable moisture transfer between the air streams. The driving potential for moisture transfer between the air streams is the difference between their vapour concentrations or vapour pressures. In this thesis, the humidity ratio is used to express vapour concentrations and is defined as the ratio of the mass of water vapour over the mass of dry air. Therefore, in order for the liquid desiccant to transfer moisture between the two air streams, the equilibrium air humidity ratio of the desiccant (i.e., the humidity ratio of the air in equilibrium with the surface layer of the desiccant) has to fall between the humidity ratios of the two air streams. In this thesis, the equilibrium air humidity ratio of the desiccant is referred to as the humidity ratio of the desiccant for brevity.

Liquid desiccants are ideal coupling fluids because they are able to produce a wide range of humidity ratios depending on their type, concentration, and temperature. Figure 2.1 shows the equilibrium relationship between humidity ratio, temperature, and concentration for a desiccant solution of LiBr (Afshin 2010). At a constant desiccant concentration, the humidity ratio increases exponentially as temperature increases. These trends are very similar to curves of constant relative humidity. The liquid

desiccant also exhibits a saturation concentration curve at which concentration the solution can, at equilibrium, not contain anymore desiccant and will begin to crystallize on the closest available nucleation point or surface if more water is removed from the solution. The relationship shown in Figure 2.1 applies to liquid desiccants other than LiBr except that the iso-concentration curves for given concentrations would correspond with different constant relative humidity curves and the saturation concentration value and position would differ. These variations between the properties of different liquid desiccants and complications associated with crystallization in the desiccant, requires careful selection of the desiccant based on the requirements of the RAMEE. The work by Afshin (2010) focused on selecting the optimal liquid desiccant for the RAMEE.

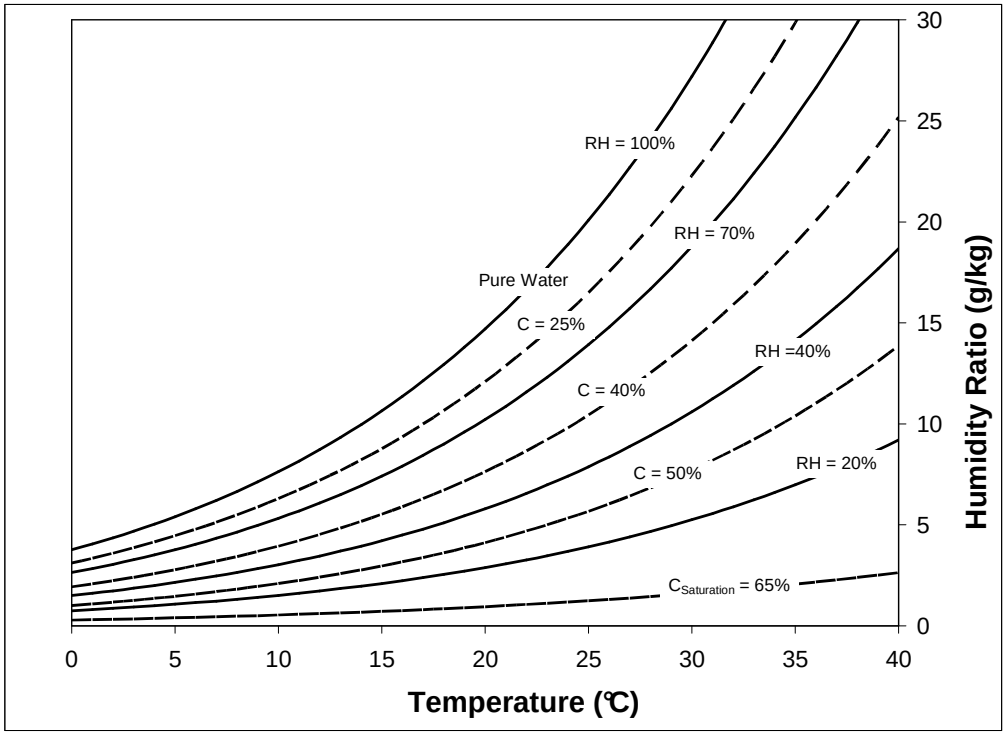

Figure 2.1: Equilibrium surface vapour pressure, concentration (C), temperature relationship of LiBr with lines of constant relative humidity (RH).

The concentration of the liquid desiccant (C) is defined as the mass of salt divided by the mass of solution. In this study, the solution mass fraction (X) is preferred

over the concentration, which is equal to mass of water divided by the mass of salt in the solution. The mass fraction of desiccant is analogous to the humidity ratio of air.

2.2.3 Liquid-to-Air Membrane Exchanger

The LAMEE is the core element of the RAMEE system. LAMEEs are flat plate exchangers with alternating solution and air channels of thickness δ_{Sol} and δ_{Air}, respectively, which are separated by a membrane of thickness δ_{Mem} (Figure 2.2). The flow regime in the model can be either cross, counter, or a combination between cross and counter flows. The counter flow regime is predominantly used in this study and so only governing equations pertaining to it will be shown (numerical simulations of the experimental prototypes use the combination between cross and counter flows). The equations for the other flow regimes can be found in the work of Vali (2009).

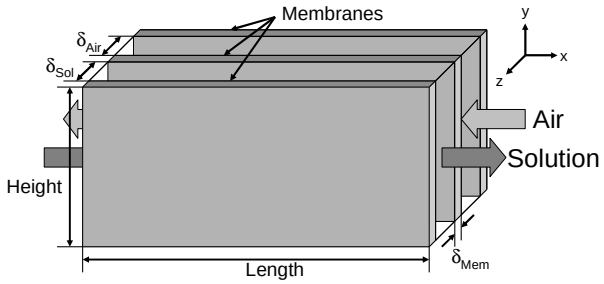

Figure 2.2: LAMEE control volume with counter flow air and solution streams.

Conservation of Moisture

Moisture transfer is governed by the conservation of mass between the air and desiccant solution fluid streams. Two equations, one for the air stream and the desiccant solution stream, describe the mass transfer. These equations are:

$$\frac{\partial X_{Sol}}{\partial x} = \frac{2U'_m}{J_{Sol}\delta_{Sol}}(W_{Air} - W_{Sol,mem}), \tag{2.1}$$

$$\frac{\partial W_{Air}}{\partial x} = -\frac{2U'_m}{J_{Air}\delta_{Air}}(W_{Air} - W_{Sol,mem}), \tag{2.2}$$

where

$$U'_m = \left[\left(h_{m,Air} \right)^{-1} + \left(k_m / \delta_{Mem} \right)^{-1} \right]^{-1}, \tag{2.3}$$

and X is the mass fraction of the solution [kg_{Water}/kg_{Salt}],

W is the humidity ratio of the air [kg_{Water}/kg_{Air}],

U'_m is the modified overall mass transfer coefficient [$kg/(m^2 \cdot s)$],

J is the mass flux [$kg/(m^2 \cdot s)$],

h_m is the convective mass transfer coefficient [$kg/(m^2 \cdot s)$],

k_m is the membrane water vapour permeability [$kg/(m \cdot s)$],

and subscripts:

Air denotes air (bulk),

Sol denotes solution (bulk), and

Sol,mem denotes properties at membrane-solution interface.

In order to determine T_{Air} and W_{Air} by solving equations (2.1) and (2.2), the bulk concentration of the solution has to be related to its equilibrium air humidity ratio at the membrane-solution interface, which is not known. This is accomplished through equations (2.4-2.6) that are iteratively solved. Cisternas and Lam (1991), [also presented in Afshin (2010)], developed a correlation that relates the equilibrium air humidity ratio with the temperature and concentration of the solution at the membrane-solution interface,

$$W_{Sol,mem} = f\left(T_{Sol,mem}, X_{Sol,mem} \right). \tag{2.4}$$

The temperature and concentration of the desiccant at the membrane-solution interface are determined through heat and mass flux balances at this interface. The moisture mass flux at the membrane-solution interface is expressed as:

$$\dot{m}'' = \frac{W_{Air} - W_{Sol,mem}}{\left(h^{w}_{m,Air}\right)^{-1} + \left(k_m / \delta_{Mem}\right)^{-1}} = h^{x}_{m,Sol}\left(\frac{1}{1+X_{Sol}} - \frac{1}{1+X_{Sol,mem}}\right), \tag{2.5}$$

and the heat flux at the membrane-solution interface is given by:

$$q'' = \frac{T_{Air} - T_{Sol,mem}}{\left(h_{Air}\right)^{-1} + \left(k / \delta_{Mem}\right)^{-1}} + \frac{W_{air} - W_{Sol,mem}}{\left(h^{w}_{m,Air}\right)^{-1} + \left(k_m / \delta_{Mem}\right)^{-1}} h_{fg} = h_{Sol}\left(T_{Sol,mem} - T_{Sol}\right), \tag{2.6}$$

where $\dot{m}''$ is the mass flux of moisture [kg/(m^2·s)],

q" is the heat flux [W/m^2],

T is the temperature [°C],

h is the convective heat transfer coefficient [W/(m^2·K)],

k is the membrane thermal conductivity [W/(m·K)], and

h_{fg} is the latent heat of vapourization [J/kg],

and superscripts

X denotes a convective mass transfer coefficient based on a difference in X, and

W denotes a convective mass transfer coefficient based on a difference in W.

Equations (2.5) and (2.6) are rearranged to solve for $X_{Sol,mem}$ and $T_{Sol,mem}$ respectively, which are then used in equation (2.4) to determine the $W_{Sol,mem}$. Equations (2.4-2.6) are coupled and therefore they are iterated to determine the humidity ratio of the solution at the membrane-solution interface, which allows equations (2.1) and (2.2) to be solved when the bulk temperature and mass fraction of the desiccant are known.

The resistance to mass transfer in the solution is accounted for by equations (2.5) and (2.6), which was neglected in Vali's model (2009), where $W_{Sol,mem}$ was based on the bulk solution temperature and mass fraction.

Conservation of Energy

Heat transfer is governed by the conservation of energy between the air and desiccant solution fluid streams. This heat transfer is described by one equation for the air and another for the desiccant solution. These equations are also for a counter flow configuration and are:

$$\frac{\partial T_{Sol}}{\partial x} = \frac{2}{C_{p,Sol} J_{Sol} \delta_{Sol}} \left[U(T_{Air} - T_{Sol}) + U'_m (W_{Air} - W_{Sol,mem}) h_{fg} \right], \tag{2.7}$$

$$\frac{\partial T_{Air}}{\partial x} = - \frac{2U}{C_{p,Air} J_{Air} \delta_{Air}} (T_{Air} - T_{Sol}), \tag{2.8}$$

where

$$U = \left[(h_{Air})^{-1} + \left(k / \delta_{Mem} \right)^{-1} + (h_{Sol})^{-1} \right]^{-1}, \tag{2.9}$$

and U is the overall heat transfer coefficient [W/(m^2·K)], and

C_p is the specific heat capacity [kJ/kg].

Air, Solution, and Membrane Properties

The thermal conductivity and specific heat of the air and solution are required in the analysis (equations (2.1-2.9)). These air properties are only mildly dependent on temperature and therefore constant values obtained from Incropera and DeWitt (2002 are used). The properties of the liquid desiccant are more complex and depend on the salt type, concentration, and temperature. Empirical correlations contained in Zaytsez and Aseyev (1992) are used to determine the solution properties (also contained in Afshin 2010). The convective heat transfer coefficients in the air and desiccant are

determined from the Nusselt number for constant heat flux in a laminar flow between parallel plates (Shah and London 1978). The air and solution convective mass transfer coefficients are given by the Chilton-Colburn analogy (Incropera and DeWitt 2002).

Unless otherwise specified, the membrane used in the numerical model is based on the properties of Propore™, which was used in the experimental prototypes of Erb (2010) and Mahmud et al. (2010). The properties for Propore™ were determined by Larson (2006) and are presented in Table 2.1. Also, the thicknesses for the air and solution channels are presented in Table 2.1. These thicknesses are also based on the experimental prototype of Mahmud et al. (2010) and will be used in this study unless specified otherwise.

Table 2.1: LAMEE channel thicknesses and membrane properties for Propore™.

Property	Value
Channel Thicknesses	
Air	4.2 mm
Solution	2.7 mm
Membrane Properties	
Thickness	0.2 mm
Thermal Conductivity	0.334 W/(m·K)
Water Vapour Permeability	1.66×10^{-6} kg/(m·s)

2.2.4 LAMEE Numerical Procedure

Equations (2.1-2.9) enable temperature and moisture content (humidity ratio/mass fraction) distributions in the LAMEE air and solution channels to be determined. The boundary conditions for the governing equations are the temperature and humidity ratio of the air inlet and the temperature and mass fraction of the solution inlet. The air conditions at the LAMEE inlets are the outside conditions for the supply exchanger and the indoor conditions for the exhaust exchanger. Various indoor and outdoor air conditions are used in this study and will be highlighted when they are

applied. Commonly used conditions are the summer and winter AHRI standard test conditions (AHRI 2005) which are shown in Table 2.2.

Table 2.2: AHRI test conditions.

	Summer		Winter	
	Indoor	**Outdoor**	**Indoor**	**Outdoor**
T	24℃	35℃	21°	1.7℃
W	9.3 g/kg	17.5 g/kg	7.1 g/kg	3.5 g/kg
RH	50%	49%	46%	82%

The governing equations (2.1, 2.2, 2.7, & 2.8) are discretized by an implicit finite difference method using an upwind scheme in order to determine the air and solution temperature and moisture content distributions in the exchangers. Grids of over 100 nodes in the discretized directions were used, which were shown to provide grid independent results (Vali 2009). A Gauss-Seidel iteration technique is used to solve the discretized governing equations. The convergence criteria is satisfied when the root-mean-square difference between successive iterations for all the air and solution properties (i.e., T, W, and X) are less than $1x10^{-5}$. The convergence criteria are very conservative in that the change in effectivenesses caused by increasing the criteria from $1x10^{-4}$ to $1x10^{-5}$ is less than $1x10^{-3}$% at the AHRI summer condition. The conservative criteria ensure satisfactory convergence for a variety of outdoor and indoor air conditions. Once convergence occurs, the exchanger outlet conditions are determined based on the nodal air/solution values at the exchanger outlets adiabatically mixing.

2.2.5 RAMEE Numerical Procedure

The RAMEE numerical procedure combines the supply and exhaust LAMEEs together to determine the temperature and mass fraction of the solution at the LAMEE inlets during quasi-steady state operations. This is achieved through an iterative process that begins by assuming an initial solution condition at the supply exchanger solution

inlet. The LAMEE numerical procedure is used to determine the temperature and mass fraction of the solution at the supply exchanger outlet based on its boundary conditions. The solution condition at the supply exchanger outlet becomes the inlet conditions for the exhaust exchanger. This assumes no heat or moisture is transferred in the piping system which is justified with adequately insulated piping. The LAMEE numerical procedure is then used again to determine the solution conditions at the exhaust exchanger outlet, which is then used as the inlet solution condition for the supply exchanger. This process is continued until convergence occurs, which for the RAMEE is defined as when the moisture and energy transfer between the supply and exhaust exchangers are within $5x10^{-4}$ of each other. This is also a conservative criterion with the change in effectiveness being less $1x10^{-3}$% when the convergence criterion is increased from $1x10^{-4}$% to $1x10^{-5}$% at AHRI summer conditions. At this steady state, all the inlet and outlet conditions of the exchangers are known and do not change significantly with further iterations. The results from the RAMEE analysis are for steady state conditions.

2.2.6 Non-uniform Air and Solution Channel Thicknesses

An objective of this study is to determine the effects of non-uniform air and solution channel thicknesses on the system performance. This is accomplished by imposing a variable channel thickness into the model and considering the resulting flow maldistributions in the air and solution channels and the variable heat and moisture transfer resistances. This condition is only applied to the case of a counter-flow exchanger in this thesis.

The experimental prototypes (Erb 2010, Mahmud et al. 2010, and Beriault 2010) exhibited non-uniform air and solution channel thicknesses. The variable channel

thickness is caused by the higher pressure in the solution channel causing the membrane to deflect into the air channel. The deflected panel is constrained by support structures in the air channel, which results in the membrane bulging into complex two-dimensional patterns. This pattern is simplified as a sinusoidal pattern, which is shown in Figure 2.3. In this arrangement, the average thickness of the solution channel increases and the average thickness of the air channel decreases. The modeled sinusoidal bulges are continuous over the length of the exchanger and parallel to the fluid flows. The bulges are also assumed to be identical in all the channels.

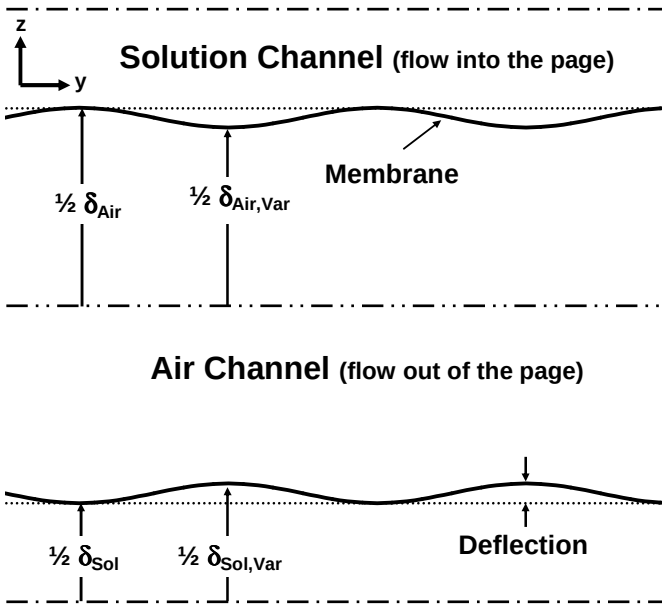

Figure 2.3: Schematic of air and solution channel variations (Var).

The non-uniform channels are divided into sections (j-indexed) in the y-direction that extend the length and thickness of the channel. The pressure drop across the length of each section is the same, which allows the flow to become maldistributed due to the sections having variable thicknesses. The maldistributed flow consists of higher flow rates in the wider sections and lower flow rates in the narrow sections. The flow rates

through the variable thickness sections can be determined according to Poiseuille flow. This analysis neglects the fluid shear stresses between adjacent sections which results in a greater calculated flow maldistribution than in reality. The analytical solution for Poiseuille flow in a uniform channel is:

$$V = \frac{1}{48} \cdot \frac{D_h^2}{\mu} \cdot \frac{dP}{dx}, \tag{2.10}$$

where V is the fluid velocity [m/s],

D_h is the hydraulic diameter of the parallel plates [m],

μ is the dynamic viscosity [kg/(s·m)], and

$\frac{dP}{dx}$ is the pressure gradient [Pa/m].

Using equation (2.10) and discretizing the channel width (y-direction in Figure 2.3), a relationship can be derived to describe the fraction of fluid flowing through a discrete channel width at a given thickness. For the air and solution channels, the relationship is:

$$\frac{\dot{m}^j}{\dot{m}_{Tot}} = \frac{D_h^{j\,3}}{\sum_{j=1}^{n} D_h^{j\,3}}, \tag{2.11}$$

where

$\frac{\dot{m}^j}{\dot{m}_{Tot}}$ is the fraction of the total channel fluid mass flow rate in section j, and

D_h^j is the hydraulic diameter of channel section j [m].

The channel thickness variation also influences the heat and moisture transfer rates by changing the convective heat and mass transfer coefficients in the air and solution. The Nusselt number, which is constant for flow between parallel plates (Shah

and London 1978), relates the convective heat transfer coefficient to the hydraulic diameter of the channel (Incropera and DeWitt 2002). Therefore if the channel width is discretized (as was previously done for the mass flow rate), the convective heat transfer coefficient can be described as:

$$h^j = \frac{Nu \cdot k}{D_h^j}, \tag{2.12}$$

where Nu is the Nusselt number, and

k is the conductivity of the fluid [W/(m·K)].

The convective mass transfer coefficient can be determined from the convective heat transfer coefficient with the Chilton-Colburn analogy (Incropera and DeWitt, 2002). In discretized form, the convective mass transfer coefficient can be determined from:

$$h_m^j = h^j \cdot \frac{Le^{-2/3}}{\rho C_P}, \tag{2.13}$$

where Le is the Lewis number of the fluid,

ρ is the fluid density [kg/m^3], and

C_P is the fluid specific heat capacity [J/(kg·K)].

The air and solution channel thickness variations in the LAMEE result in flow maldistributions and variable overall heat and mass transfer coefficients. These two effects are accounted for by equations (2.11-2.13) and allow for the effects of the non-uniform channel thicknesses on the system performance to be evaluated.

2.3 Performance Indicators

The performance of the RAMEE system is quantified in terms of the actual energy transfer and effectiveness at steady state. The energy transfers of interest are the sensible, latent, and total energy, which describe the heat, moisture, and enthalpy

transferred between the air streams. In this study, the transfers are described as the change in temperature (°C), humidity ratio (g/kg), and enthalpy (kJ/kg) of the supply air. Based on the heat exchanger steady-state definition of effectiveness, the effectiveness values are defined as the actual energy transfer rate divided by the maximum possible energy transfer for an exchanger with an infinite area (equations 2.14-2.16). In a balanced system (i.e., equal supply and exhaust mass flow rates), these steady-state effectivenesses are defined as:

$$\varepsilon_{Sen} = \frac{T_{Air,S,In} - T_{Air,S,Out}}{T_{Air,S,In} - T_{Air,E,In}} = \frac{T_{Air,E,Out} - T_{Air,E,In}}{T_{Air,S,In} - T_{Air,E,In}}, \quad (2.14)$$

$$\varepsilon_{Lat} = \frac{W_{Air,S,In} - W_{Air,S,Out}}{W_{Air,S,In} - W_{Air,E,In}} = \frac{W_{Air,E,Out} - W_{Air,E,In}}{W_{Air,S,In} - W_{Air,E,In}}, \quad (2.15)$$

$$\varepsilon_{Tot} = \frac{H_{Air,S,In} - H_{Air,S,Out}}{H_{Air,S,In} - H_{Air,E,In}} = \frac{H_{Air,E,Out} - H_{Air,E,In}}{H_{Air,S,In} - H_{Air,E,In}}, \quad (2.16)$$

where ε is the effectiveness,

T is the temperature [°C],

W is the humidity ratio [g/kg],

H is the enthalpy [kJ/kg],

and subscripts

Sen denotes sensible,

Lat denotes latent,

Tot denotes total,

Air denotes the air stream properties,

S denotes the supply exchanger,

E denotes the exhaust exchanger,

In denotes the exchanger inlet, and

Out denotes the exchanger outlet.

The actual energy transfers (and consequential effectiveness values) in the supply and exhaust exchanges are slightly different (less than 1% in most conditions) because the specific heat capacities of the air streams are slightly different and due to numerical errors and the convergence criteria. As a result, the effectiveness values presented in this study are averaged between the supply and exhaust exchangers.

2.4 Design and Operating Condition Parameters

Several parameters are used to describe the design and operating conditions of the RAMEE. The design parameter describes the size of the system, while the operating conditions describe the fluid flow rates in the system at particular outdoor air conditions.

The RAMEE size (design parameter) is characterized by the number of thermal transfer units (NTU) and number of mass transfer units (NTUm) in each exchanger. In this study, the supply and exhaust exchangers are the same size and have equal air mass flow rates. Therefore these parameters are defined as:

$$\mathrm{NTU} = \frac{\mathrm{UA}}{\dot{m}_{\mathrm{Air}} C_{\mathrm{p,Air}}}, \tag{2.17}$$

$$\mathrm{NTUm} = \frac{U'_{m} A}{\dot{m}_{\mathrm{Air}}}, \tag{2.18}$$

where

U is the overall convective heat transfer coefficient [W/(m^2·K)],

U'_m is the overall convective mass transfer coefficient [kg/(m^2·s)],

A is the surface area of the membrane in the exchanger [m^2],

$\dot{m}$ is the mass flow rate of dry air through the exchanger [kg/s], and

C_P is the specific heat capacity [kJ/(kg·K)].

The operation of the system is characterized by the ratio of the solution heat capacity rate with the air heat capacity rate (Cr*). This ratio (Cr*) is similar to the heat capacity ratio used in the literature for heat exchangers (Incropera and DeWitt 2002) except that the solution properties are always in the numerator. Using Cr* to describe the RAMEE is convenient because, under practical operation, the air flow rate is kept constant and therefore the solution flow rate is directly related to Cr*. The definition of Cr* is:

$$Cr^* = \frac{\dot{m}_{Sol} C_{p,Sol}}{\dot{m}_{Air} C_{p,Air}}. \tag{2.19}$$

The operating condition factor, H*, is a dimensionless number that is the ratio of the latent to sensible energy differences between the air inlets of the exchanger (Simonson and Besant 1999b), which is expressed as:

$$H^* = \frac{\Delta H_{Lat}}{\Delta H_{Sen}} \approx 2500 \frac{\Delta W}{\Delta T}. \tag{2.20}$$

Figure 2.4 shows the values of H* for different outdoor conditions when the indoor condition is at 24°C and 9.3 g/kg. When the indoor and outdoor air humidity ratios are the same, H* = 0, and when the indoor and outdoor air temperatures are equal, H* = ±∞. Typical energy recovery applications have H* values that vary between -6 to +6.

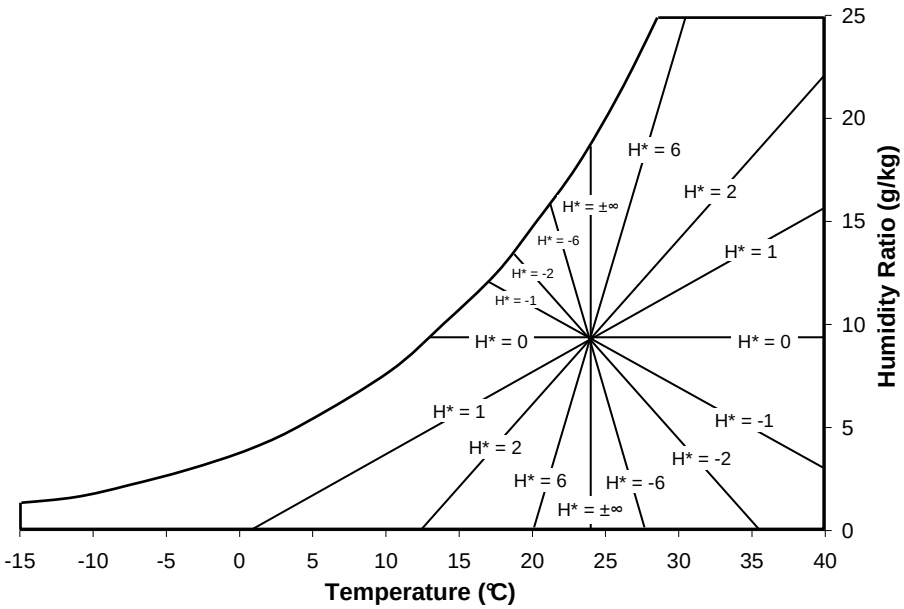

Figure 2.4: Psychometric chart showing H* values for indoor condition of 24°C and 9.3 g/kg.

The operating condition factor can also be used to determine the total effectiveness from the sensible and latent effectivenesses determined in equations (2.14-2.15). The total effectiveness can be determined from (Simonson and Besant 1999b):

$$\varepsilon_{Tot} = \frac{\varepsilon_{Sen} + H^* \varepsilon_{Lat}}{1 + H^*}. \tag{2.21}$$

Another parameter can be used in conjunction with H* to fully describe the conditions at the air inlets. This parameter considers the enthalpy difference between the air inlets which is represented by ΔH and defined by:

$$\Delta H = H_{exhaust} - H_{supply}. \tag{2.22}$$

Using both H* and ΔH allows the exact outdoor air condition relative to the indoor condition to be described.

2.5 Chapter 2 Summary

This chapter presented the numerical model that is used in this thesis to investigate the RAMEE system. The model was created by Vali (2009) and has undergone some modifications to more accurately represent the system and achieve the objectives of this study. The assumptions used in the model were presented and justified and then the properties of the desiccant solution were described. The governing equations that describe heat and moisture transfer in the LAMEE were then shown. The numerical methods used to solve the governing equations and determine the steady-state performance of the LAMEE and RAMEE were explained. The modification of the model for non-uniform air and solution channels to determine its effects on RAMEE performance was described. Finally, the indicators used to determine the performance of the system were illustrated as well as key design and operating condition parameters which describe the size and operation of the system and the outdoor air conditions it is operating in.

Chapter 3

EFFECTS OF OUTDOOR AIR CONDITIONS ON PEAK PERFORMANCE

3.1 Introduction

Previous numerical investigations into the RAMEE (Fan et al. 2006, Ahmadi et al. 2009 a&b, Vali 2009, Erb et al. 2010) have shown different performances at standard summer and winter test conditions (AHRI 2005). These differences are demonstrated in Figure 3.1, which shows the total effectiveness of a counter-flow RAMEE (NTU = 10 and NTUm = 2.7) operating at summer and winter conditions. The plots of total effectiveness as a function of Cr* for summer and winter conditions show similar trends in that as Cr* increases from zero, the effectiveness increases rapidly from zero to a maximum effectiveness and then slowly decreases to a plateau. However, the maximum or peak effectiveness and the Cr* value at which the peak total effectiveness occurs are different for the summer and winter test conditions. Sensible and latent effectivenesses versus Cr* plots (not shown here) demonstrate similar relationships with different peak effectiveness values and Cr* values at which the peak occurs.

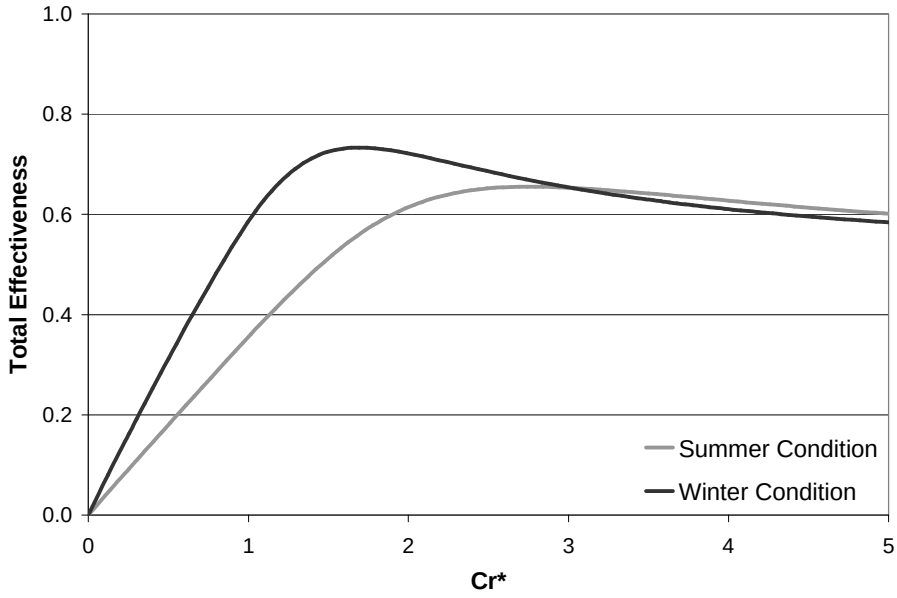

Figure 3.1: RAMEE total effectiveness at summer and winter test conditions. NTU = 10, NTUm = 2.7.

This chapter presents the complex relationship between the system performance (i.e., effectivenesses and energy transfers) and the operating parameters, namely the solution flow rate (i.e., Cr*) and the outdoor air conditions (i.e., H* and ΔH). This is achieved by simulating a range of outdoor conditions over a range of operating Cr*. The range of outdoor conditions represents the typical conditions that a given location would experience in a typical year (Figure 3.2 shows the range for Chicago, IL). From these results, the relationships between outdoor air conditions and the peak total, sensible, and latent performances are shown and explained. Additionally, the relationship between the Cr* values that cause these peak performances and the outdoor air condition are shown. The performance of the RAMEE at negative H* conditions and its potential applications are discussed. Lastly, the effects of NTU/NTUm and indoor conditions on the system are considered.

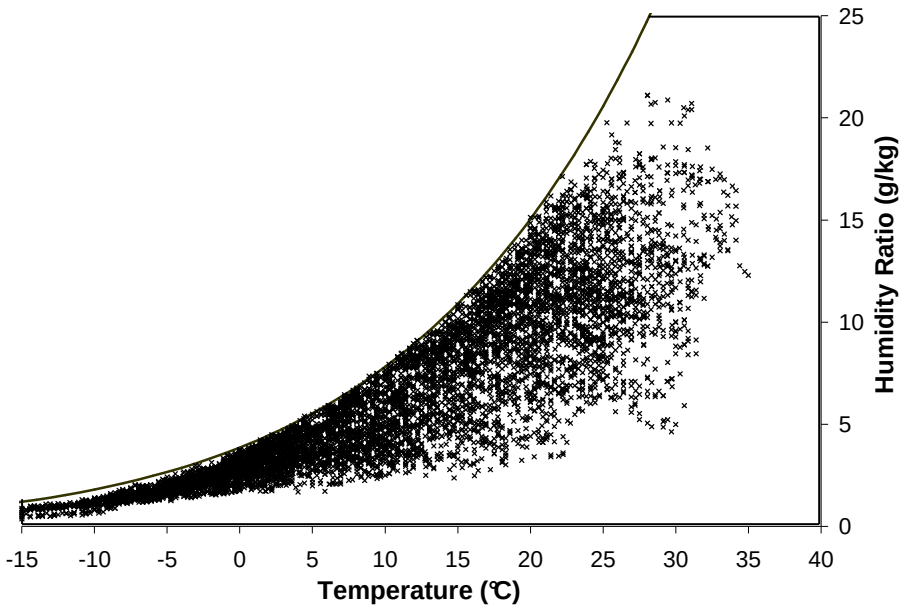

Figure 3.2: Hourly outdoor air conditions for a typical year in Chicago, IL.

The results in this chapter apply to a counter-flow RAMEE system operating with a LiBr desiccant solution. The exchangers in the system have an NTU of 10 and NTUm of 2.7, which corresponds to a maximum total effectiveness of about 65% (ε_{Sen} = 76.5%, ε_{Lat} = 59.9%, ε_{Tot} = 65.7%) at summer test conditions (AHRI 2005). The indoor air conditions are constant at 24°C and 9.3 g/kg. The outdoor air conditions range between -15°C to 40° and 0 g/kg to 25 g/kg at 1°C and 1 g/kg increments with 682 conditions simulated. The effects of frosting in the RAMEE at the low temperature conditions are neglected in this analysis. All other simulation conditions and factors are outlined in Chapter 2.

3.2 Peak Total Performance

The peak total performance is the maximum total energy transferred between the supply and exhaust air streams at a constant NTU. The total energy is comprised of the sensible energy (heat) and the latent energy (moisture) which is described by the sensible and latent performances. The peak total performance of the RAMEE is

important because in most situations, energy recovery systems operating at their peak total performance will allow the maximum amount of energy recovery in a year (Rasouli et al. 2010). Knowing the relationship between peak total performance and outdoor air conditions allows for the annual energy savings of the RAMEE to be determined which is useful in cost-benefit analyses.

The peak total performance for a specific outdoor condition occurs at a certain Cr*. This Cr* is referred at as the optimal Cr* because at this point the system energy recovery is at a maximum. Knowing the relationship between the optimal Cr* and the outdoor air conditions will allow the RAMEE to operate at peak total performance and therefore achieve maximum energy recovery.

This section presents the relationships of the outdoor air conditions with the peak total performance and the optimal Cr*. The causes of these relationships are also explained and discussed.

3.2.1 Performance Contour Plots

The results for the RAMEE performance as a function of the outdoor conditions are presented as contour plots on the psychometric chart. The values on the chart correspond to the performance of the system for the given outdoor air temperature and humidity ratio when the system is operating at the optimal Cr*. Plots of effectiveness and energy transfer are used to describe the sensible, latent, and total performances. Using both of these indices aids in observing and describing the various trends that are present.

Sensible Performance

The contour plots for the sensible performance (Figure 3.3) contain the sensible effectiveness and the temperature change in the supply air. The sensible effectiveness contour lines (Figure 3.3A) are similar to lines of constant H* (see Figure 2.4) and the effectiveness increases as H* increases. However unlike lines of constant H*, the sensible effectiveness contours have slight curvatures, which indicates that the sensible effectiveness still depends on another parameter (i.e., ΔH). The sensible effectiveness also goes to infinity when H* goes to infinity (i.e., indoor and outdoor air temperatures are equal). Several large $\pm$H* conditions ($-6 < H^* > 6$) produce effectiveness values that are less than 0% or greater than 100%. The sensible effectiveness for more than half of the outdoor conditions considered in this chapter, range between 60-100%.

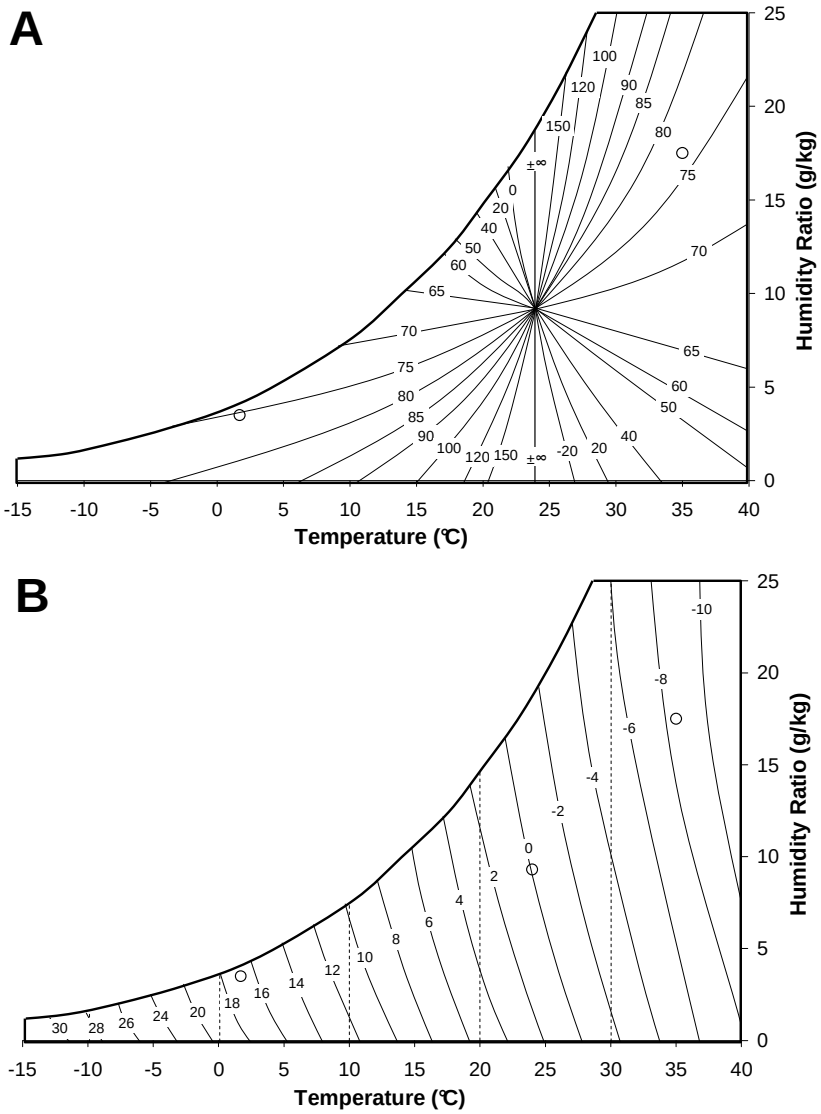

Figure 3.3: Sensible performance of the RAMEE operating at optimal Cr* for different outdoor air conditions. A) Sensible effectiveness (%). B) Supply air temperature change (°C). Dashed lines are lines of constant temperature change and circles correspond to AHRI outdoor summer and winter conditions and the indoor condition (24°C, 9.3 g/kg) at NTU = 10 and NTUm = 2.7.

The temperature change plot (Figure 3.3B) consists of near vertical lines that curve down and to the right (i.e., toward lower humidity ratios and higher temperatures). The distance between the contours is relatively constant and their curvatures are greater at lower temperatures. A constant sensible effectiveness energy recovery system (i.e., moisture transfer does not influence heat transfer) would have a temperature change contour plot with vertical lines with a constant distance between the contours. The

contours in Figure 3.3B show the sensible effectiveness is mildly influenced by temperature (relatively constant distance between the contours) and strongly influenced by humidity ratio (contour curvatures).

Latent Performance

The latent performance contour plots (Figure 3.4) shows the latent effectiveness and the supply air humidity ratio change. The latent effectiveness contour lines are similar to lines of constant H* (Figure 3.4A), except the effectiveness contour lines are slightly curved (like the sensible effectiveness contours). The latent effectiveness values increase as the inverse of H* increases, which means that the highest latent effectiveness occurs when $H^* = 0^+$ and the lowest latent effectiveness occurs when $H^* = 0^-$. The latent effectivenesses go to infinity when the outdoor and indoor humidity ratios are equal. Several conditions where the outdoor humidity ratio is near the indoor humidity ratio (i.e., $H^* < \pm 0.5$) produce effectiveness values that are less than 0% or greater than 100%. The majority of the simulated outdoor conditions produce effectiveness values between 40-70%.

The moisture change contour plot (Figure 3.4B) consists of nearly horizontal lines that curve up and to the left (i.e., towards higher humidity ratios and lower temperatures). The distance between the contour lines is relatively constant and their curvatures are greater at lower humidity ratios. A moisture change contour plot with equally spaced horizontal contours would represent an energy recovery system with constant latent effectiveness (i.e., one where heat transfer does not influence moisture transfer).

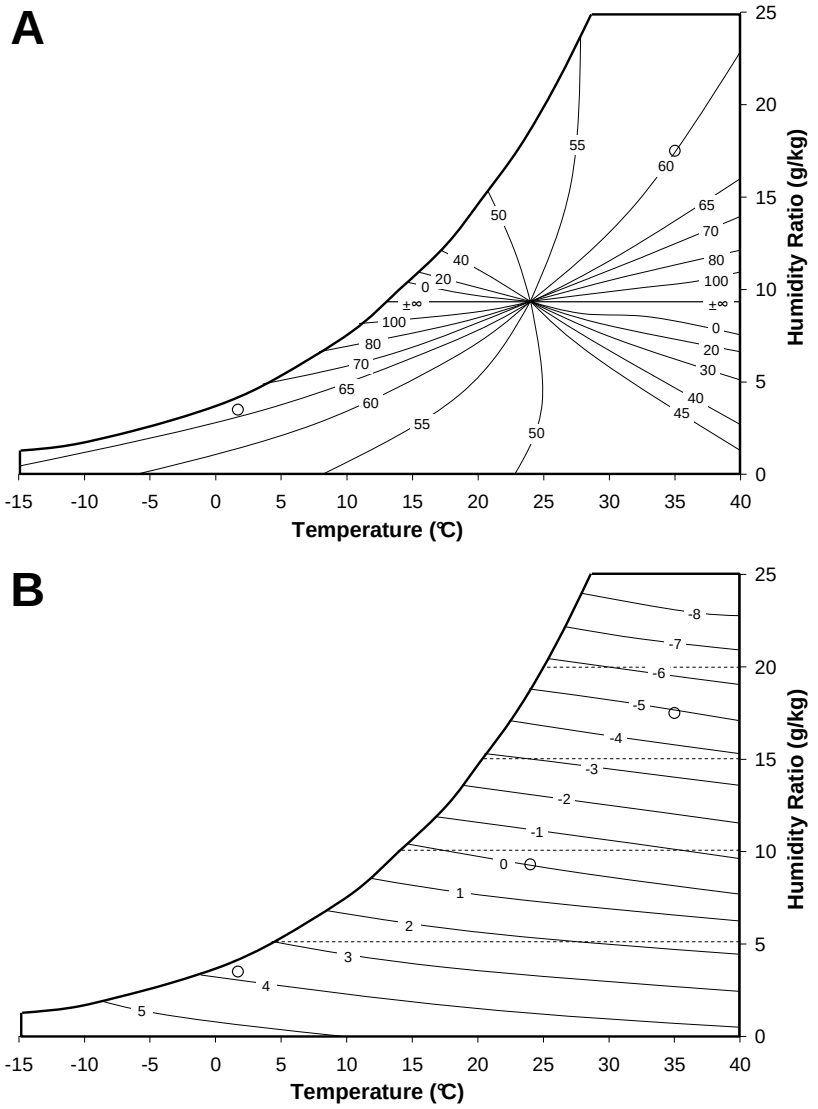

Figure 3.4: Latent performance of the RAMEE operating at optimal Cr* for different outdoor air conditions. A) Latent effectiveness (%). B) Supply air moisture change (g/kg). Dashed lines are lines of constant humidity ratio change and circles correspond to AHRI outdoor summer and winter conditions and the indoor condition, NTU = 10 and NTUm = 2.7.

Total Performance

The total energy performance of the system is harder to characterize than the sensible and latent performances because the total effectiveness is a function of the sensible effectiveness, the latent effectiveness and the outdoor air conditions (H*, see Equation (2.21)). As a result of this, the total effectiveness of an energy recovery

system is variable for different outdoor air conditions even if the sensible and latent effectiveness are constant. The exception to this occurs when the sensible and latent effectivenesses are also equal to each other and constant. In this situation, the sensible, latent, and total effectivenesses are the same and constant for all outdoor air conditions.

Effectiveness and supply air enthalpy change contour plots are presented in Figure 3.5. The total effectiveness contour lines are similar to lines of constant H* and also have slight curvatures (Figure 3.5A). The total effectiveness contour line values increase as H* decreases from -1 to -∞ and then from +∞ to -1. As H* goes to -1 (i.e., the outdoor air enthalpy approaches the indoor air enthalpy), the total effectivenesses approaches ±infinity. Several outdoor conditions near H* = -1 (-0.5 > H* > -1.2) have effectiveness values less than 0% or greater than 100%. Over half of the conditions simulated have total effectiveness values between 55-75%.

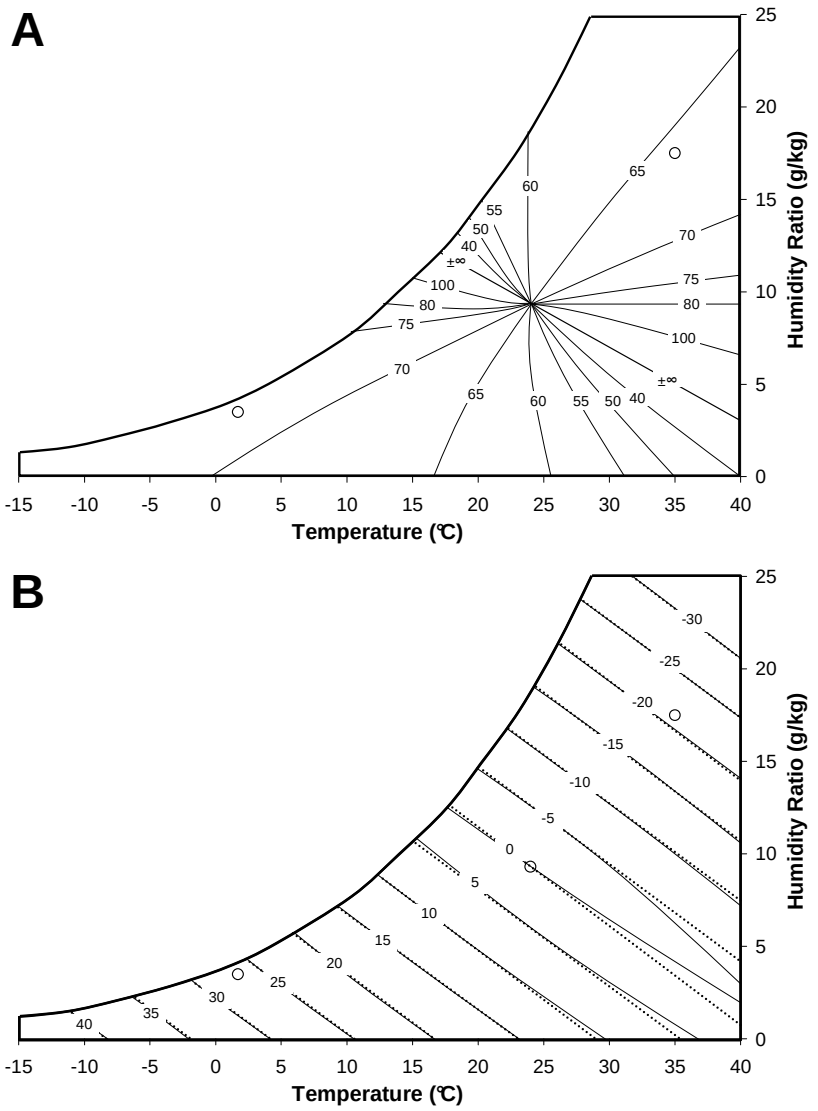

Figure 3.5: Total performance of the RAMEE operating at optimal Cr* for different outdoor air conditions. A) Total effectiveness (%). B) Supply air enthalpy change (kJ/kg). Dotted lines represent enthalpy change for a constant effectiveness system (ε_{Sen}=80%, ε_{Lat}=61%). Circles correspond to AHRI outdoor summer and winter conditions and the indoor condition.

The actual total energy transfer (Figure 3.5B) consists of contours with slopes similar to lines of constant enthalpy, but they are slightly steeper (i.e., greater change in humidity ratio for a given temperature change). The total energy contours are slightly curved, especially near the indoor air condition. The total energy transfer is comparable to the total energy transfer of a constant effectiveness system with ε_{Sen} = 80% and

ε_{Lat} = 61%, which are slightly different from the RAMEE effectiveness values at AHRI summer conditions (ε_{Sen} = 77% and ε_{Lat} = 60%). These constant effectiveness values are determined by minimizing the difference (based on root-mean-square) between the air enthalpy change in a constant effectiveness system and the RAMEE (variable effectiveness) for all the simulated outdoor air conditions. Figure 3.5B shows the enthalpy change contour lines for the RAMEE system (solid lines) and a constant effectiveness system (ε_{Sen} = 80%, ε_{Lat} = 61%, dotted lines). The slope of the contour lines and the distance between adjacent lines in both systems are very similar. The only deviations between the contours of the two systems occur at –H* conditions (i.e., outdoor air conditions that are warmer and drier or colder and more humid than the indoor conditions) but these deviations are minimal. These deviations occur because the sensible and latent effectiveness values show the greatest temperature dependency in these areas.

The total performance of the system summarizes the sensible and latent performances. The contour plots for the total performance show that the RAMEE behaves very similar to a system with constant sensible and latent effectiveness. This indicates that the variations in the sensible and latent performances of the RAMEE roughly cancel each other out (i.e., as one effectiveness increases, the other decreases). Therefore the total energy recovery of the RAMEE can be determined based on a constant sensible and latent effectiveness system (ε_{Sen} = 80%, ε_{Lat} = 61%). However this approach would inaccurately determine the sensible and latent performances of the RAMEE.

3.2.2 Heat and Moisture Transfer Driving Potentials

The previous sectioned showed that the RAMEE effectivenesses strongly depends on H*. The relationship between H* and the RAMEE performance can be understood by considering the driving potentials for heat and moisture transfer.

Classically, the heat (moisture) transfer driving potential is the temperature (humidity ratio) difference between the outdoor and indoor air (referred to as primary driving potential in this study). Therefore as the temperature (humidity ratio) difference between the indoor and outdoor air increases, the amount of heat (moisture) transferred between the air streams increases as well. An energy recovery system that operates only with a primary driving potential would have constant effectivenesses at different outdoor conditions and the amount of heat (moisture) transferred would be dependent on the temperature (humidity ratio) difference between the indoor and outdoor air streams and independent of the humidity ratio (temperature) difference. Heat wheels, run-around coil, and flat plate exchangers are examples of air-to-air energy recovery systems that operate only with a primary driving potential.

However, Figure 3.3-Figure 3.5 show that the heat and moisture transfer in the RAMEE at different operating conditions is more complex than an energy recovery system that is only governed by a primary driving potential. Therefore, a secondary driving potential is required to fully describe the RAMEE performance at different outdoor air conditions. In the RAMEE, the secondary driving potential for heat (moisture) transfer is the humidity ratio (temperature) difference between the indoor and outdoor air. Thus, heat (moisture) transfer in the RAMEE is primarily driven by the difference in temperature (humidity ratio) between the indoor and outdoor air and to a lesser, secondary, extent by the humidity ratio (temperature) difference. Appendix A

elaborates on how the humidity ratio (temperature) difference between the indoor and outdoor air affects the heat (moisture) transfer in the RAMEE.

The interplay between the primary and secondary driving potentials depends on their magnitudes compared to each other, which can be described by H*. When H* is close to zero, the heat transfer primary driving potential (i.e., ΔT between the indoor and outdoor air) is very large compared to the secondary potential (i.e., ΔW between the indoor and outdoor air) and as a result the secondary driving potential has minimal influence. However, at H* values close to infinity (i.e., $\Delta H_{Lat} >> \Delta H_{Sen}$), the secondary driving potential becomes predominant, which can result in sensible effectiveness values that are greater than 100% or less than 0% (Figure 3.3A). An analogous description is applicable for the moisture transfer, except that the secondary driving potential is predominant at H* values close to zero (i.e., $\Delta H_{Lat} << \Delta H_{Sen}$), which leads to latent effectiveness values that are greater than 100% or less than 0% (Figure 3.4A).

The effects of the secondary driving potentials are also revealed by considering the amount of heat (moisture) transferred to the air stream. With regards to heat transfer (Figure 3.3B), at a constant outdoor temperature and therefore constant primary driving potential, the temperature change increases as H* increases. In other words, the secondary potential increases as H* increases, which slightly increases the temperature change in the air. A similar explanation can also be applied to the change in the air humidity ratio in Figure 3.4B.

The major features of the sensible and latent contour plots are explained by considering the primary and secondary driving potentials for heat and moisture transfer and how the outdoor air conditions influence them. Additional factors also influence the

contour plots (Figure 3.3, Figure 3.4) and they account for the minor features in the contour plots (e.g., curvatures of contour lines), which are briefly discussed in Chapter 4.

3.2.3 Optimal Cr* Contour Plots

The relationship between effectiveness and Cr* (see Figure 3.1) shows that the total effectiveness has a maximum value at a specific Cr*. see Figure 3.1 also shows that the value of this specific Cr* depends on the outdoor air conditions. This specific Cr* is referred to as the optimal Cr* because the maximum amount of energy is transferred between the air streams when the RAMEE is operating at this Cr*. Therefore in order for the RAMEE to maximize energy transfer when the outdoor air conditions are variable, the relationship between the optimal Cr* and the outdoor air conditions must be known.

The optimal Cr* contour plot in Figure 3.6 shows a complex relationship between the optimal Cr* values and the outdoor air conditions. The optimal Cr* ranges between 1 and infinity for the outdoor conditions considered. The majority of outdoor conditions have optimal Cr* values between 1.5 and 3.0. A discontinuity in the plot occurs at H* = -1, which corresponds to the line of constant enthalpy that passes through the indoor air conditions. This discontinuity has the optimal Cr* values approaching 1 or infinity depending on the side of the discontinuity. Hot and humid summer outdoor conditions typically have optimal Cr* values greater than 2.5 while cold and dry winter outdoor conditions have optimal Cr* values less than 2.0. Therefore if it is desired to control the RAMEE on a seasonal basis, the winter operating Cr* would be around 2.0 and the summer operating Cr* would be around 2.5. The exact values of the summer

and winter operating Cr* values would depend on the climate and would be different for each location.

The effects of the outdoor conditions on the RAMEE performance were discussed in Section 3.2.2. However, the effects on the optimal Cr* appear to be more complex and are not properly described by the previous discussion. A thorough discussion into the relationship between the optimal Cr* and the outdoor condition is beyond the scope of this study and is not done.

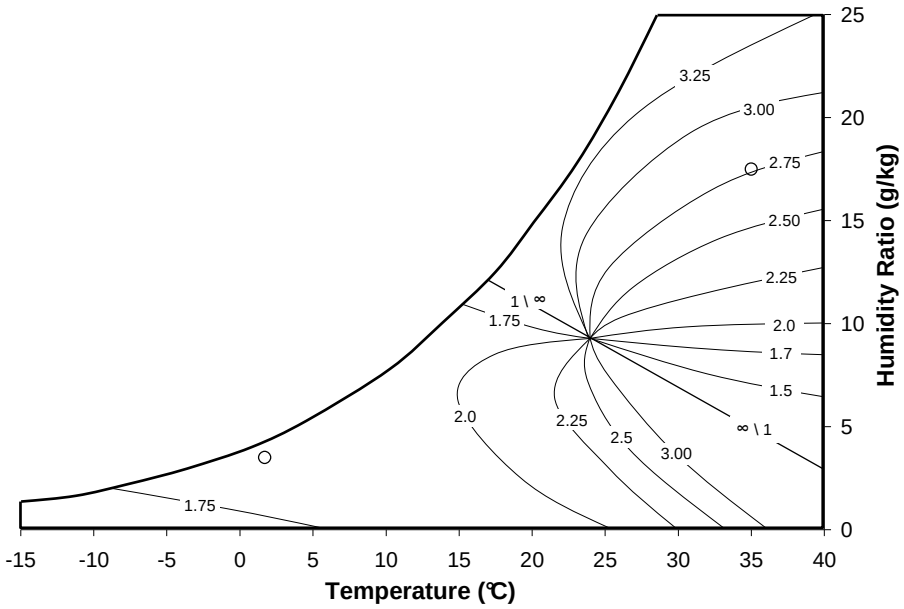

Figure 3.6: Optimal Cr* of the RAMEE system for different outdoor air conditions. Circles correspond to AHRI outdoor summer and winter conditions. NTU = 10 and NTUm = 2.7.

3.3 Peak Sensible and Latent Performances

The previous section (3.2) presented contour plots to describe the RAMEE when it is operating with its maximum total effectiveness. However, when the RAMEE is operating at its maximum total effectiveness, the sensible and latent effectiveness are not necessarily at their maximum values for that given outdoor air condition. Figure 3.7 shows the sensible, latent and total effectiveness plots for the RAMEE operating at

AHRI summer conditions. Under these conditions it can be seen that the sensible and latent effectiveness plots have similar trends as the total effectiveness plot. Both the sensible and latent effectivenesses have maximum values, but the peak values do not occur when the RAMEE is operating at the optimal Cr*.

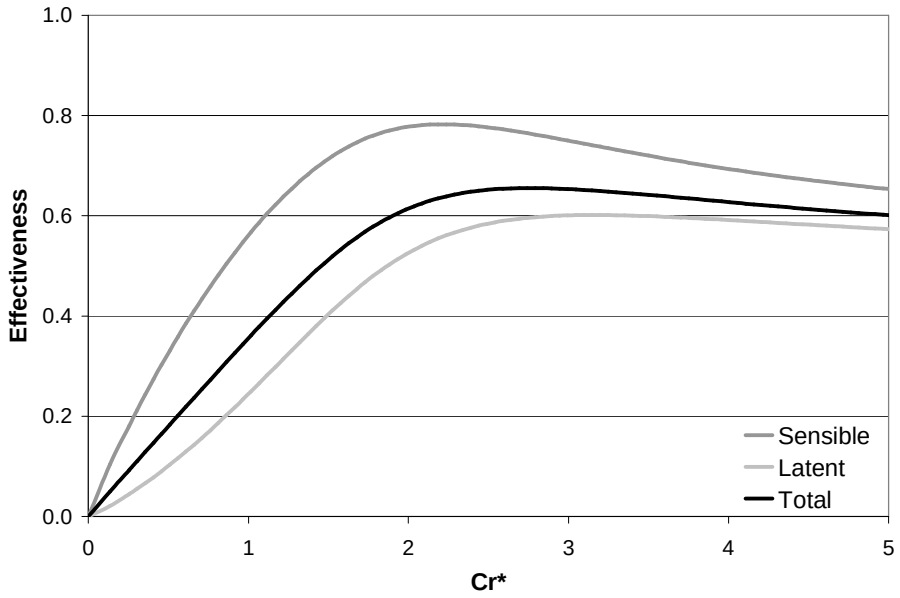

Figure 3.7: RAMEE system effectiveness values at AHRI summer test conditions.

This section presents contour plots for cases when the RAMEE is operating at the Cr* values that cause maximum sensible and maximum latent effectiveness values. The operating Cr* values are referred to as peak sensible Cr* or peak latent Cr* if it causes the RAMEE to operate at peak sensible effectiveness or peak latent effectiveness, respectively. These contour plots are able to further describe the performance of the RAMEE under different outdoor air conditions. The plots can be used to contrast the differences in performance between when the system is operating at either peak sensible or latent effectiveness conditions compared to peak total effectiveness conditions. Also, the contour plots for peak sensible Cr* and peak latent Cr* are presented.

The plots and only a brief description are presented because the underlying explanation to their trends is outlined in Section 3.2.2. Understanding the peak sensible and peak latent performances and how to achieve them is beneficial because in some conditions and/or control strategies it is desirable to maximize either the heat transfer (e.g., cold winter operations) or moisture transfer (e.g., humid hot summer conditions).

3.3.1 Peak Sensible Performance

The peak sensible effectiveness contour plots for the RAMEE when it is operating at the peak sensible Cr* are shown in Figure 3.8. The sensible effectiveness has a minimum value of 64% and goes to infinity as the outdoor temperature approaches the indoor temperature of 24°C. The minimum sensible effectiveness occurs at outdoor conditions near an H* of -1. Several outdoor air conditions produce effectiveness values that are greater than 100%. The supply air temperature change contour plot (Figure 3.8B) compares the temperature change when the system is operating at peak sensible effectiveness (solid line) and peak total effectiveness (dashed line). This comparison shows similar temperature changes at positive H* (+H*) conditions (hot and humid or cold and dry) with the change being slightly greater for peak sensible operations. However, at negative H* (–H*) conditions the performance is significantly different. These results indicate that the sensible effectiveness is near its maximum when the RAMEE is operating at optimal Cr* for +H* conditions, while at –H* conditions the sensible effectiveness achieved at the optimal Cr* is much lower than its maximum value.

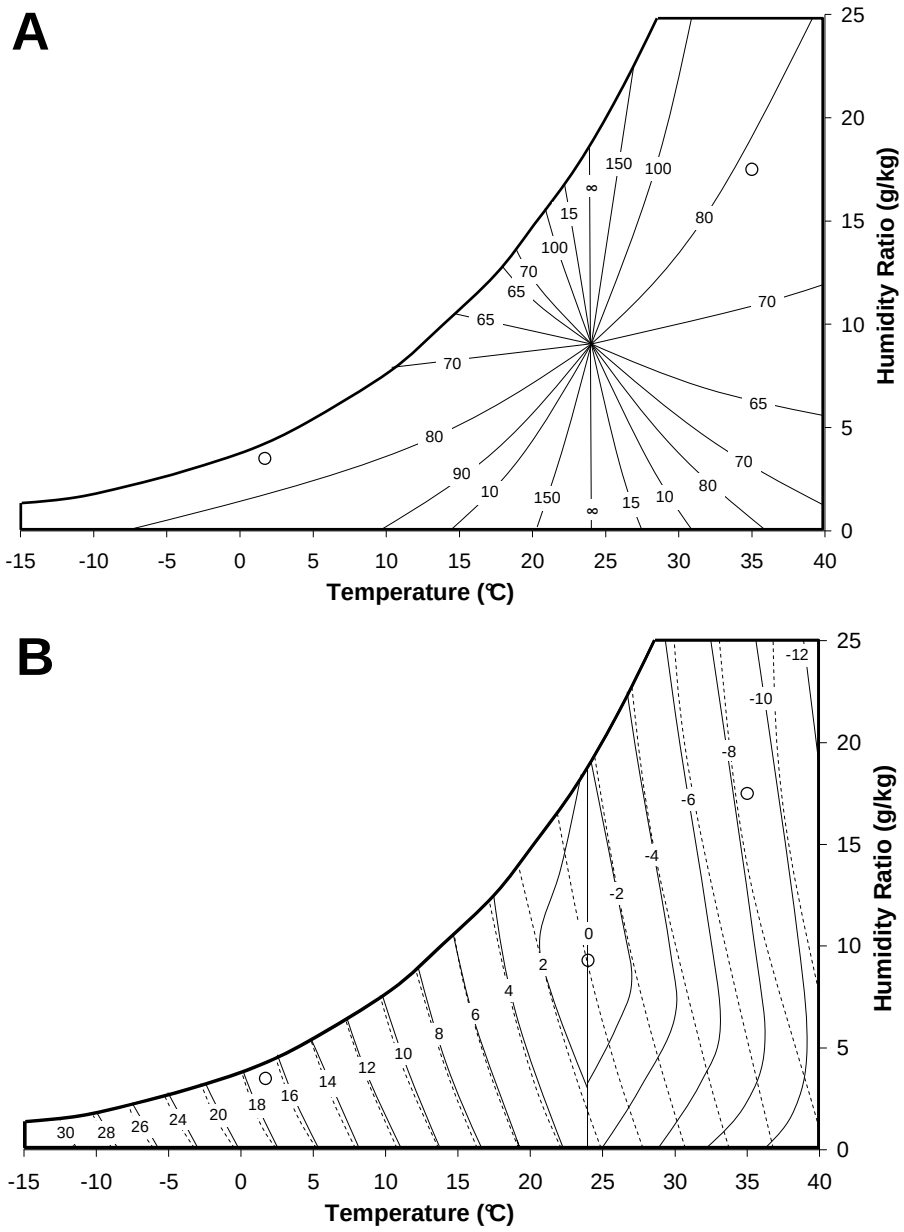

Figure 3.8: Peak sensible performance of the RAMEE for different outdoor air conditions. A) Sensible effectiveness (%). B) Supply air temperature change (°C). Dashed lines represent the temperature change corresponding to peak total effectiveness conditions (Figure 3.3).

The contour plot of the peak sensible Cr* (operating Cr* that results in peak sensible performance) is presented in Figure 3.9. The peak sensible Cr* contour plot shows similar trends as the optimal Cr* contour plot (Figure 3.6). The values are very similar at +H* conditions, but significantly different at –H* conditions. This comparison agrees with the observation that the RAMEE is near its peak sensible

performance when it is operating at its optimal Cr* at +H* conditions. Conversely at -H* conditions, the peak sensible Cr* and optimal Cr* are significantly different, which also agrees with the differences in the sensible performances.

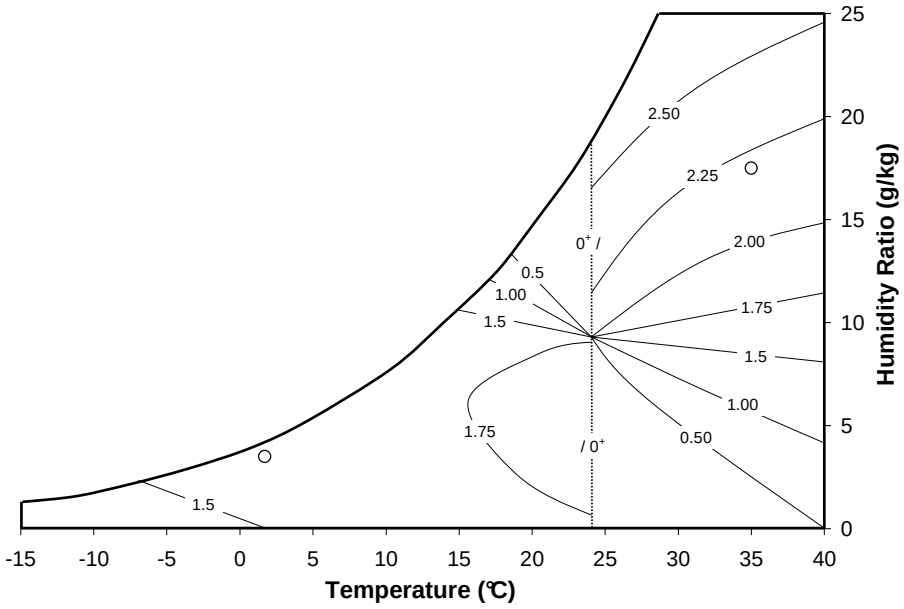

Figure 3.9: Peak sensible Cr* in the RAMEE system for different outdoor air conditions.

3.3.2 Peak Latent Performance

The peak latent performance contour plots are shown in Figure 3.10. These results correspond to when the RAMEE is operating at peak latent Cr*. The minimum latent effectiveness occurs at H* conditions near -1 where it decreases to 43%. The effectiveness values approach infinity as the outdoor humidity ratio nears the indoor humidity ratio (9.3 g/kg). The changes in the supply air humidity ratio that occur when the system is operating at either maximum latent effectiveness or maximum total effectiveness (Figure 3.10B) are very similar at +H* and large –H* conditions, but very different at small –H* conditions. At small –H* conditions, the humidity ratio change is significantly higher when the RAMEE is operating at peak latent effectiveness conditions compared to when it is operating at peak total effectiveness.

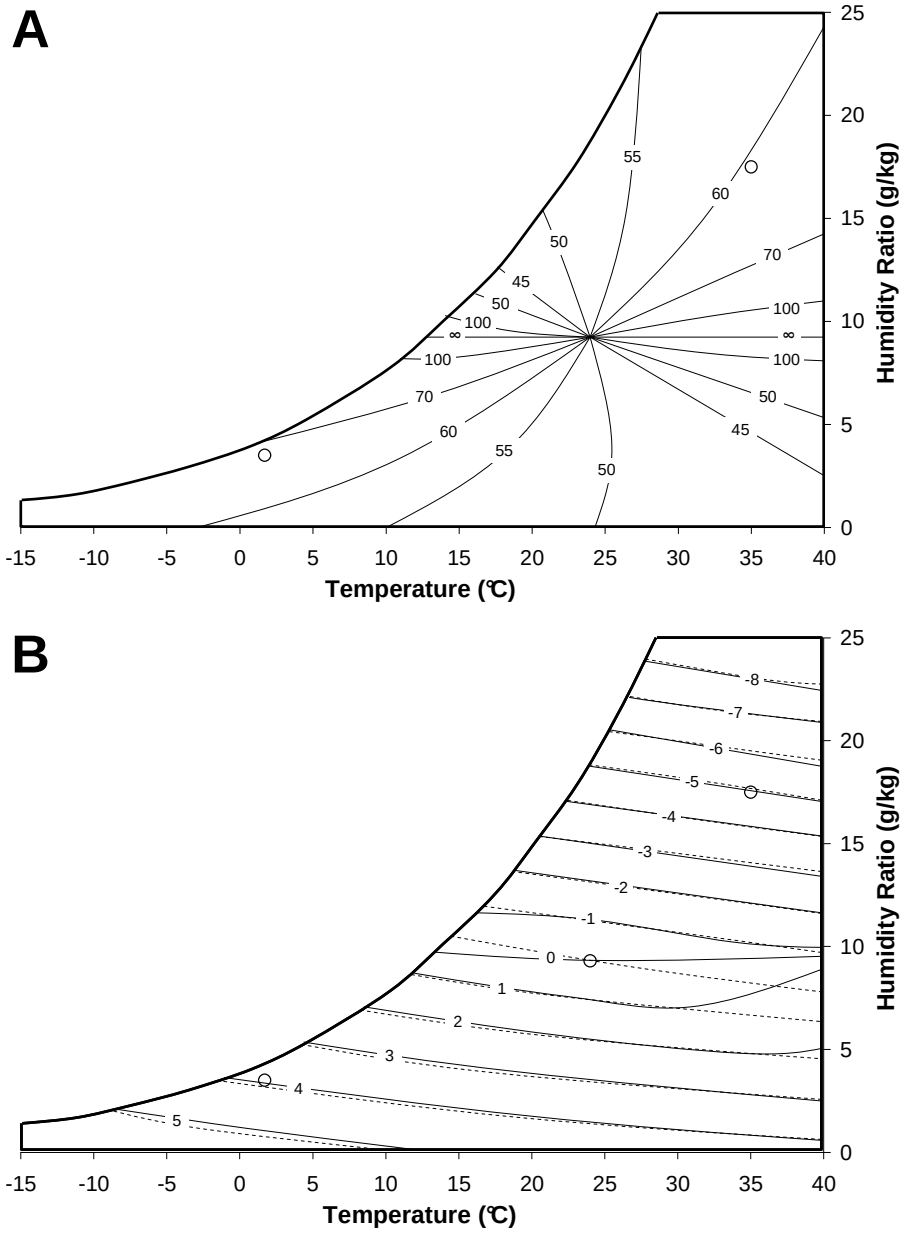

Figure 3.10: Peak latent performance of the RAMEE for different outdoor air conditions. A) Sensible effectiveness (%). B) Supply air humidity ratio change (g/kg). Dashed lines represent the humidity ratio change corresponding to peak total effectiveness conditions (Figure 3.3).

The peak latent Cr* contour plot shown in Figure 3.11 shows the relationship between the outdoor air conditions and the operating Cr* value that results in the maximum latent performance in the RAMEE. The peak latent Cr* contour plot is very similar to the optimal Cr* plot (Figure 3.6) and is only significantly different when H* is

between 0 and -1. This corroborates why in Figure 3.10B the only discrepancy in the change in humidity ratio when the RAMEE is operating at either peak latent or peak total (optimal) performances occurs at low –H* conditions.

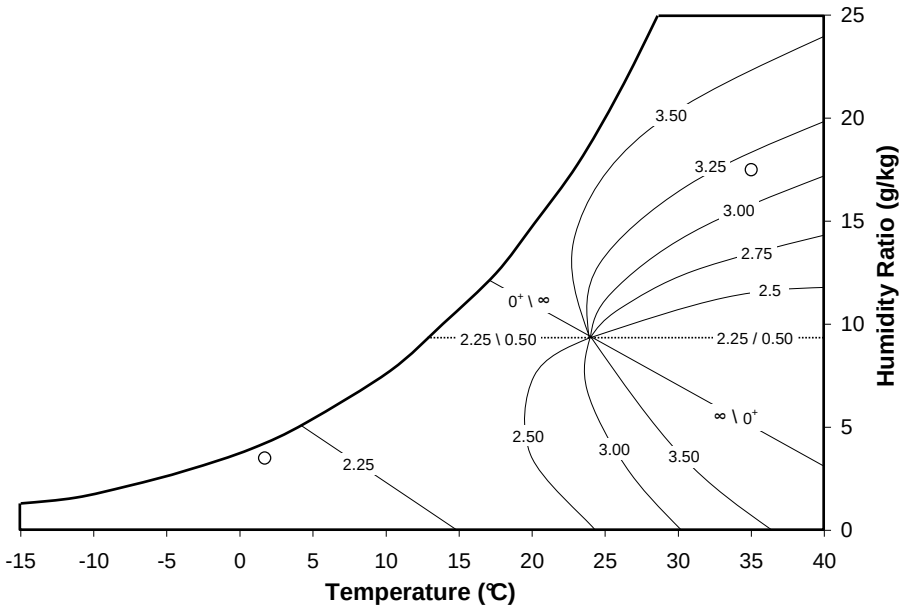

Figure 3.11: Peak latent Cr* in the RAMEE system for different outdoor air conditions.

3.3.3 Peak Sensible and Latent Performance Comparison

The evaluation and comparison of the peak sensible, latent, and total performances for different outdoor air conditions, and the operating Cr* values that they occur at, reveal some interesting characteristics of the RAMEE.

At +H* conditions (outdoor air is hot and humid or cold and dry), the operating Cr* values that cause the peaks in sensible and latent effectivenesses are very similar to each other for a given outdoor condition. At a given +H* condition, if the operating Cr* value is increased from zero, the peak sensible occurs first, followed by the peak total, and then the peak latent. The difference between the Cr* values that cause the peak sensible and latent effectivenesses is less than 1 for +H* conditions. For +H*

conditions, the optimal Cr* value is closer to the peak sensible Cr* at low H* conditions, while the optimal Cr* value is closer to the peak latent Cr* at higher H* conditions. As a result of the small range in the peak Cr* values and the effectiveness-Cr* plots being similar, the performances (sensible, latent, and total) of the RAMEE at each of these peaks are very similar.

At –H* conditions (outdoor air is hot and dry or cool and humid), the peak Cr* values differ significantly from each other for a given condition. The order of the peak Cr* values is not as consistent and depends on the -H* condition, with either the sensible peak Cr* or the latent peak Cr* occurring at the lower Cr* values. Also, the difference between the operating Cr* that causes peak sensible and latent effectivenesses is much larger at –H* conditions and can be greater than 3 for some H* conditions. Therefore, at –H* conditions when the RAMEE is operating at one of the peak Cr* values (sensible, latent, or optimal), its effectiveness (sensible, latent, and total) is very different from when it is operating at another one of its peak Cr* values.

3.4 Negative H* Conditions

The analysis of the peak sensible, latent, and total performances of the RAMEE in the previous sections reveals some interesting characteristics of how the system operates under different outdoor air conditions. The analysis shows that the operating Cr* values that cause the peak sensible, latent, and total effectivenesses are very similar at +H* conditions, but are very different at –H* conditions. Therefore, the behaviour of the RAMEE during –H* conditions is considered in more detail in this section. This investigation consists of describing the relationship between Cr* and effectiveness at different –H* conditions and discussing the practical implications of –H* operating

conditions. Also, a comparison between numerical and experimental results for the RAMEE operating at –H* conditions is made to validate the model and support these observations.

3.4.1 Cr* versus Effectiveness

A typical Cr* versus effectiveness relationship of the RAMEE under +H* conditions was previously shown in Figure 3.7 (in this case, AHRI summer conditions where H* = +1.9), which showed the sensible, latent, and total effectiveness plots. These three plots are very comparable to each other and show the same key features in that they all exhibit peak effectiveness values, which occur at similar operating Cr* values, and their effectiveness values approach zero as Cr* approaches to zero.

However at –H* conditions, the RAMEE displays a very different Cr*-effectiveness relationship as shown in Figure 3.12 where the effectiveness is a function of Cr* is presented for three different –H* conditions. The effectiveness values still demonstrate a peak, but this peak can be a maximum or minimum depending on the value of H*. Some of these minimum values even have negative effectiveness values. Also, the operating Cr*s that cause each peak sensible, latent, or total effectivenesses are very different from each other for the same H* condition.

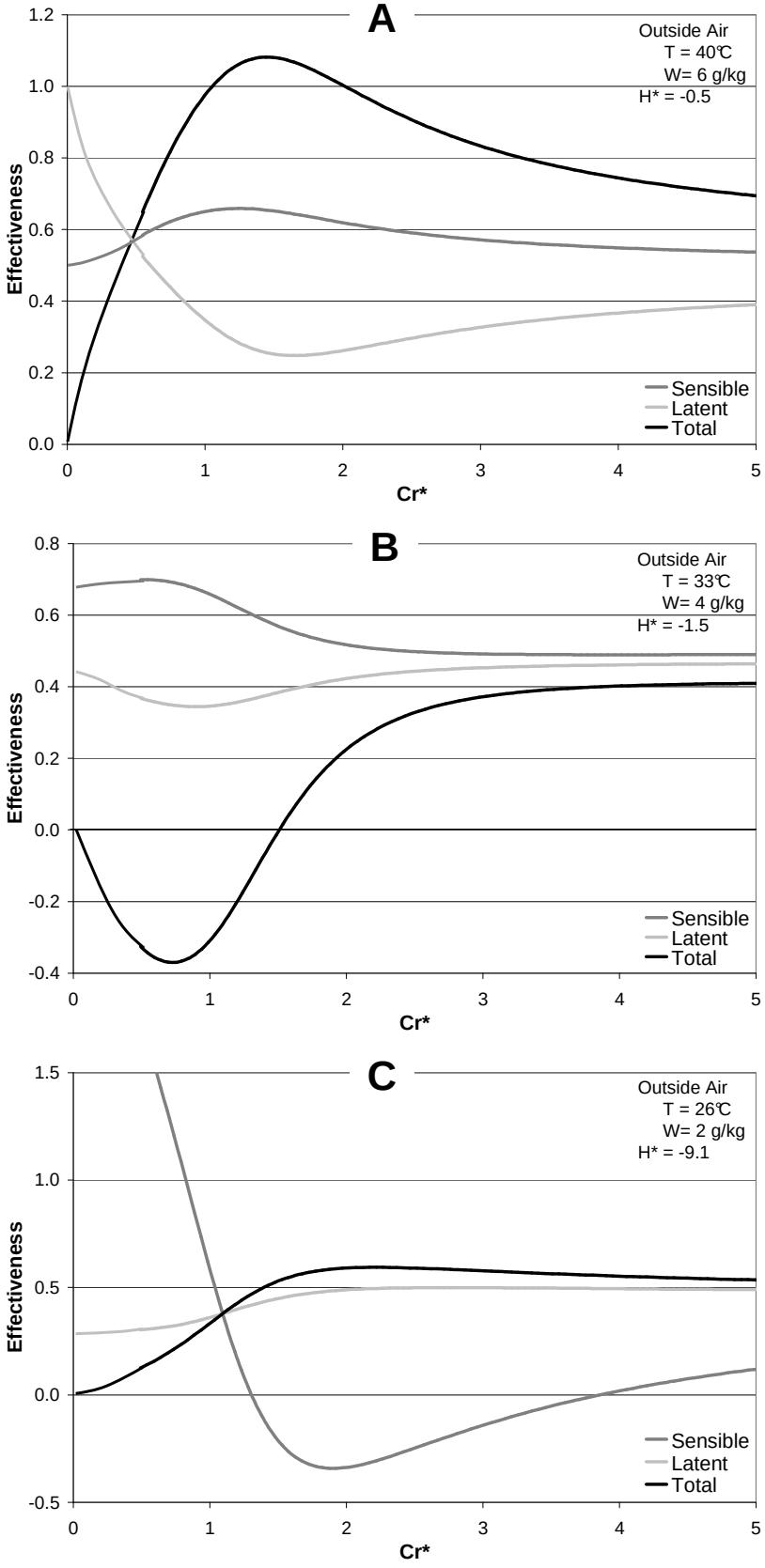

Figure 3.12: Effectiveness of the RAMEE as a function of Cr* at different –H* conditions.

The plots also display interesting trends at low operating Cr*. As the Cr* decreases to zero, the total effectiveness approaches zero (just like in +H* regions), but the latent and sensible effectiveness approach non-zero values, which in some conditions may be very large. The effectiveness plots at near-zero operating Cr* display a trend from small to large –H* conditions (Figure 3.12). This trend has the near-zero Cr* latent effectiveness decreasing and the near-zero Cr* sensible effectiveness increasing as |H*| increases.

The performance characteristics of the RAMEE when it is operating at –H* conditions as shown in Figure 3.12 are also present to some extent at high and low +H* conditions (i.e., +H*<0.7 or +H*>6). Figure 3.13 shows the effectiveness plots of the RAMEE operating at a low and high +H* conditions. The trend of effectiveness with Cr* for these high and low +H* conditions are similar to the trends of effectiveness with Cr* for moderate +H* conditions when the Cr* values are greater than 1.5 (see Figure 3.7), but the trends are significantly different at low operating Cr*. For low +H* conditions (Figure 3.13A) with the RAMEE operating at a near-zero Cr* value, the latent effectiveness has a large negative value, while the sensible effectiveness maintains an intermediate positive effectiveness. A similar trend occurs at high +H* conditions (Figure 3.13B), except it is the sensible effectiveness rather than the latent effectiveness that has a large negative value as Cr* goes to zero. The absolute effectiveness values at near-zero Cr* values for high and low +H* conditions are less than the values for the -H* conditions. Also, the magnitude of the near-zero Cr* effectiveness values at high and low +H* conditions decrease as the +H* becomes more moderate. As the +H* condition becomes more moderate the effectiveness plots transition into the plots like

the one shown in Figure 3.7, which has sensible and latent effectiveness values of zero as Cr* approaches zero.

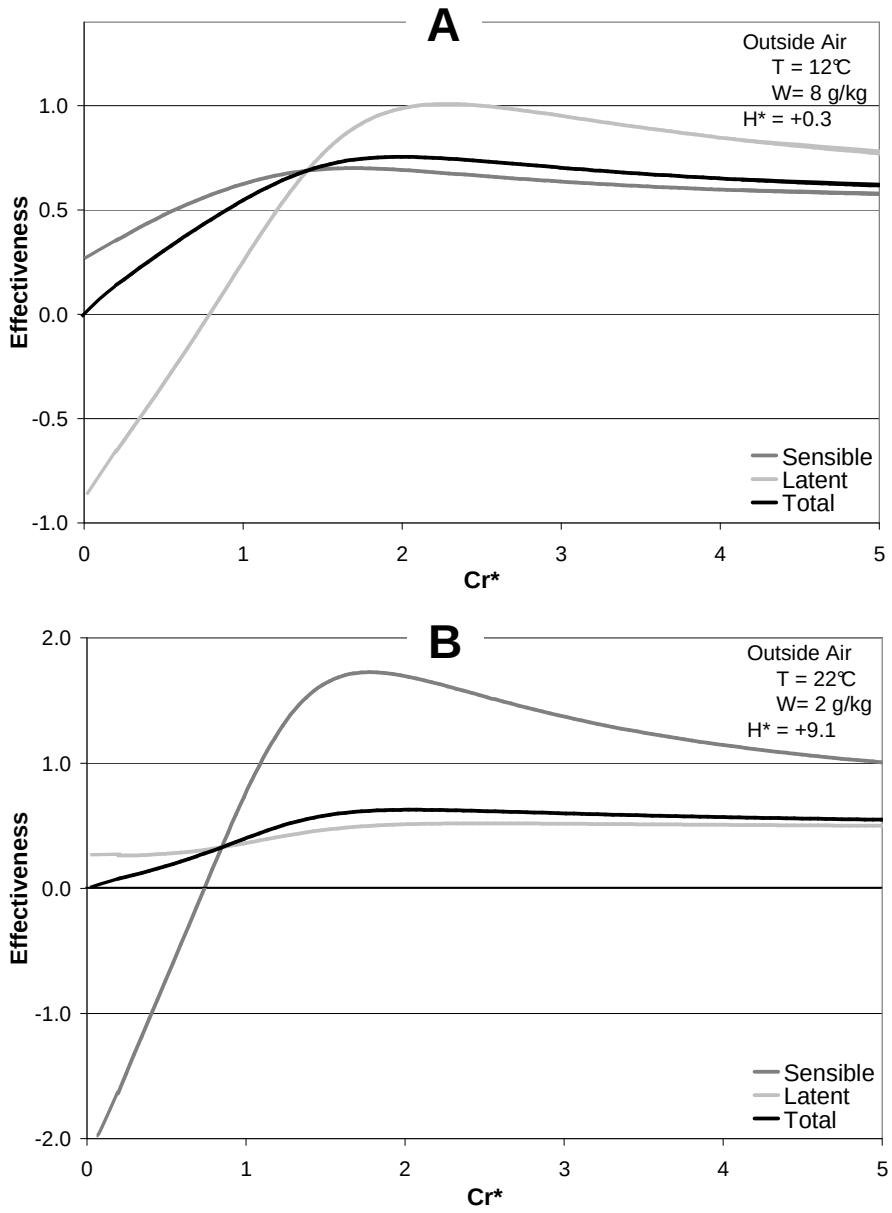

Figure 3.13: Effectiveness of the RAMEE as a function of Cr* at high and low +H* conditions.

Another interesting characteristics of the RAMEE at –H* conditions (and some high and low +H* conditions) are the negative effectivenesses that occur at some Cr* values (Figure 3.12 and Figure 3.13). The negative effectiveness values are significant because heat and/or moisture are being transferred in the direction that is opposite to the

primary driving potential established by the outdoor and indoor air streams. This is possible because the secondary driving potentials are larger and in the opposite direction of the primary potentials. These negative effectiveness values can be advantageous in certain situations where it is beneficial for the supply air to be conditioned away from the exhaust air (i.e., the temperature difference between the supply and indoor air is greater than the difference between the indoor and outdoor air)..

3.4.2 Experimental Validation of Performance at –H* Conditions

The performance of the RAMEE at –H* conditions is very different from the standard test conditions (i.e., H* = 1.9) results reported by Fan et al. (2006) and Vali (2009). Therefore experimental results are used to validate the numerical results for -H* conditions.

Experimental results were produced on Prototype #4, which was constructed and tested by Beriault (2010). The prototype used a combination cross-counter flow configuration. The key dimensions of the exchangers and the membrane properties are contained in Table 3.1. These exchanger properties are different than the ones presented in Chapter 2 and were applied to the model simulations in this section. The prototype was tested at a range of Cr* values (0.5 to 5) at a constant NTU and NTUm of 17 and 4.5, respectively. The inlet and outlet air conditions during the test were at 25.7±0.7°C, 6.3±0.5 g/kg and 16.5±0.8°C, 8.8±0.5 g/kg, respectively, which results in an H* value of -0.68±0.05. A full description of the RAMEE prototype #4, experimental set-up, and testing procedure is contained in the thesis of Beriault (2010).

Table 3.1: RAMEE Prototype #4 specifications

Property	Value
Panel Dimensions	
Length	1 220 mm
Width	305 mm
Entrance Length	64 mm
Channel Thicknesses	
Air	5.4 mm
Solution	2.6 mm
Membrane Properties	
Thickness	0.5 mm
Thermal Conductivity	0.334 W/(m·K)
Water Vapour Permeability	3.4×10^{-6} kg/(m·s)

The experimental results consist of 9 measurements taken at constant NTU, NTUm, and H*, but different Cr* values. The experimental sensible, latent, and total effectiveness values are presented as a function of Cr* in Figure 3.14, which also contains the results from the numerical simulation of the prototype. The experimental results show a high degree of scatter at some points, but some general trends are present. The scatter can be attributed to flow maldistribution in the channels and heat gains and losses between the system and the environment. Also, the experimental uncertainty due to temperature and humidity measurements is more significant because the differences between the humidity ratios and enthalpies of the two air streams are small (<3 g/kg and <3 kJ/kg).

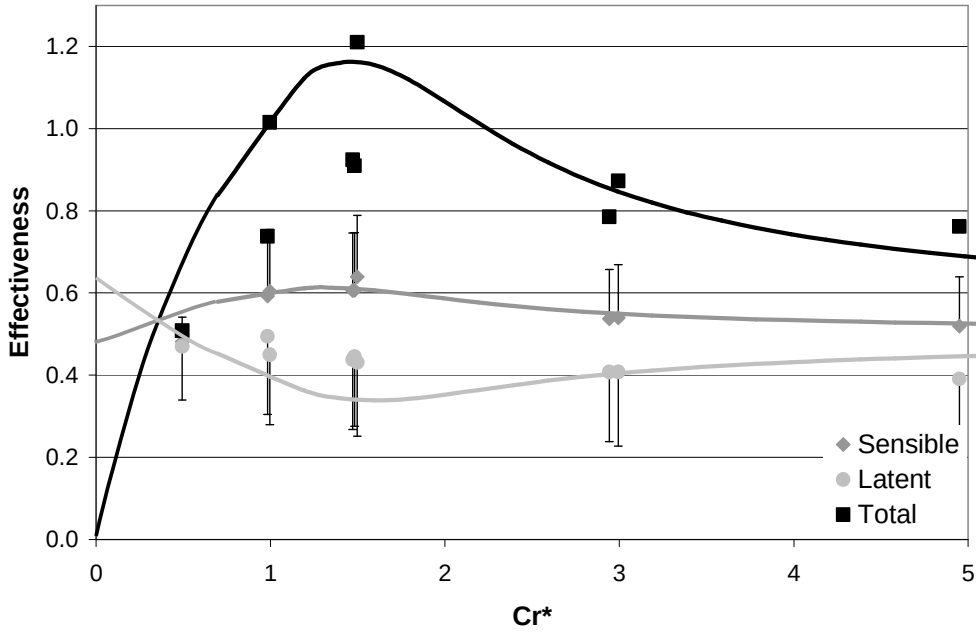

Figure 3.14: Comparison between experimental (Beriault 2010) and numerical results for Prototype #4 operating at NTU=17, NTUm=4.5, and H*=-0.68. Experimental and numerical results are represented by symbols and lines respectively. Error bars are only shown on one side, but apply to both.

Figure 3.14 shows reasonable agreement between the numerical and experimental results. Both results show that the total effectiveness increases as Cr* increases from zero and reaches a maximum value of over 100% at Cr* ≈1.5. As Cr* increases above Cr* ≈1.5, total effectiveness decreases. The experimental sensible effectiveness values are relatively constant and have a maximum value of around 60%, which agrees with the numerical results. The agreement between the experimental and numerical results for the latent effectiveness is not as good because the numerical data shows a local minimum at Cr* = 1.5, while the experimental data does not. Nevertheless, the differences between the experimental and numerical data for latent effectiveness are not large and within the bounds of the experimental uncertainty.

The comparison in Figure 3.14 shows that the general trends in the effectiveness plots predicted by the numerical model are present in the experimental results, which

provides reasonable validation of the numerical model. Therefore, the unique performance characteristics of the RAMEE at –H* conditions discussed in this section can confidently be used to investigate –H* conditions further.

3.4.3 Performance at Near-Zero Cr*

Investigations of the RAMEE performance at –H* conditions reveal some noteworthy characteristics at low operating Cr*. These characteristics have the sensible and latent effectivenesses approaching non-zero values as Cr* decreases to zero. Some of these effectiveness values are very large and often exceed 100% when the magnitude of -H* is high or low. These characteristics also extend to high and low +H* conditions ((i.e., +H*<0.7 or +H*>6)) except that either the sensible or latent effectivenesses has a very large negative value that often exceeds -100%. In all of these cases, the sensible effectiveness divided by the latent effectiveness at near-zero operating Cr* values is equal to the negative value of the H* condition. Therefore, at near-zero operating Cr*; $\varepsilon_{Sen} = \varepsilon_{Lat}$ when H* = -1, $\varepsilon_{Sen} > \varepsilon_{Lat}$ when H* < -1, and $\varepsilon_{Sen} < \varepsilon_{Lat}$ when H* > -1. Also, the total effectiveness decreases to zero as Cr* approaches zero. The explanation of these characteristics is considered in this section.

At near-zero Cr* values, the solution flow rate is very low. As a result, the desiccant temperature and concentration (and thus humidity ratio) undergoes a large change as it travels through the exchangers. For moderate +H* conditions (i.e., 1<H*<6), the heat and moisture both transfer in the same direction which results in the desiccant quickly coming into equilibrium with the air stream temperature and humidity ratio. Therefore, only a small amount of the transfer surface between the desiccant and air stream has any substantial temperature and humidity ratio difference across it, which

results in very little heat or moisture transfer between the air and the desiccant. For -H*conditions (and some +H* conditions), the heat and moisture transfers are in the opposite directions and these enhance each other.

The enhancement can be understood by considering the interactions between heat and moisture transfers with the desiccant. When moisture is transferred to the air, the latent energy is provided by the desiccant, which lowers the desiccant temperature and subsequently cools the air. When moisture is removed from the air, the latent energy is absorbed by the desiccant which increases the desiccant temperature and then warms the air. At near-zero Cr* values, the total energy transferred is very low since the latent and sensible energies are transferred in the opposite direction. This behaviour of non-zero latent and sensible effectivenesses at near-zero Cr* extends to high and low +H* conditions because the heat and moisture still transfer in the opposite directions at low Cr* even though the conditions of the indoor and outdoor air indicate they should transfer in the same direction. Heat and moisture are able to transfer in the opposite direction at low and high +H* conditions when the RAMEE is operating at low Cr* because the temperature-humidity ratio of the desiccant (see Section 2.2.2) allows the temperature or humidity ratio of the desiccant to extend beyond the region of conditions between the indoor and outdoor air conditions. As the +H* condition becomes less extreme (i.e., $1 < H^* < 6$), the temperature and humidity ratio of the desiccant are between the indoor and outdoor air conditions and this results in the heat and moisture transferring in the same direction.

The operation of the LAMEEs at near-zero Cr* can be viewed as either an evaporative cooler or condensing heater. One of the LAMEEs humidifies the air and the

latent energy used to evaporate the moisture indirectly cools the air, while the other LAMEE dehumidifies the air and indirectly uses the released latent energy to warm the air. When the RAMEE is operating in this fashion only moisture and no energy is transferred between exchangers.

The circulation of the solution (albeit at a very low rate) between the exchangers is also essential for the non-zero sensible and latent effectivenesses at near-zero Cr*. The transit of the desiccant through the exchanger is required for the temperature and humidity ratio differences between the desiccant and air streams to exist in the exchanger. The circulation of the desiccant between the exchangers couples them together and keeps the desiccant temperature and humidity ratio in equilibrium with the indoor and outdoor air conditions. However, if the solution stops circulating (i.e., Cr* = 0), the two exchangers become decoupled and the temperature and humidity ratio of the desiccant in each exchanger will change over time and eventually come into equilibrium with the condition of their respective air stream. As this is happening, the heat and moisture transfer rates would decay and eventually reach zero once the desiccant in each exchanger reaches equilibrium with their respective air stream.

3.4.4 Selective Heat or Moisture Transfer

The unique performance of the RAMEE at –H* and high and low +H* conditions allows heat or moisture to be selectively transferred to some extent. At these conditions, the difference between the indoor and outdoor temperature (high H* conditions) or humidity ratio (low H* conditions) is small. The selective transfer is possible when the difference between the sensible and latent effectiveness values at a given Cr* is large. A larger sensible effectiveness allows heat to be preferentially

transferred while a larger latent effectiveness preferentially transfers moisture. These large differences in effectiveness values are most prevalent at high or low ±H* conditions (Figure 3.12A,C, & Figure 3.13) and are minimal at moderate ±H* conditions (Figure 3.7 & Figure 3.12B).

The effectiveness plots for the RAMEE at high and low H* conditions are shown in Figure 3.15 for –H* conditions and Figure 3.16 for +H* conditions. The plots demonstrate two regions of operating Cr* where the differences between the sensible and latent effectiveness values are greatest, which are denoted as Regions I & II in Figure 3.15 and Figure 3.16. In Region I the latent effectiveness is greater than the sensible effectiveness and in Region II the sensible effectiveness is greater than the latent effectiveness. Therefore, if it is beneficial for the building HVAC system to preferentially transfer moisture instead of heat, the RAMEE should be operated with a Cr* that resides in Region I. Conversely, if heat transfer is preferred instead of moisture transfer, then the RAMEE should be operated with a Cr* in Region II. Figure 3.15 and Figure 3.16 also reveal that the values of the operating Cr* for each region depend on H*. The operating Cr* values in the regions are either near-zero or close to the optimal Cr* (Cr* = ~1-3). For low –H* and high +H* conditions, Region I is near a Cr* of zero, while Region II is near the optimal Cr*. For high –H* and low +H*, Region I is near the optimal Cr* and Region II is near a Cr* of zero.

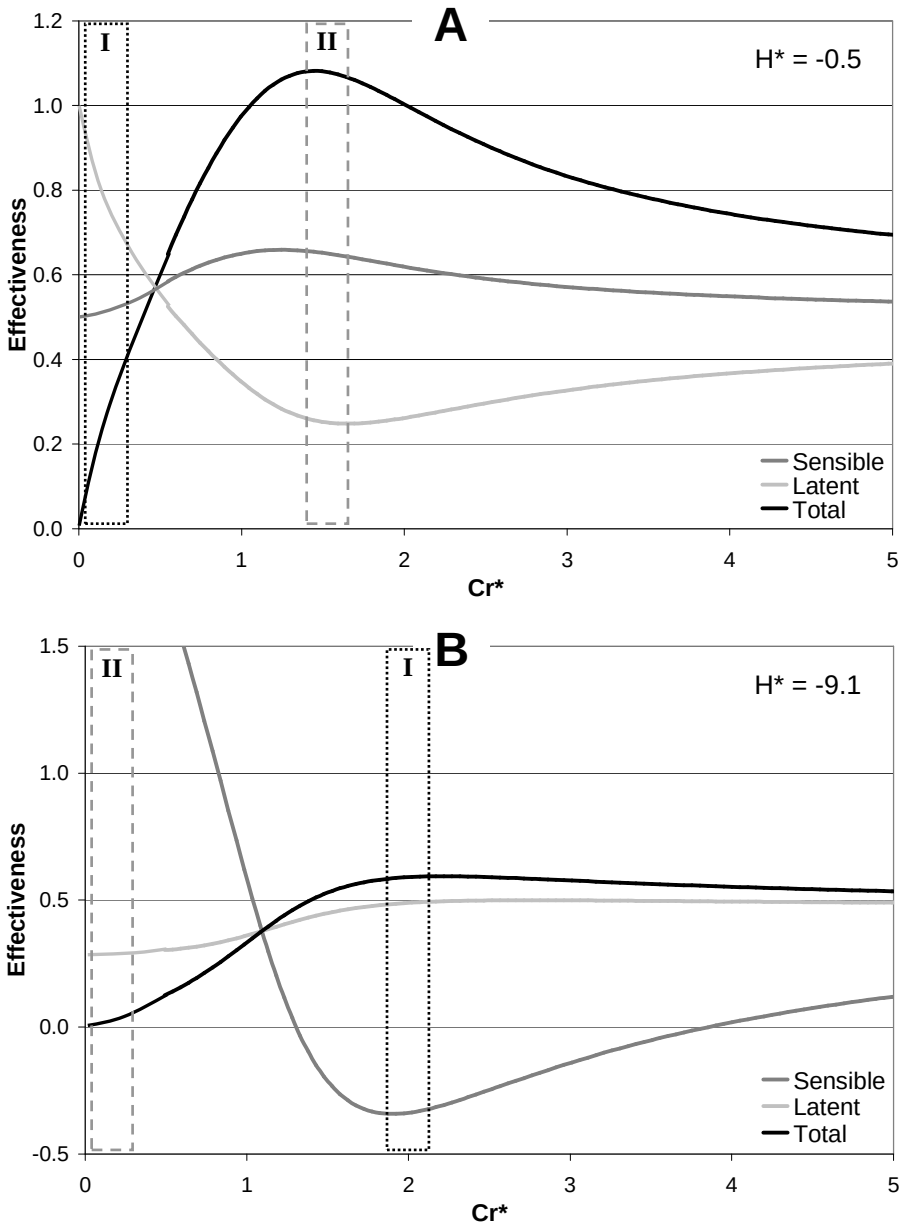

Figure 3.15: RAMEE effectiveness as a function of Cr* at different -H* conditions. Boxed regions denote greatest positive effectiveness differences between: I) latent and sensible, and II) sensible and latent.

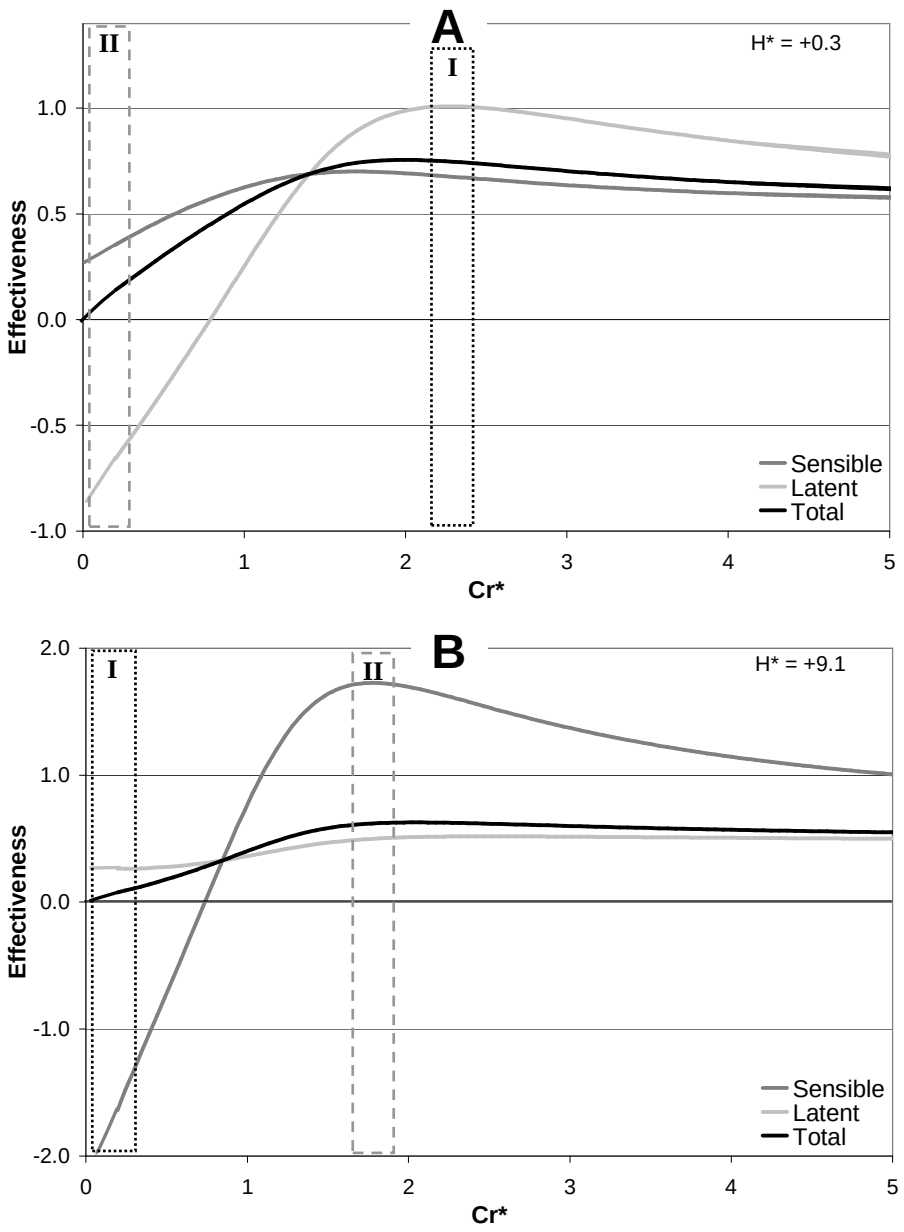

Figure 3.16: RAMEE effectiveness as a function of Cr* at different +H* conditions. Boxed regions denote greatest positive effectiveness differences between: I) latent and sensible, and II) sensible and latent.

Applications for Selective Heat and Moisture Transfer

Selectively transferring heat or moisture would provide practical benefits in building HVAC systems as well as in numerous industrial applications where specific air conditions are required. The benefits to building ventilation can be understood by considering a typical HVAC system and the energy required to condition the ventilation

air. Figure 3.17 shows a typical dedicated outdoor air HVAC system with a RAMEE and an auxiliary heating/cooling unit. The conditions of the air streams as they travel through the HVAC system are indicated by numbers. The outdoor air (state 1) is pre-conditioned by the supply LAMEE (state 2) and then fully conditioned by the heating/cooling unit (state 3) after which the air is supplied to the building space. The exhaust stream consists of the indoor air (state 4) that passes through the exhaust LAMEE (state 5) and then exhausted from the building. The condition of the supply air (state 3) entering the space depends on whether the space is cooled by the air or a separate cooling system. In the following discussion, the supply air is assumed to cool the space and therefore the desired supply air conditions are 13°C and 7 g/kg.

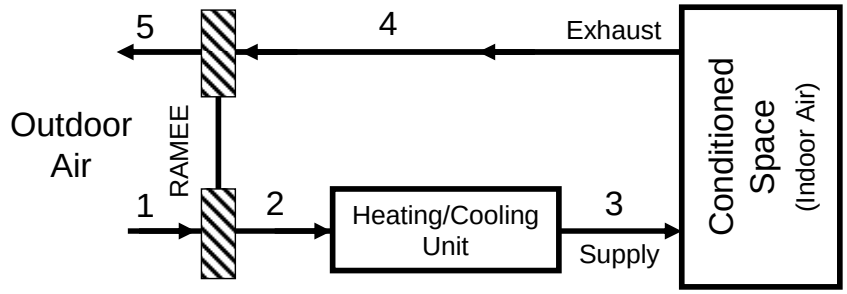

Figure 3.17: Schematic of a typical HVAC system equipped with a RAMEE.

The amount of energy used to fully condition the air to the desired supply conditions is determined by the difference between the conditions of the air at the supply LAMEE outlet (state 2) and the desired supply air (state 3). The RAMEE decreases the amount of conditioning energy required by pre-conditioning the supply air. The conditioning energy is minimized when the condition of the air leaving the supply LAMEE is as close to the condition of the desired supply air as opposed to the condition of the exhaust air, which the RAMEE is interacting with. Since the RAMEE is interacting with the exhaust air and not the desired supply air, at some outdoor air conditions the difference between the conditions of the air leaving in the supply LAMEE

and the desired supply air increases, which would increase the energy used to fully condition the air. Therefore at some outdoor air conditions, controlling the RAMEE would minimize the conditioning energy.

The ability of controlling the RAMEE to condition the air towards the desired supply air condition depends on the outdoor condition and how the RAMEE performs at that condition. The outdoor conditions can be arranged into different zones based on how the RAMEE should be controlled (Figure 3.18). The divisions between the zones shown here are generalizations and would be different for some HVAC applications and control strategies. A more concise analysis of how an energy recovery system can be controlled in different outdoor conditions is presented by Rasouli (2010b). The description of each zone and how the RAMEE would operate in each zone are given below.

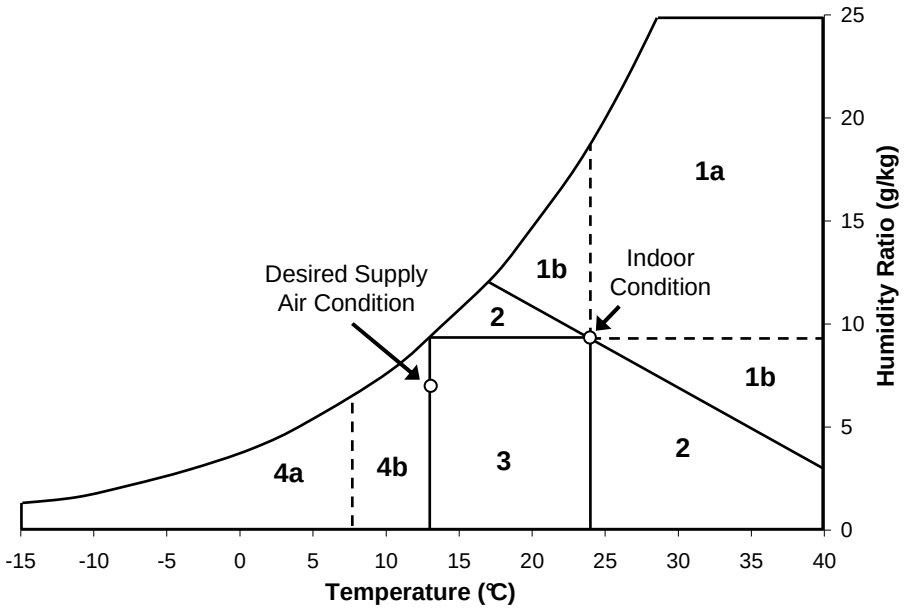

Figure 3.18: Outdoor air conditions control zones.

Zone 1: This zone contains outdoor air conditions that have a higher enthalpy than the indoor air. The zone is subdivided into 1a (+H* conditions) and

1b (–H* conditions). In Zone 1, the RAMEE would operate at its optimal Cr*, which allows for maximum energy transfer. In Zone 1a, operating the RAMEE at optimal Cr* also selectively transfers heat or moisture depending on the outdoor air conditions.

Zone 2: This zone encompasses –H* outdoor air conditions that have a lower enthalpy than the indoor air conditions. Operating the RAMEE at near-zero Cr* selectively transfers heat and moisture and allows the supply LAMEE to condition the air towards the desired supply air condition. If the RAMEE was transferring maximum total energy, the conditions of the air at the supply LAMEE outlet become more different from the desired supply air conditions, thus requiring more energy to fully condition the air.

Zone 3: The outdoor air conditions in this zone are +H* and have a temperature that is lower than the indoor air, but greater than the desired supply air (i.e., 13°C). Normally during these conditions an economizer would be used which increases the ventilation rate of outdoor air allowing supply air with a temperature that is warmer than 13°C to cool the space. However, the RAMEE could operate at near-zero Cr* and utilize its selective heat or moisture transfer capabilities and condition the air towards the desired supply air condition without over conditioning it.

Zone 4: This zone contains +H* conditions where the outdoor temperature is lower than 13°C and the outdoor humidity ratio is lower than the indoor air (i.e., 9.3 g/kg). The RAMEE would operated at its optimal Cr* for

maximum total energy transfer. In order to not over-condition the air at some of the warmer conditions (Zone 4b), the RAMEE could be partially bypassed and operated at part load or be operated by controlling Cr* and selectively transfer heat or moisture.

The selective transfer of heat and moisture is required in some of the zones (1b, 2, 3, & 4b) in order to maximize energy savings. Examples of outdoor air conditions from these zones are presented to illustrate how the RAMEE could condition the air in these zones (Figure 3.19, Table 3.2). In each of these cases, the RAMEE is operated at the Cr* that conditions the supply air as close as possible to the desired supply condition.

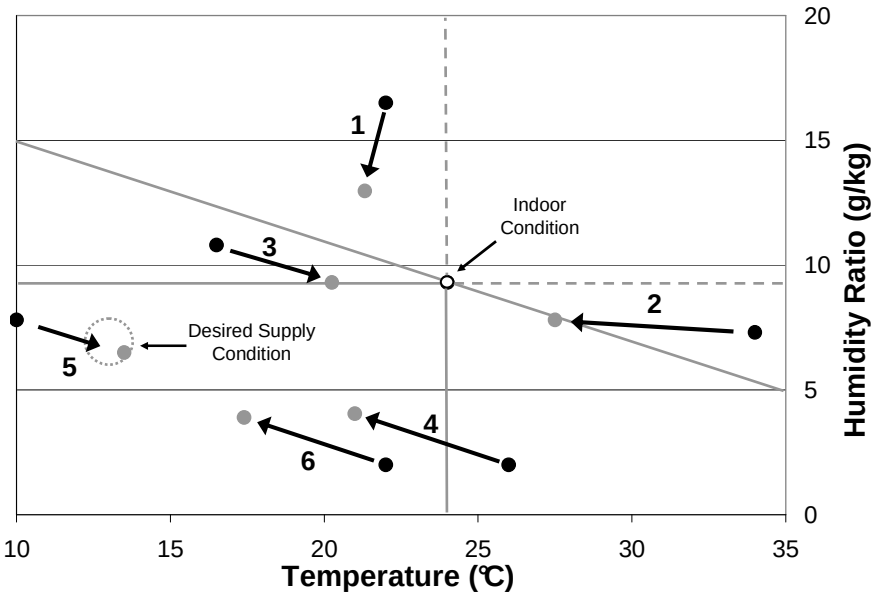

Figure 3.19: Psychometric chart showing cases where selective heat and moisture transfer in the supply exchanger conditions the outdoor air towards the desired supply condition. Black and grey dots denote supply LAMEE inlet and outlet respectively. Grey lines divide conditions into described zones.

Table 3.2: RAMEE operation for select outdoor air conditions.

Case	Outdoor Condition			H*	Region	Cr* Value	Effectiveness (%)		Supply LAMEE Outlet Condition	
	Zone	T (℃)	W (g/kg)				Sensible	Latent	T (℃)	W (g/kg)
1	1b	22.0	16.5	-9.0	I	2.0	-34	49	21.3	13.0
2	1b	34.0	7.3	-0.5	II	1.5	65	25	27.5	7.8
3	2	16.5	10.8	-0.5	I	0^+	50	100	20.3	9.3
4	2	26.0	2.0	-9.1	II	0^+	250	28	21.0	4.0
5	4b	10.0	7.8	0.3	I	0^+	25	-87	13.5	6.5
6	3	22.0	2.0	9.1	II	0^+	-230	26	17.4	3.9
Indoor		24.0	9.3							

Figure 3.19 shows some interesting features of the RAMEE performance at these extreme H* conditions. Some of the cases demonstrate the RAMEE's ability to cool the supply air below the indoor temperature (Cases 1, 4, & 6) or dehumidify the supply air below the indoor humidity ratio (Case 5). Also, at most conditions (Cases 3, 4, 5, & 6), no energy is transferred between the supply and exhaust air (i.e., $\varepsilon_{Tot} \approx 0$) and the LAMEEs operate as either evaporative coolers or condensing heaters.

These cases demonstrate the benefits of selective transfer at high and low ±H* conditions. In all of the cases, with the exception of Case 3, the supply LAMEE conditions the air towards the desired supply condition, which decreases the amount of energy required to fully condition the supply air. Case 3 is an exception in this discussion because the supply LAMEE does not condition the air towards the desired supply condition, but it does decrease the humidity ratio of the air and it would be beneficial if the humidity ratio is lowered to an acceptable level. If the humidity ratio is decreased sufficiently, the supply air only has to be cooled (no dehumidification required) to fully condition it, which would significantly decrease the consumed energy. Cases 5 and 6 represent examples of where the selective transfer in the RAMEE can be used as an alternative to partially bypassing the RAMEE or using an economizer.

The benefits of minimizing the energy used to fully condition the supply air by selective heat and moisture transfer in the RAMEE are only based on a preliminary study. The discussion does not consider the energy consumed controlling the solution flow rate for different conditions or the number of hours during a year that a location experiences the outdoor conditions where selective heat and moisture transfer is possible (which is usually very small). A more in-depth analysis of the operation and benefits of the RAMEE at extreme H* conditions is beyond the scope of this study (see Rasouli 2010 for a detailed analysis). This discussion is intended as a general introduction to the benefits and potential applications for the RAMEE at these outdoor air conditions.

3.5 Additional Factors Influencing System Performance

The analysis in this chapter (not including the results for Prototype #4 in Section 3.4.2, Figure 3.14) has focused on the effects of the outdoor air conditions on the system performance with NTU = 10, NTUm = 2.7, and constant indoor air conditions (AHRI summer conditions). The effects of the exchanger size (NTU and NTUm) and the indoor air conditions are briefly considered here, but a detailed analysis is left for further investigation.

3.5.1 NTU and NTUm

The effects of changing NTU and NTUm independently and concurrently at AHRI summer air conditions are presented in Table 3.3. The results show an increase in sensible effectiveness and a slight increase in latent effectiveness when NTU is increased and NTUm is kept constant. When NTU is kept constant and NTUm is increased, the sensible effectiveness increases slightly while the latent effectiveness increases significantly. When NTU and NTUm are increased concurrently, the sensible

and latent effectiveness both show significant increases. The changes in effectiveness when NTU and NTUm are increased together from the base case are slightly greater than the sum of the increases that occur when NTU and NTUm are increased independently. This result implies that a slight degree of synergy occurs in the RAMEE when NTU and NTUm are increased at the same time.

Table 3.3: RAMEE system effectiveness at different NTU and NTUm values at AHRI summer conditions.

NTU	NTUm	System Effectiveness (%)			Difference From Base Case (%)		
		Sensible	Latent	Total	Sensible	Latent	Total
10.0	2.7	76.5	59.9	65.7			
13.6	2.7	79.0	60.7	67.1	2.42	0.83	1.39
10.0	3.8	77.4	66.0	70.0	0.85	6.12	4.27
13.6	3.8	79.9	67.1	71.6	3.35	7.25	5.88

The trends of sensible and latent effectiveness increasing with NTU and NTUm respectively follow the sensible analytical solutions (Incropera and DeWitt 2002) and latent empirical correlations (Zhang and Niu 2002) for single exchangers. The other trends of sensible effectiveness increasing with NTUm and latent effectiveness increasing with NTU is further evidence of how the moisture transfer influences sensible performance and heat transfer influences latent performance.

As a result of these findings and the literature (Incropera and DeWitt 2002, Zhang and Niu 2002), the RAMEE performance contour plots would change when NTU and NTUm are changed. Increasing NTU would increase the values of the contour lines on the sensible performance plots significantly while only slightly changing the latent performance plots. Increasing NTUm would significantly increase the latent performance contour plot line values, but only mildly increase the sensible contour plot values. The magnitude of the change to the contour line values depends on the amount

NTU and NTUm are changed and the relative proportion of the change. More detailed conclusions would require contour plots at multiple NTU and NTUm configurations to be created which is beyond the scope of this study. However, the effects of NTU and NTUm are considered further in Chapter 4 during the development of the RAMEE correlations.

3.5.2 Indoor Air Conditions

The effects of the indoor air conditions on the system performance are considered by comparing the effectiveness at different indoor conditions (Table 3.4). The indoor conditions considered consist of the region bounded by AHRI summer and winter indoor conditions. This region covers the range of indoor conditions that the system would normally encounter. In order to account for the effects of heat and moisture transfer, the temperature and humidity ratio differences between the indoor and outdoor air are kept constant at 10°C and 7 g/kg for all the indoor conditions considered. This means that H* and ΔH are constant in all cases.

Table 3.4: RAMEE system effectiveness at different indoor air conditions. Outdoor air temperatures and humidities are 10°C and 7 g/kg higher than indoor conditions (H*=1.8).

Indoor Air Condition			System Effectiveness			Difference From AHRI Summer Indoor Conditions (%)		
T (℃)	W (g/kg)	RH (%)	Sensible (%)	Latent (%)	Total (%)	Sensible	Latent	Total
24.0	9.3	50	76.2	59.9	65.8			
21.0	9.3	60	76.2	60.0	65.9	0.0	0.1	0.1
24.0	7.1	39	79.0	58.6	66.1	2.9	-1.2	0.2
21.0	7.1	47	79.0	58.7	66.1	2.8	-1.3	0.2

Table 3.4 shows that the indoor air condition slightly affects the system performance. Changing the indoor temperature has a minimal effect on the effectiveness values ($\geq$0.1%), while changing the indoor humidity ratio has a moderate effect on both the sensible and latent effectiveness values (ε_{Sen} = 2.9% and ε_{Lat} = 1.3%).

However the variations in sensible and latent effectiveness offset each other and as a result, the total effectiveness only varies by 0.2% for the conditions considered.

The RAMEE contour plots are based on an indoor air condition of 24°C and 9.3 g/kg, and the above results show that the plots can be applied to other similar indoor air conditions as long as the humidity ratio difference between the two indoor conditions is less than 2 g/kg. In order to apply the contour plots to different indoor conditions, the contours must be shifted by the temperature and humidity ratio differences between the new and original indoor air conditions that the contours are based on (i.e., 24°C and 9.3 g/kg). Shifting the plots allows the zero transfer contour lines to cross the new indoor air condition. The shifted plots will have minimum errors (<0.2%) in the total effectiveness and slight to moderate (<3%%) errors in the latent and sensible energy effectivenesses if the new indoor condition is within 2°C and 0.2 g/kg of the original indoor condition of 24°C and 9.3 g/kg. These errors increase with the difference between the new indoor condition and the original indoor air condition increases, especially as the difference in humidity ratios increase above 0.2 g/kg.

The system performance is very sensitive to NTU and NTUm and slightly depends on the indoor air conditions. The system performance contour plots only apply to a system with a NTU of 10 and NTUm of 2.7, but the trends would still apply to other values. The indoor air conditions influence the sensible and latent performance of the system. These effects offset each other and as a result the influence on total performance is negligible for a small range of indoor air conditions (±2°C and ±0.2 g/kg) around 24°C and 9.3 g/kg.

3.6 Chapter 3 Summary

In this chapter the relationships between the RAMEE performance and the outdoor air conditions were presented. Previous investigations revealed the RAMEE operated differently under summer and winter standard test conditions, but the extent of this variation for other outdoor conditions was unknown. Therefore additional conditions were simulated that represent the range of outdoor air conditions that would be encountered in a typical year for most climate locations. The results showed the effects of the outdoor air conditions on the peak total, sensible, and latent effectivenesses and the operating Cr* that causes these peaks. The underlying causes of the RAMEE performance at the different outdoor air conditions were also elucidated.

The results for the peak total performance were presented as contour plots that showed the relationships between sensible, latent, and total performances and the outdoor air conditions. These results showed that heat and moisture transfer in the RAMEE is governed by primary and secondary potentials. For heat transfer, the primary and secondary potentials are the temperature and humidity ratio differences, respectively, between the outdoor and indoor air. While for moisture transfer, the primary and secondary potentials are the difference between the indoor and outdoor humidity ratio and temperature. The presence of secondary driving potentials for heat and moisture are unique to the RAMEE and result in it being able to achieve effectiveness values that are greater than 100% or less than 0% for some outdoor conditions. The contour plot for the operating Cr* that causes the system to perform with the maximum total effectiveness was also shown. Knowing this optimal Cr*,

allows the energy recovery in the RAMEE to be maximized at different outdoor conditions

Additional contour plots were presented that show the peak sensible and latent performances and the Cr* values at which they occur. These plots further described the relationship between the RAMEE performance and the outdoor air conditions and demonstrated the maximum heat and moisture transfer rates in the RAMEE.

The unique performance of the RAMEE at –H* conditions was also investigated. These conditions were shown to cause very interesting results with sensible and latent effectivenesses greater than 100% or less than 0% for some conditions. The results showed that at some Cr* values, the difference between the sensible and latent effectiveness values are considerable which allows heat or moisture to be selectively transferred over each other. The investigation also showed that at low operating Cr* values, the individual LAMEEs function as either a evaporative cooler or a condensing heater and the RAMEE would transfer very little total energy between the air streams. The potential applications of the RAMEE at these conditions were proposed and the numerical model was validated at these conditions with experimental findings.

Lastly, the effects of the exchanger size (NTU/NTUm) and the indoor conditions on the system performances and how they would modify the presented contour plots were considered.

Chapter 4

RAMEE EFFECTIVENESS CORRELATIONS

4.1 Introduction

Chapter 3 showed that the effectiveness of the RAMEE is extremely variable and a function of design (i.e., NTU) and operating condition (i.e., Cr* and outdoor air conditions) parameters. In this thesis, the RAMEE performance is determined through numerical simulations which use the design and operating condition parameters as inputs. However, these simulations are computational intensive due to their iterative nature and are cumbersome to use, which makes them impractical for designing and operating HVAC systems that use a RAMEE for energy recovery.

In practice, correlations are used to describe the performance of air-to-air energy recovery systems. Numerous correlations exist in the literature that are used to describe heat exchangers (Incropera and DeWitt 2002), flat plate energy exchangers (Zhang and Niu 2002), heat wheels (Shah 1981) and energy wheels (Simonson and Besant 1999a). The correlations are simple explicit equations that determine the exchanger performance (often in terms of effectiveness) based on several input parameters. This chapter develops a set of correlations to describe the RAMEE effectiveness for different design and operating condition parameters.

4.2 RAMEE Dependency on Design and Operating Condition Parameters

In order to develop correlations for the RAMEE sensible and latent effectiveness, the individual relationship between effectiveness and design and each operating condition parameters must be determined. Some of these relationships (i.e., outdoor air conditions) were briefly shown in Chapter 3, but are considered here in more detail. The parameters considered in this study are NTU (design parameter), Cr* (operating condition parameter), and H* and ΔH (operating condition parameter / outdoor air condition). The relationship between each parameter and the RAMEE effectiveness is demonstrated by varying one parameter while maintaining the remaining parameters constant. The design parameter of NTUm is indirectly considered in the analysis because it is related to NTU by the properties of the LAMEE (see eqs. (2.17) & (2.18)). Because of this coupling, NTU and NTUm are not considered independently and NTU/NTUm is constant at 3.6 for all the operating conditions considered.

4.2.1 Effects of NTU on Effectiveness

The relationship between NTU (design parameter) and RAMEE effectivenesses is shown in Figure 4.1. The figure shows the sensible and latent effectivenesses increasing as NTU increases with the greatest rate of change occurring at low NTU values and the effectiveness values leveling off at higher NTU values.

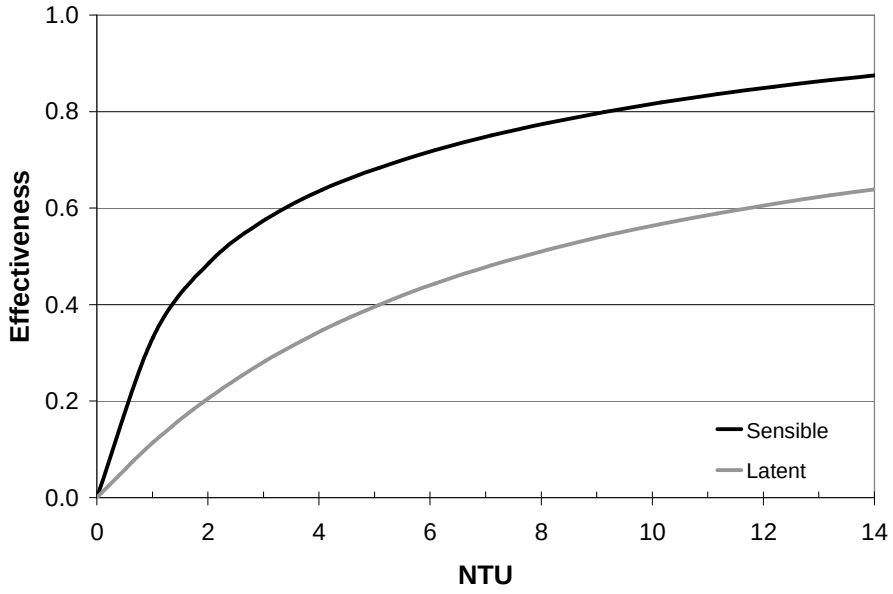

Figure 4.1: RAMEE effectiveness as a function of NTU (Cr* = 3, H* = 3, and ΔH = -43 kJ/kg).

4.2.2 Effects of Cr* on Effectiveness

The relationship between Cr* and RAMEE effectiveness has been shown previously, but is reintroduced in Figure 4.2. The figure shows the sensible and latent effectivenesses rapidly increasing from zero to maximum values and then slowly decreasing to plateaus as Cr* increases from zero to higher values. This relationship is similar to a run-around heat (sensible) exchanger except that the peak effectivenesses occurs when Cr* is equal to 1 for a run-around heat exchanger (London and Kays 1951).

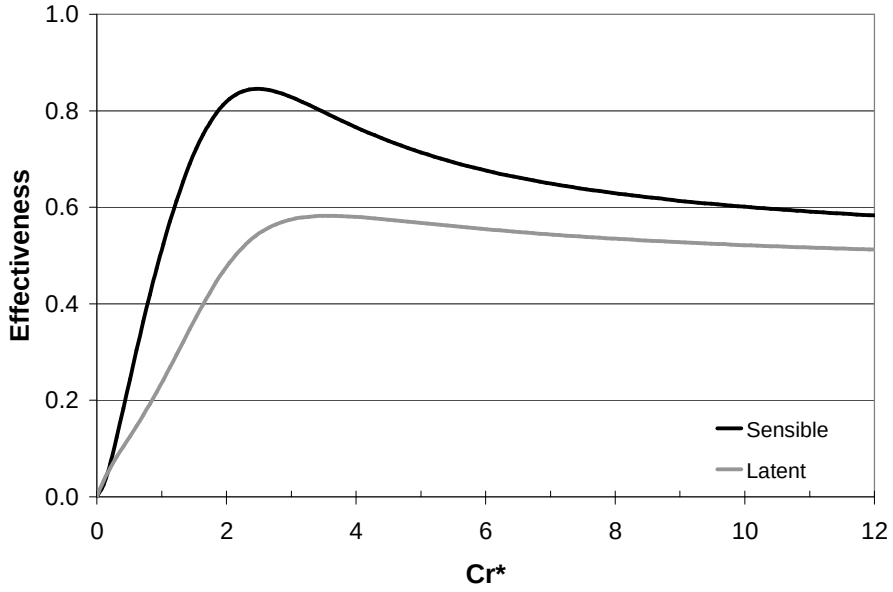

Figure 4.2: RAMEE effectiveness as a function of Cr* (NTU = 10, H* = 3, and ΔH = -43 kJ/kg).

4.2.3 Effects of H* on Effectiveness

In Chapter 3, the RAMEE effectiveness contour plots (Figure 3.3A - Figure 3.5A) show that the contours resemble lines of constant H* (Figure 2.4). Figure 4.3 shows the relationship between the RAMEE effectiveness and H*. In general, the sensible effectiveness is linearly related to H* and increases as H* increases, while the latent effectiveness is inversely related to H*. However near H* = -1, the actual

relationship between effectiveness and performance (diamonds/circles in Figure 4.3) slightly deviates from the general relationship as shown by the lines in Figure 4.3.

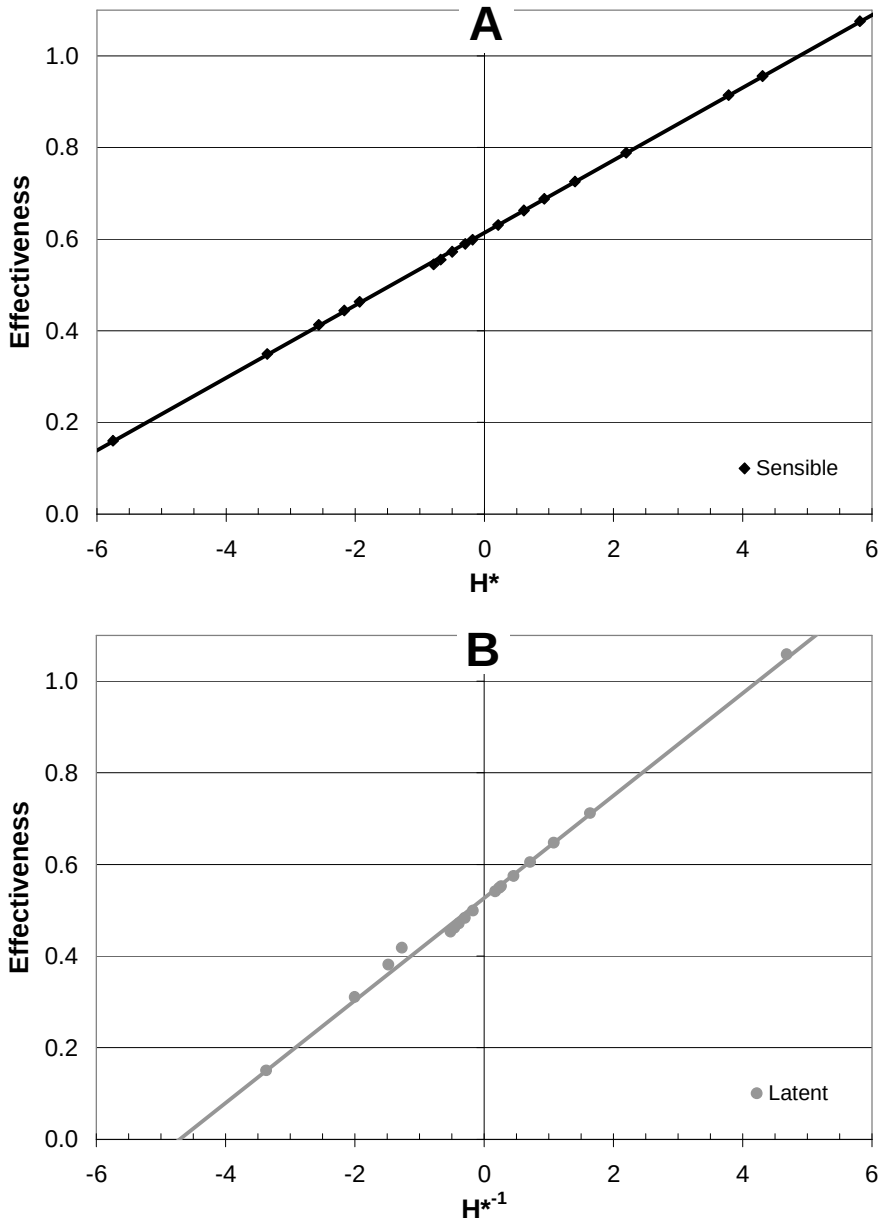

Figure 4.3: RAMEE effectiveness as a function of H* (NTU = 10, Cr* = 3, and ΔH = -5 kJ/kg).

4.2.4 Effects of ΔH on Effectiveness

The contours from the effectiveness contour plots (Figure 3.3A - Figure 3.5A) are slightly curved, which indicates that H* does not adequately describe the effects of the outdoor air conditions of the RAMEE performance. Therefore, ΔH is used as another parameter to further describe the relationship between the outdoor air conditions and the RAMEE performance. Figure 4.4 shows that effectivenesses are linearly related to ΔH with minor deviations (indicated by scatter of diamonds/squares around a linear trend line). As ΔH increases (i.e., outdoor air enthalpy decreases, see eq.. (2.22)), the sensible effectiveness increases while the latent effectiveness decreases. Over the range considered (-60 kJ/kg to +30 kJ/kg), the change of the effectivenesses is small (+5% for sensible and -5% for latent). This shows that ΔH has a minor effect on effectiveness compared to NTU, Cr*, and H*.

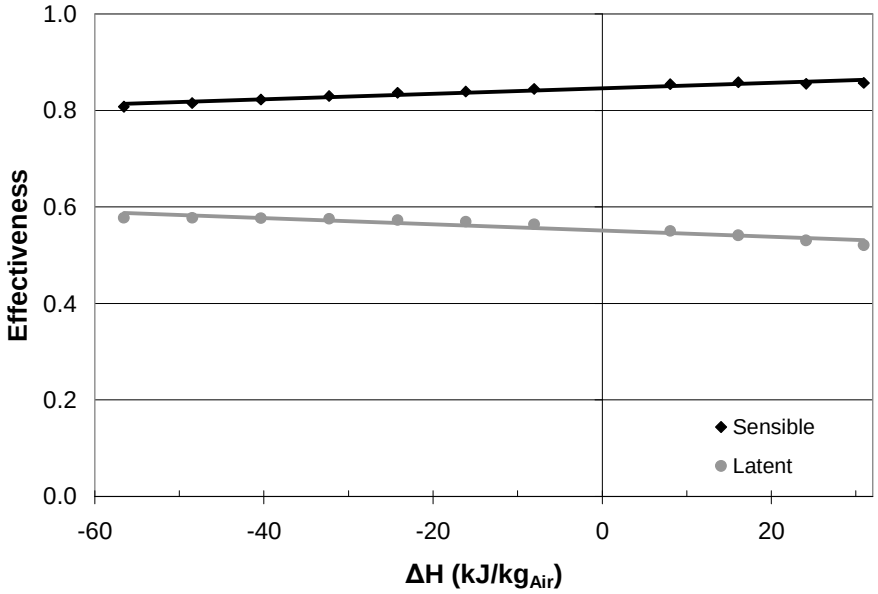

Figure 4.4: RAMEE effectiveness as a function of ΔH (NTU = 10, Cr* = 3, and H = -3).

4.3 Peak Total Performance

Figure 4.1 - Figure 4.4 show the relationships between RAMEE effectiveness and the design and operating condition parameters. Developing effectiveness correlations that consider all the parameters would be extremely difficult and produce very complex results. However, correlations that describe the RAMEE when it is operating at peak total effectiveness only require the NTU, H*, and ΔH parameters. Therefore the peak total effectiveness correlations would be easier to develop because they do not depend on Cr*, which is the parameter with the most complex relationship with effectiveness.

Developing correlations describing the peak total effectiveness of the RAMEE is desirable because of the controlled strategy introduced in Section 3.4.4 (and thoroughly discussed by Rasouli (2010b)) has the RAMEE operating at its peak total effectiveness for the given conditions. These strategies call for the RAMEE to be operated at peak total effectiveness for most outdoor air conditions (predominantly +H*) in order to maximize energy recovery which in return minimizes the energy required by auxiliary equipment to fully condition the air in the building. The control strategies for –H* conditions are more complex and sometimes require that Cr* be controlled to give an effectiveness that is different from the maximum total effectiveness. These –H* conditions are left for future work. Therefore, the correlations developed in this thesis are for only +H* conditions.

In order to operate the RAMEE (i.e., control Cr*) at its peak effectiveness for a given condition, the optimal Cr* for that given condition must be known. Therefore, a correlation to describe the optimal Cr* is required and should accompany the

effectiveness correlations. This correlation is developed for the same range of conditions as the effectiveness correlations and therefore is only valid for +H* conditions.

The development of correlations for the peak total effectiveness will allow the energy saving potential of the RAMEE to be easily determined for a range of conditions (i.e., NTU, +H*, and ΔH) without the need of the computational intensive numerical model. Additionally, the optimal Cr* correlation would facilitate operating the RAMEE at its peak total performance under various conditions.

4.3.1 Data Range and Correlation Development

This section details the range of the input parameters and the methodology that are used to develop the correlations. The outdoor air conditions are shown in Figure 4.5 and consist of 51 +H* conditions with respect to standard indoor air conditions (24°C, 9.3 g/kg, 50% RH). The outdoor temperatures range between -6°C to 38°C while the humidity ratio ranges between 2 g/kg to 24 g/kg. The NTU values range between 1 and 14 at increments of 1 and are manipulated by changing the air mass flow rate. NTUm is not considered directly but has the same proportionality to NTU for all conditions (i.e., NTU/NTUm = 3.6). The relationship between NTU and NTUm is based on the LAMEE properties of Prototype #3 (Mahmud et al. 2010). The simulated Cr* values range between 1 and 5 at 0.05 increments. The range of Cr* is adequately sized to ensure that the optimal Cr* values for all the conditions considered falls within the range.

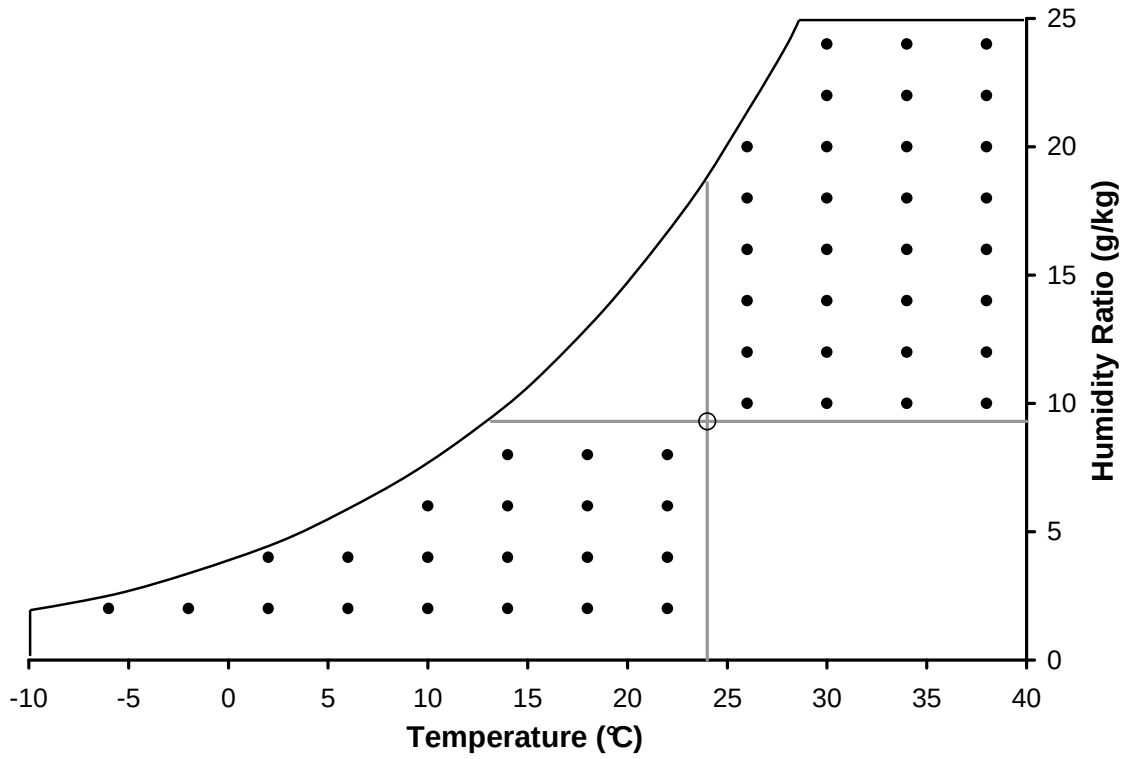

Figure 4.5: Simulated outdoor air conditions used to develop the effectiveness correlations.

The correlations are developed from the simulated data set consisting of results from the various input parameters. The data set has 714 points from the 51 outdoor air conditions and 14 NTU values considered. The peak total effectiveness is taken as the maximum total effectiveness that occurs between the simulated range Cr* of 1 to 5. The Cr* that causes the peak total effectiveness is taken as the optimal Cr* and the sensible and latent effectivenesses at the optimal Cr* are used in the data set. Using Cr* increments of 0.05 ensure that the peak total effectiveness is very close to the actual peak value.

The general forms of the correlations are based on the trends observed in Figure 4.1, Figure 4.3, and Figure 4.4. Linear relationships are used to relate H* and ΔH (H* ΔH^{1}) to sensible (latent) effectiveness. Power and logarithmic relationships are used to describe the relationship between NTU and effectiveness and were selected by trial and

error since they provide a better fit than other basic functions (e.g., high order polynomial, exponential and power relationships). The relationships for the individual parameters are incrementally combined (H*, ΔH, and then NTU) to form the correlations. The coefficients for each correlation are determined by minimizing the root mean square difference between the simulated and correlated results for each data point, which is achieved by the solver function in Microsoft Excel®. The coefficients are rounded to simplify the correlations. For the sensible effectiveness correlation, the temperature change in the supply LAMEE is used for the root mean square difference, while the humidity ratio change is used for the latent effectiveness correlation. The temperature and humidity ratio changes are used as the results instead of the sensible and latent effectivenesses because the temperature and humidity ratio changes describe the actual energy recovery of the RAMEE and the subsequent energy savings. This method results in some of the correlated effectivenesses having large errors compared to the simulated values, but the errors in the temperature/humidity ratio changes are small.

4.3.2 Correlations

Sensible Effectiveness

The correlation for the sensible effectiveness when the RAMEE is operating at peak total effectiveness is given in equation (4.1). The correlation shows that the sensible effectiveness increases linearly with H* and ΔH. As NTU increases, the sensible effectiveness also increases but at a decaying rate of change.

$$\varepsilon_{Sen} = 0.0093 \cdot NTU \cdot H^* - 45 \cdot (NTU + 4)^{-3} + 8x10^{-5} \cdot (H^* + 0.4) \cdot NTU \cdot \Delta H + 0.678 \quad (4.1)$$

The accuracy of the correlation is shown in Figure 4.1 which compares the correlated and simulated change in the supply air temperature (ΔT). The differences between the simulated and correlated temperature changes ($\delta\Delta T$) has 95% of the considered points with $\delta\Delta T < 0.2°C$, 75% of the points with $\delta\Delta T < 0.1°C$, and a maximum difference of 0.31°C. Based on the comparison and the small differences between the simulated and correlated supply air temperature changes, the sensible effectiveness correlation is able to successfully determine the sensible energy transfer in the RAMEE when it is operating at peak total effectiveness within the range of conditions considered.

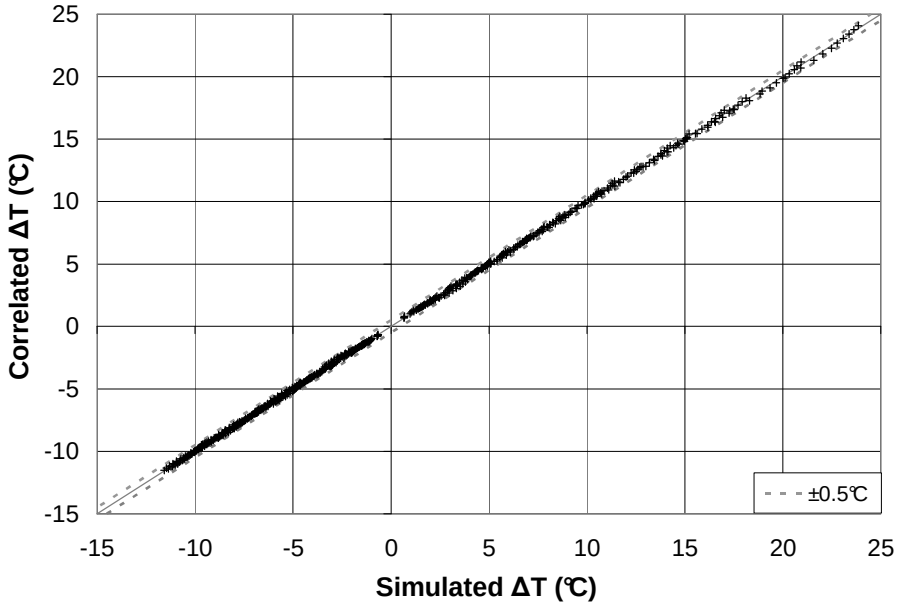

Figure 4.6: Comparison between correlated and simulated supply air temperature change.

Latent Effectiveness

The correlation for latent effectiveness is shown in equation (4.2). The latent effectiveness decreases linearly as ΔH increases and decreases linearly as the inverse of

H* increases. The latent effectiveness also increases with NTU, but at a decaying rate of change.

$$\varepsilon_{Lat} = 0.01 \cdot NTU \cdot H^{*-1} - 67 \cdot (NTU + 10)^{-2} - 3x10^{-5} \cdot \left(H^{*-1} + 2\right) \cdot NTU \cdot \Delta H + 0.671 \quad (4.2)$$

The accuracy of the latent effectiveness correlation is shown in Figure 4.7, which displays the comparison between the correlated and simulated change in supply air humidity ratio. The difference between the correlated and simulated supply air humidity ratio changes ($\delta\Delta W$) has a maximum value of 0.12 g/kg with 91% of the points having $\delta\Delta W < 0.05$ g/kg and 64% of the points having $\delta\Delta W < 0.025$ g/kg. These low differences between the correlated and simulated humidity ratios show the latent effectiveness correlation is able to accurately describe the latent performance of the RAMEE.

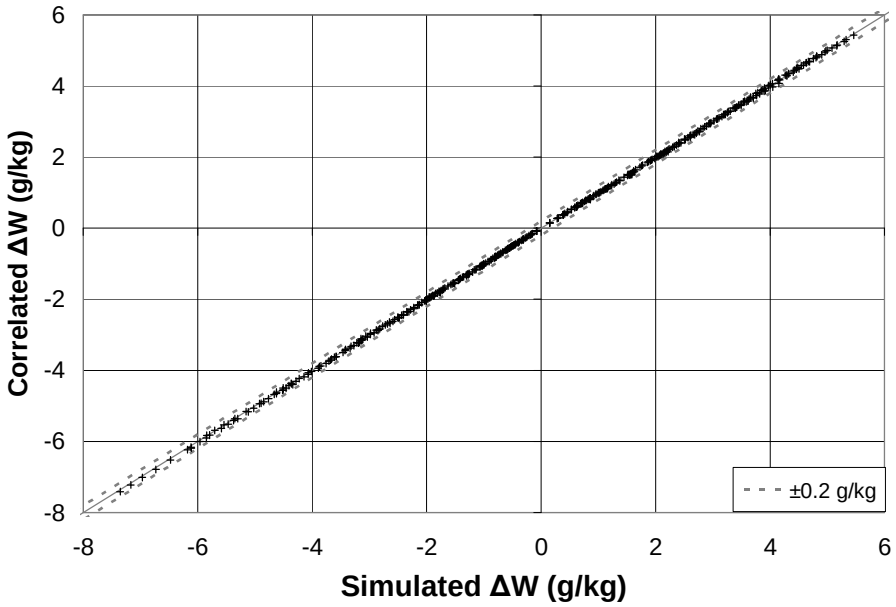

Figure 4.7: Comparison between correlated and simulated supply air humidity ratio change.

Total Performance

The total effectiveness of the RAMEE is determined from the sensible and latent effectiveness and H* according to equation (4.3) (Simonson, Besant 1999b).

$$\varepsilon_{Tot} = \frac{\varepsilon_{Sen} + H^* \varepsilon_{Lat}}{1 + H^*} \tag{4.3}$$

The accuracy of the total effectiveness correlation is shown in Figure 4.8, which compares the change in the supply air enthalpy between the simulation and correlation. The differences between the correlated and simulated supply air enthalpy change ($\delta\Delta H$) has a maximum value of 0.47 kJ/kg and 96% of the points have $\delta\Delta H < 0.25$ kJ/kg and 65% of $\delta\Delta H < 0.1$ kJ/kg.

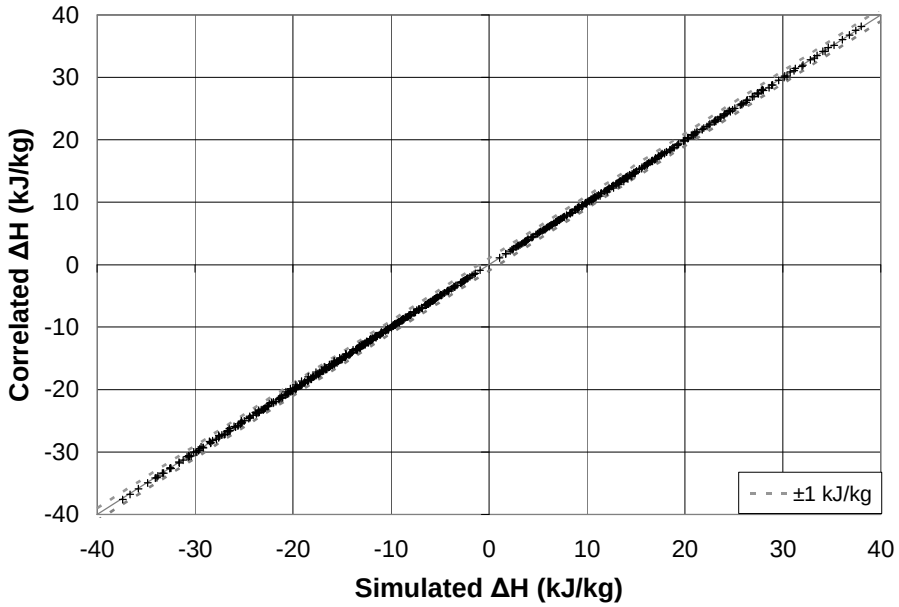

Figure 4.8: Comparison between correlated and simulated supply air enthalpy change.

Optimal Cr*

The correlation for optimal Cr* provides the Cr* value that has the RAMEE operating at its maximum total effectiveness for a given outdoor air condition and NTU, which is shown in equation (4.4).

$$Cr*_{Optimal} = \left[Ln(NTU)+10\right]\cdot H*^{0.1} + \left[(H*+5)^{-2.4} - 0.023\right]\cdot \Delta H + 0.177 \qquad (4.4)$$

The optimal Cr* as a function of the outdoor air conditions (H* and ΔH) and NTU is extremely complex, but the developed correlation is able to achieve a moderate degree of accuracy as can be seen in Figure 4.9. The comparison between the simulated and correlated optimal Cr* has a maximum error ($\delta Cr*_{Optimal}$) of 0.30 and 85% of the points have $\delta Cr*_{Optimal} < 0.1$ and 59% of the points have $\delta Cr*_{Optimal} < 0.05$. Using a Cr*

that is 0.3 off the optimal Cr* can results in the total effectiveness being off by 2%, which equates to temperature and humidity ratio change errors of 0.8°C and 0.03 g/kg.

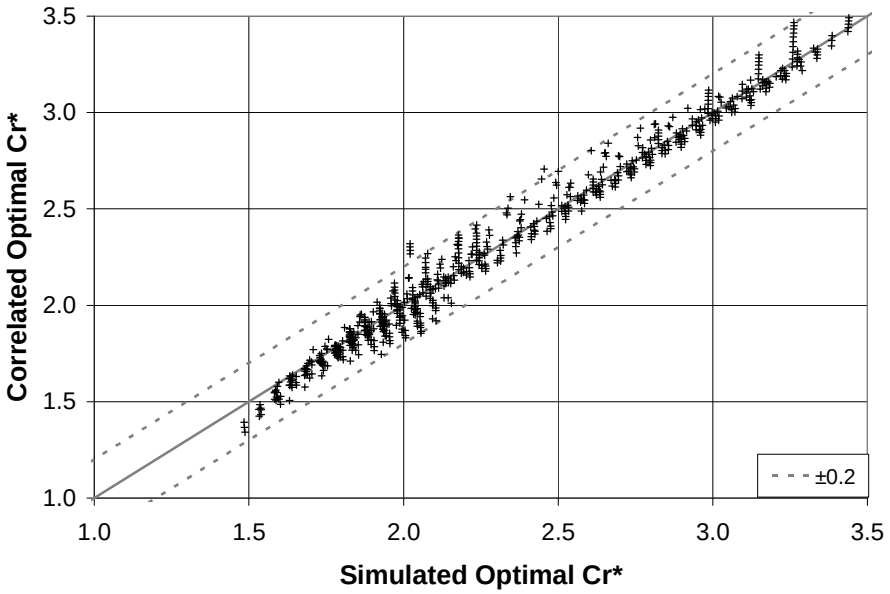

Figure 4.9: Comparison between correlated and simulated optimal Cr*.

4.4 Chapter 4 Summary

In this chapter the effects of the system (i.e., NTU) and operating (i.e., Cr*, H*, ΔH) parameters on the RAMEE performance were shown. These relationships were quantitatively described and used to create a set of correlations that describe the RAMEE effectivenesses and optimal Cr*. The developed correlations use NTU, H*, and ΔH as input parameters to determine the optimal Cr* and the sensible and latent effectivenesses of the RAMEE when it is operating at maximum total effectiveness. The correlations are able to determine the changes in the supply air temperature, humidity ratio, and enthalpy and the optimal Cr* with minimal error (0.31°C, 0.12 g/kg, and 0.47 kJ/kg, 0.30) and are valid for all +H* conditions between -6°C to 38°C and 0 to 24 g/kg and NTU values from 1 to 14 with NTU/NTUm = 3.6.

Chapter 5

EFFECTS OF NON-UNIFORM EXCHANGER CHANNELS

5.1 Introduction

Non-uniform exchanger channels in the LAMEE are an inherent design and construction challenge. Since the membrane that separates the air and salt solution is very flexible, it readily deforms due to the pressure difference across each membrane between the two fluids. Deformations in the membrane mean the flow channel thickness varies throughout each LAMEE, which causes non-uniform air and solution velocities in each LAMEE. Varying channel thicknesses also cause a spatial variation in the heat and moisture transfer coefficients for each fluid. The effects of the fluid flow maldistribution and variable heat and moisture transfer coefficients on the RAMEE performance (effectiveness) are investigated in this chapter. The investigation presents two somewhat independent methods of estimating the change in effectiveness when simple geometric deflections are imposed in the flow channel, i.e., algebraic and numerical simulation methods. As well, these numerical predictions are compared to some experimental results.

5.2 Geometry of Deformed Channel

The deformed air and solution channels used in this chapter are significantly different than the undeformed channels used to develop the model presented in previous chapters. Figure 5.1 shows the expected geometric differences between the uniform and

non-uniform channels in each LAMEE. Uniform flow channels were used in the numerical analysis in Chapters 3 and 4 where the membrane panels are parallel to each other. The non-uniform flow channels, considered in this Chapter, have the membrane bulging into the air channel, which form a sinusoidal pattern as shown in Figure 5.1B. This sinusoidal pattern is used to approximate the dominant membrane deformation shape in each exchanger which is caused by the solution channel bulging into the air channel because of the pressure differential between the channels. The membrane forms a sinusoidal shape because the membrane bulges between evenly spaced air channel support structures, which are used to prevent the air channel from collapsing on itself. This sinusoidal membrane shape is repeated over the height of the channel in the z direction with the number of cycles depending on the number of support structures and the sinusoidal shape runs the length of the channel in the x direction.

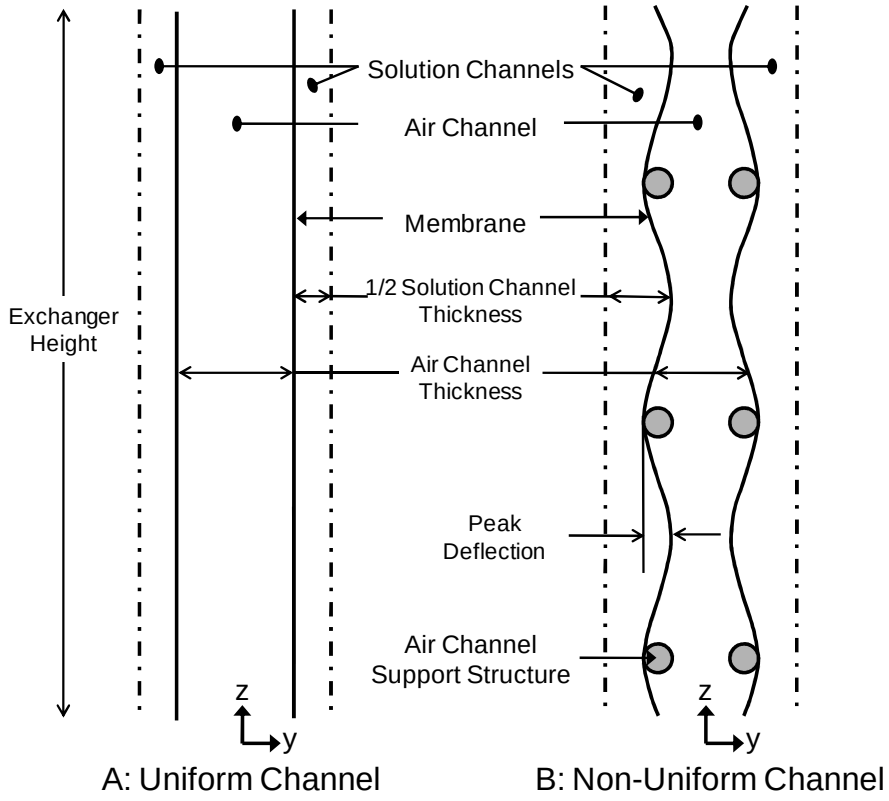

Figure 5.1: Schematics of uniform and non-uniform channels with z scale ≠ to y scale. Fluid flows are into and out of page in the x direction.

The magnitude of the membrane deflection is characterized by the size of the peak membrane deflection divided by the undeflected (nominal) air channel thickness. Therefore, a deflection of 50% would imply that the membranes would be in contact with each other at the center of the air channel. Figure 5.2 shows the shape (over one cycle) of the membrane for deflections of 10% and 20% of the nominal air channel thickness in a LAMEE. This figure represents the deflection position with a relative scale that has the peak membrane deflections occurring at relative positions of 0 and 1 and the minimum deflection occurring at 0.5. In this section and subsequent sections (i.e., 5.2 to 5.4), the LAMEE is modeled with nominal air and solution channel of 4 mm and 2 mm respectively. Also, the effects of the support structure inside the air channel are not considered in this analysis and are left for future investigations.

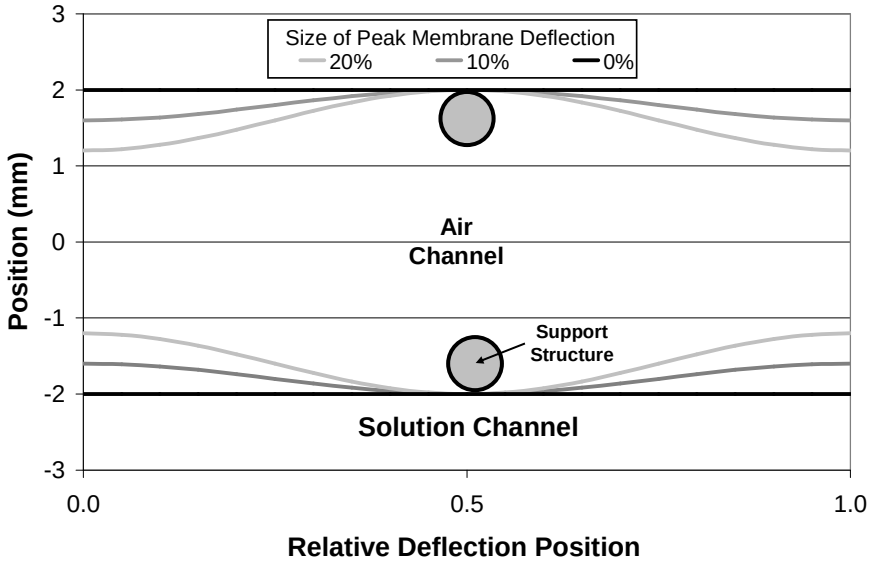

Figure 5.2: Shape of one membrane deflection cycle.

5.3 Effects of Non-Uniform Channels on RAMEE Parameters

This section describes how the non-uniform channels affect key parameters that govern the RAMEE operations. The parameters that are considered here are the local fluid flow rates in the channel (Cr*), the overall heat and moisture transfer coefficients (U and U_m), and the NTU and NTUm values. These parameters are normalized relative to these values in a RAMEE with uniform channels in each LAMEE. Therefore, a parameter with a relative value of 1 is equal to the parameter for a RAMEE with uniform channels.

5.3.1 Local Fluid Flow Rates

The non-uniform channels create flow maldistributions in the air and solution channels, with variable local mass flow rates. The local fluid mass flow rate is the flow through a channel section of variable thickness ($\delta_{Sol,Var}$, $\delta_{Air,Var}$) and equal width (Δz). The resulting maldistributed mass flow rate is determined by eq. (2.11) which determines the mass flow distribution based on fully developed Poiseuille flow and that

the pressure drop along the length of the channel is the same across the face of the channel (i.e., independent of z).

The normalized mass flow rates of the air and solution shown in Figure 5.3 and Figure 5.4 are normalized with respect to the flow in channels with uniform thicknesses. These figures show each fluid will have a higher mass flow rate in the wider sections of their channels (i.e., relative positions 0 and 1 for the air flow) and a lower flow rate in the narrower section of their channels (i.e., relative position 0.5 for the air) compared to the flow rate in a uniform channel. The variations in mass flow rate increases as the magnitude of the peak membrane deflection increases. The arrangement of the membrane bulges in the channels result in regions with high solution mass flow rates being adjacent to regions with low air mass flow rates and vice versa.

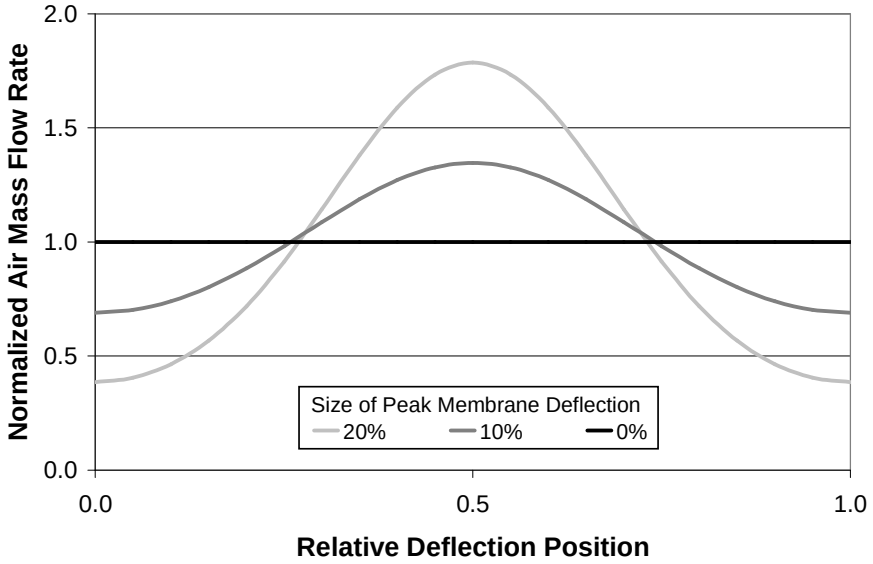

Figure 5.3: Normalized air mass flow rate distribution for one cycle of membrane deflection in the channel.

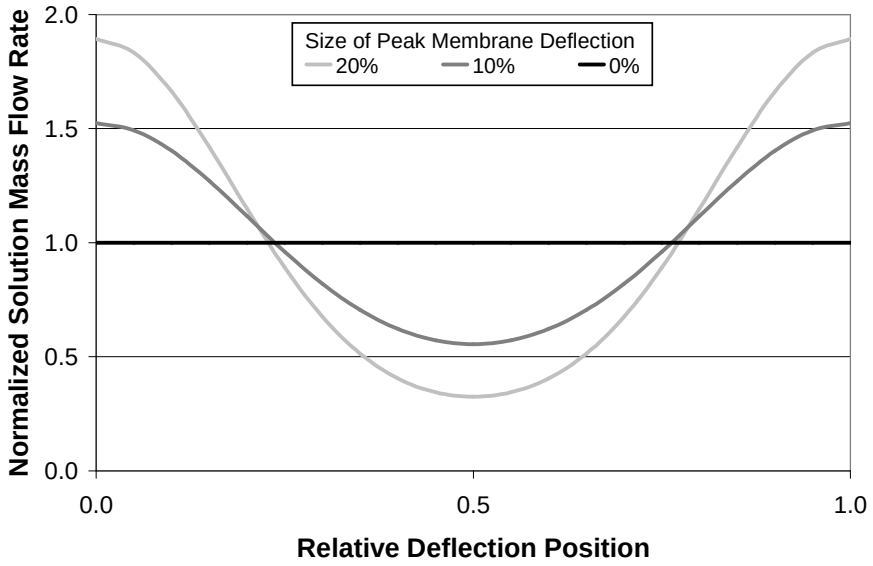

Figure 5.4: Normalized solution mass flow rate distribution for one cycle of membrane deflection in the channel.

The local Cr* values combines the distribution of the local air and solution flow rates. Figure 5.5 shows this Cr* distribution which has low values in the wide air channel sections (relative position 0.5) and large values in the narrow sections (relative

positions 0 and 1). The local Cr* in a LAMEE with non-uniform channels is therefore very different from a uniform channel system.

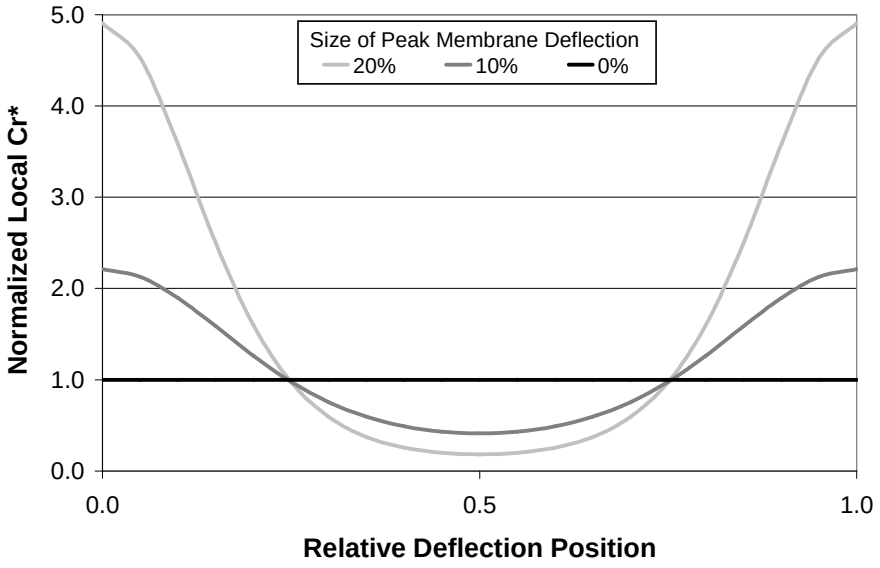

Figure 5.5: Normalized local Cr* distribution for one cycle of membrane deflection in the channel.

5.3.2 Overall Heat and Moisture Transfer Coefficients

The channel thickness variations also influence the overall heat and moisture transfer coefficients between the bulk air and solution flows. The overall heat and moisture transfer coefficients are determined from eq.. (2.3) and eq.. (2.9) and incorporate the heat and mass transfer coefficients imposed by the membrane and the air and solution boundary layers. The coefficients are listed in Table 5.1 and are based on air and solution channels of 4 mm and 2 mm respectively and fluid conditions encountered during standard summer test condition. The solution mass transfer coefficient is not incorporated in the overall coefficient but is accounted for in the governing equations (see Section 2.2.3). The flows are assumed to be laminar and fully developed, which results in the air and solution convective transfer coefficients only being affected by the channel thicknesses in the non-uniform channel according to eq..

(2.13) and independent of the fluid flow rates. Therefore the convective coefficients increase as the channel thickness decreases and vice versa.

Table 5.1: Heat and mass transfer coefficients for laminar and fully developed flow in a 4 mm air channel and 2 mm solution channel.

Heat Transfer Coefficients		
h_{Air}	27.1	
k/δ_{Mem}	1670	$W/(m^2 \cdot s)$
h_{Sol}	998	
Mass Transfer Coefficients		
$h_{m,Air}$	0.0335	$kg/(m^2 \cdot s)$
k_m/δ_{Mem}	0.0083	

Figure 5.6 and Figure 5.7 show the distributions of the normalized overall heat transfer (U) and the overall mass transfer (U_m) coefficients in the non-uniform channels, respectively. The variable overall coefficients are normalized to the coefficients for uniform channels. Both these overall coefficients are highest when the air channel is narrowest (relative positions 0 and 1), which is because the air convective coefficients are higher in the narrow section than the wide sections and the air convective coefficients make the greatest contributions to the overall coefficients. The variation in the overall coefficients increases as the size of the peak deflection increases. The change in the overall mass transfer coefficient is significantly smaller than the overall heat transfer coefficient (~20%), which is due to the membrane's transfer coefficient to mass transfer having the greatest contribution to the overall mass transfer coefficient, which is independent of membrane deflection.

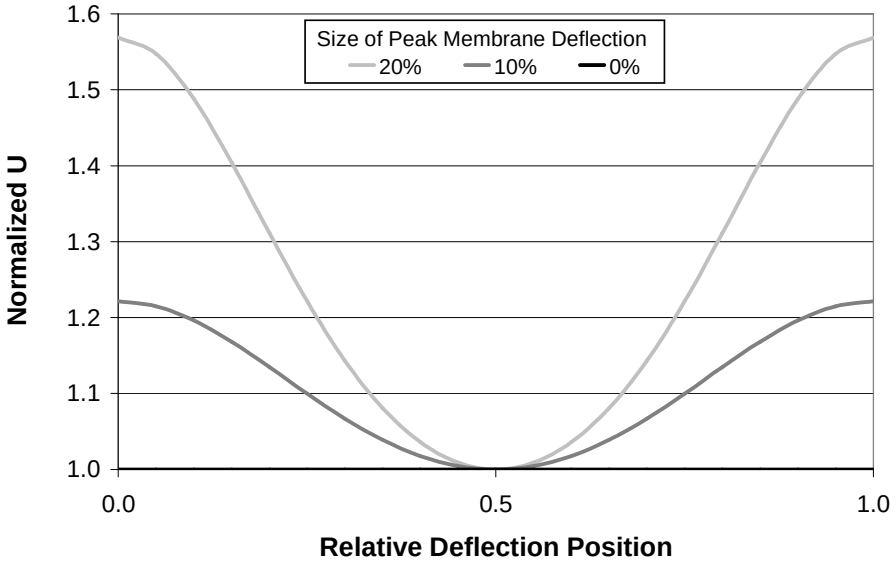

Figure 5.6: Normalized overall heat transfer coefficient (U) distribution for one cycle of membrane deflection in the channel.

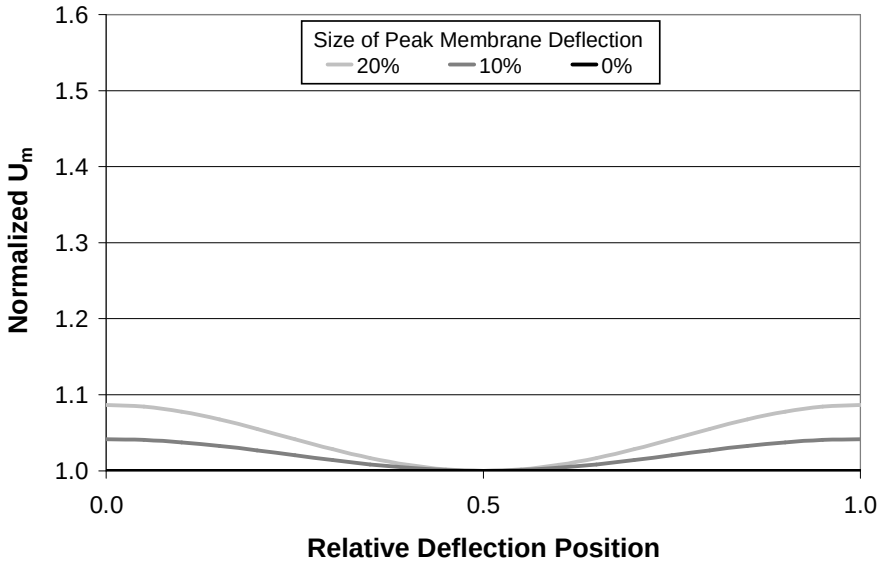

Figure 5.7: Normalized overall mass transfer coefficient (U_m) distribution for one cycle of membrane deflection in the channel.

5.3.3 NTU and NTUm

The effects of the flow maldistribution and variable overall heat and mass transfer coefficients are summarized by the local NTU and NTUm values as defined by

eqs. (2.17) and (2.18). Figure 5.8 and Figure 5.9 show the normalized local NTU and NTUm distributions in the non-uniform channel. Compared to the uniform channel, the local NTU values are depressed in the wide sections of the air channel (between relative positions 0.3 to 0.7) and enhanced in the narrow sections of the air channel. For the peak membrane deflection of 20%, the relative NTU decreases by half in the widest part of the channel and increases 4 times in the narrowest part compared to a uniform channel. The average NTU/NTUm values are greater than 1 and increases as the deflection size increases. The relative NTUm has a similar distribution as NTU except that the magnitude of the variation is not as large.

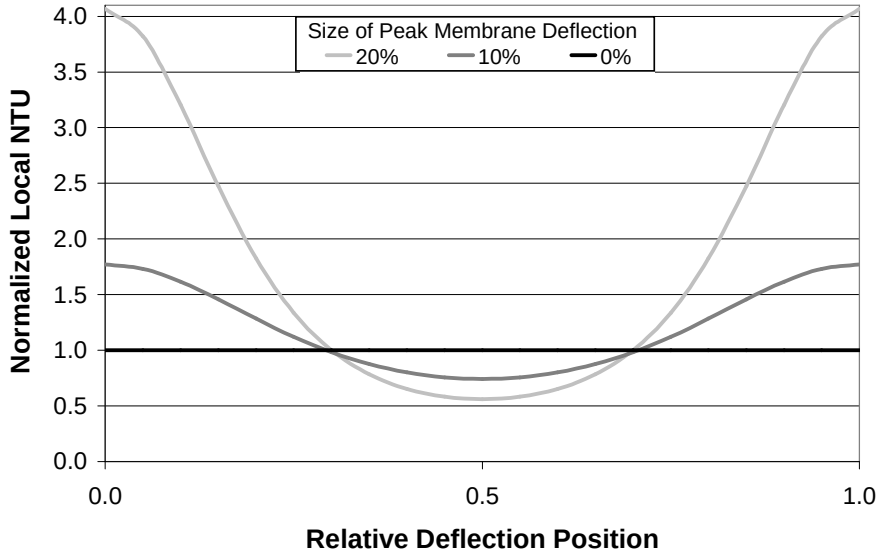

Figure 5.8: Normalized local NTU distribution for one cycle of membrane deflection in the channel.

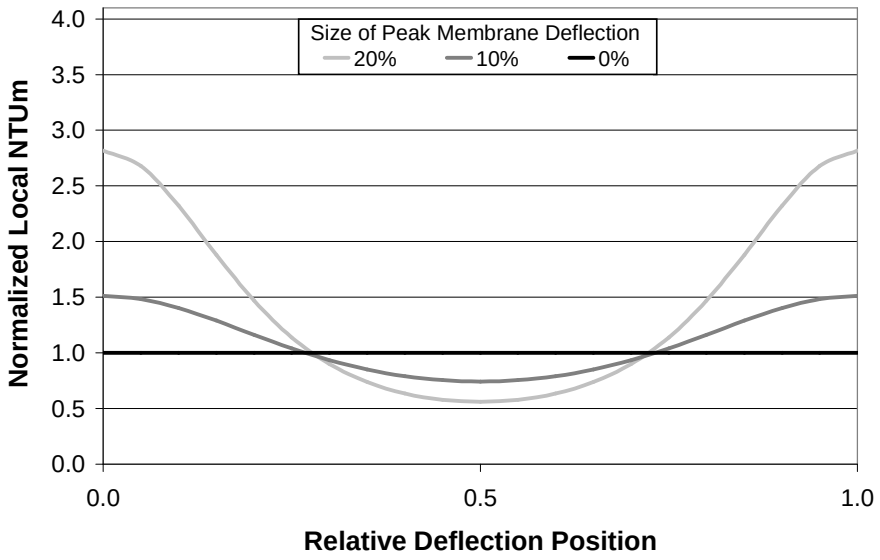

Figure 5.9: Normalized local NTUm distribution for one cycle of membrane deflection in the channel.

The relative NTU and NTUm distributions are out of phase with the relative air mass flow rate distributions, which is shown by comparing Figure 5.8 and Figure 5.9 with Figure 5.3. This arrangement results in the bulk of the air flowing through the channel sections with the lower local NTU and NTUm values.

5.4 Effects of Non-Uniform Channels on RAMEE Effectiveness

Chapter 4 showed that NTU and Cr* significantly influence a RAMEE's effectiveness, while Section 5.3 showed that the non-uniform channels create distributions in the local Cr* and NTU. Therefore, a distribution in the local NTU and Cr* caused by non-uniform channels will change the RAMEE effectiveness. This change is investigated in this section.

5.4.1 Algebraic Analysis

This section introduces a simple algebraic analysis to highlight the mechanisms that allow the variable Cr* and NTU values to influence the effectiveness. This analysis considers an exchanger with nominal air and solution channels of 4 mm and 2 mm

respectively that have a peak membrane deflection of 20%. Figure 5.10 shows one cycle of the membrane deflection in the air channel which is divided into 10 segments of equal widths.

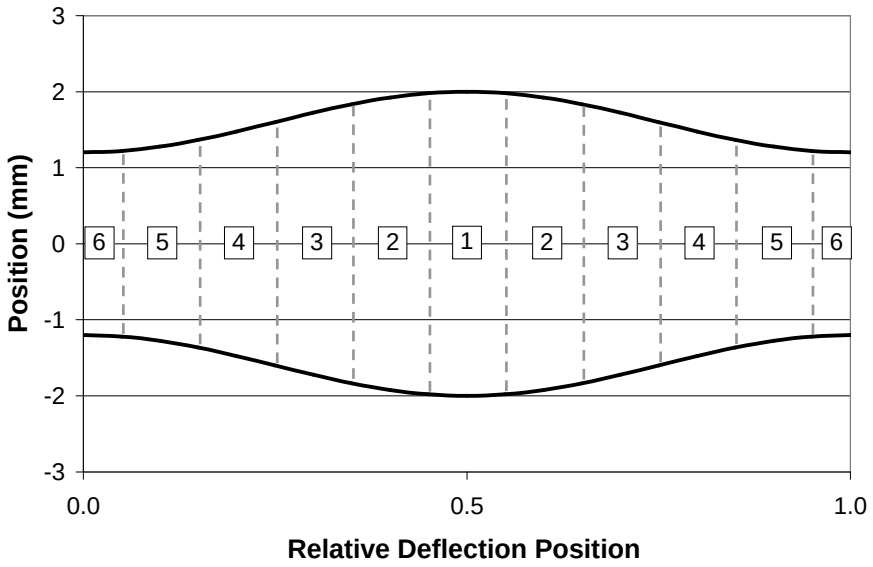

Figure 5.10: Air channel with 20% peak membrane deflection showing one deflection cycle discretized into 10 segments.

Table 5.2 contains the local values for the air mass flow rate, Cr*, NTU, and total effectiveness for each of the segments shown in Figure 5.10. The local air mass flow rate (in each segment), Cr*, and NTU are determined from the methods described in Section 5.3, while the total effectiveness is determined from the method that is discussed below. The air and solution flow rates are based on the fluid mass flow rates of a uniform channel RAMEE operating with a NTU of 6 and a Cr* of 2.6 (optimal Cr*) for the simulated AHRI summer condition. The local values for the RAMEE with uniform channels, which are constant for each segment, are also contained in Table 5.2.

Table 5.2: Local parameters and total effectiveness in discretized segments for the RAMEE operating at a NTU 6 for RAMEE channels with or without a 20% deflection.

Segment	Local Value			
	Air Mass Flow Rate (g/s)	NTU	Cr*	ε_{Tot}
Uniform Channels				
1-6	0.344	6.0	2.6	53.2
Non-Uniform Channels With 20% Deflection				
6	0.133	24.4	12.6	56.9
5	0.160	19.2	9.2	59.2
4	0.247	11.0	4.1	63.1
3	0.393	6.0	1.5	47.8
2	0.547	3.9	0.7	23.2
1	0.614	3.4	0.5	16.4
2	0.547	3.9	0.7	23.2
3	0.393	6.0	1.5	47.8
4	0.247	11.0	4.1	63.1
5	0.160	19.2	9.2	59.2
6	0.133	24.4	12.6	56.9
	Flow Rate Weighted Average			**37.9**

The results in Table 5.2 show the local air mass flow rates are higher in the wider segments (i.e., 1-3) and lower in the narrower segments compared to the local mass flow rates in the RAMEE with uniform channels. The local NTU and Cr* values have an opposite trend and their values increase (compared to the uniform channel local values) when the local air mass flow rate decreases and decrease when the flow rate increases. These patterns result in the segments of the air channel with the higher mass flows rates having lower NTU and Cr* values than the segments with the lower mass flow rates.

The local total effectiveness in each segment is determined from the local NTU and Cr* that are determined algebraically. Figure 5.11 shows the contour plot of total effectiveness as a function of NTU and Cr*. This contour plot is based on the steady state numerical simulations for a RAMEE with uniform air and solution channels of 4 mm and 2 mm respectively operating at AHRI summer conditions. The local total effectiveness values are determined by plotting the local NTU and Cr* values on the

contour plot (as indicated by the numbered circles on Figure 5.11) and interpolating the resulting effectivenesses. These local total effectiveness values are displayed in Table 5.2 and show that the segments with the higher air mass flow rates also have effectivenesses that are lower than the effectivenesses for a uniform channel exchanger. The consequence of this is that the average effectiveness of the channel, based on an air mass flow rate weighted average (to account for the maldistributed flow), is lower than the effectiveness for a RAMEE with uniform channels. For the case considered here, the average total effectiveness for the RAMEE with non-uniform channels is 37.9%, which is significantly lower than the value of 53.2% for the uniform channel RAMEE operating at the same conditions.

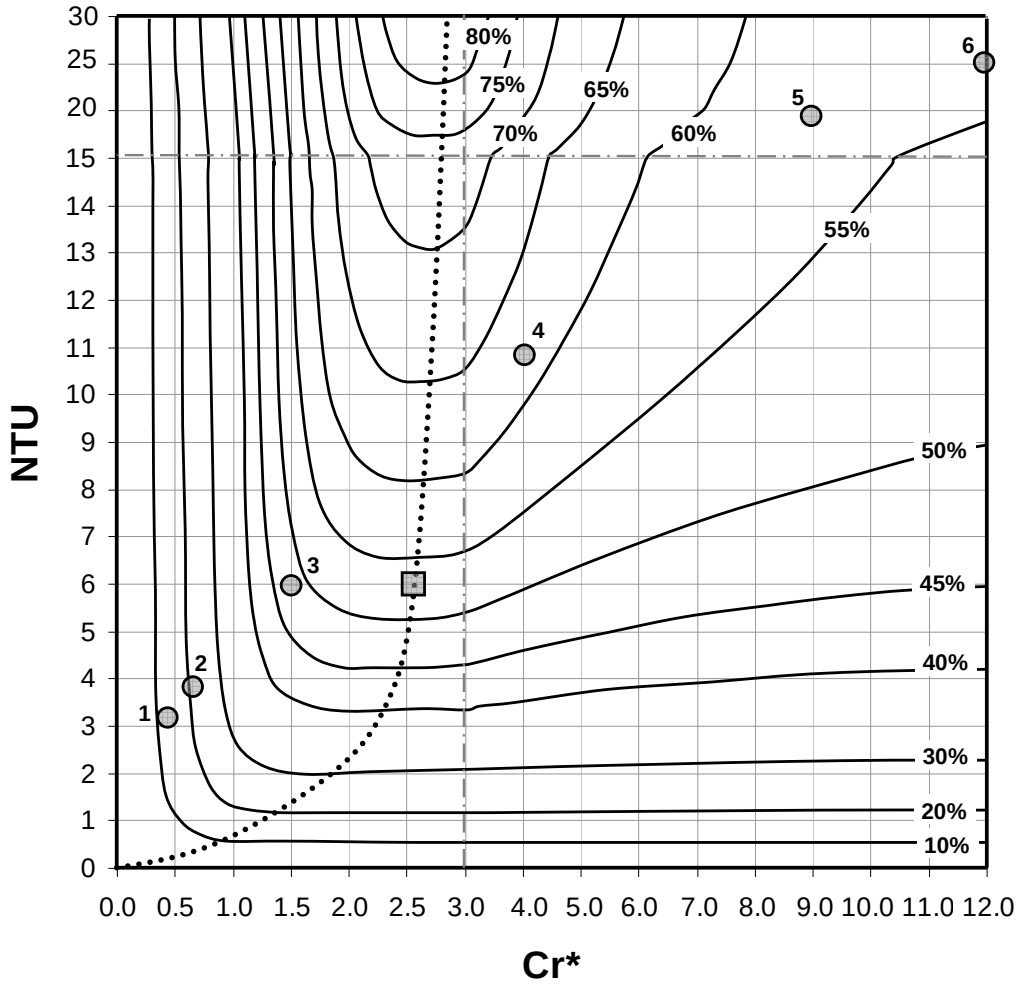

Figure 5.11: Contour plot of total effectiveness as a function of NTU and Cr* for a RAMEE with air and solution channels of 4 mm and 2 mm with NTU/NTUm = 3.8 operating at AHRI summer conditions. Dotted line indicates the maximum effectiveness for a given NTU and the corresponding optimal Cr*. Circles and square correspond to the local NTU and Cr* for discretized segments of channels with or without 20% deflections respectively.

The above analysis shows that the variable local NTU and Cr* values, that are caused by non-uniform channels, significantly decrease the total effectiveness of the RAMEE compared to a system with uniform channels. The effectiveness decreases because a higher proportion of the air flows through the wider segments of the channel that have decreased local total effectivenesses caused by the decreased local NTU and Cr* values.

Unfortunately, an invalid assumption is made in the algebraic analysis of the effects of the non-uniform channel. In the RAMEE, the solution at the exchanger outlet has temperature and concentration profiles that are related to the local effectiveness profile. The solution is then mixed before it enters the other exchanger and as a result has a constant temperature and concentration at the exchanger inlet. The algebraic analysis used up to this point in the chapter does not account for this mixing of the solution and assumes the solution temperature and concentration profiles at the exchanger outlet are the same at the inlet. As a result, the local effectiveness values obtained from Figure 5.11 and the determined average effectiveness would be slightly different since mixing occurs. Nevertheless, this analysis demonstrated the processes by which the non-uniform channels influence the RAMEE effectiveness. The next section uses numerical simulations, which account for the mixing of the solution, to more accurately determine the effects of non-uniform channels on the RAMEE effectiveness.

5.4.2 Numerical Analysis

Section 5.4.1 used a simplified algebraic approach to demonstrate the mechanisms by which the non-uniform channels influence the RAMEE effectiveness. Numerical simulations of the RAMEE are now used to describe the effects of non-uniform channels on the RAMEE effectiveness.

A counter-flow LAMEE with air and solution channel thicknesses of 4 mm and 2 mm, respectively, operating at AHRI summer conditions is simulated. Peak membrane deflections ranging between 0% and 30% are considered in order to adequately describe the effects. The total air mass flow rates are constant for all the deflections and correspond to the mass flow rates for a RAMEE with uniform channels

operating with NTU values of 6 and 12. The ratio between NTU and NTUm (i.e., NTU/NTUm) is 3.8 for the simulations.

Figure 5.12 and Figure 5.13 show the sensible, latent, and total effectivenesses that occur when the RAMEE is operating at its peak total effectiveness as a function of the peak membrane deflection for both NTU values. The figures show the total effectiveness gradually decreasing in value as the deflection size increases to 5% and then beyond 5%, the effectiveness decreases rapidly as the deflection size increases to 15%. At deflections greater than 15%, the total effectiveness decreases with deflection size in a nearly linear manner, but not as rapidly as it did between deflections of 5% to 15%. The sensible and latent effectivenesses exhibit the same trend as the total effectiveness. The decrease effectiveness for the two NTU cases is slightly higher when NTU equals 12 (based on percent change) and thus shows that the impact of non-uniform channels increase slightly with NTU.

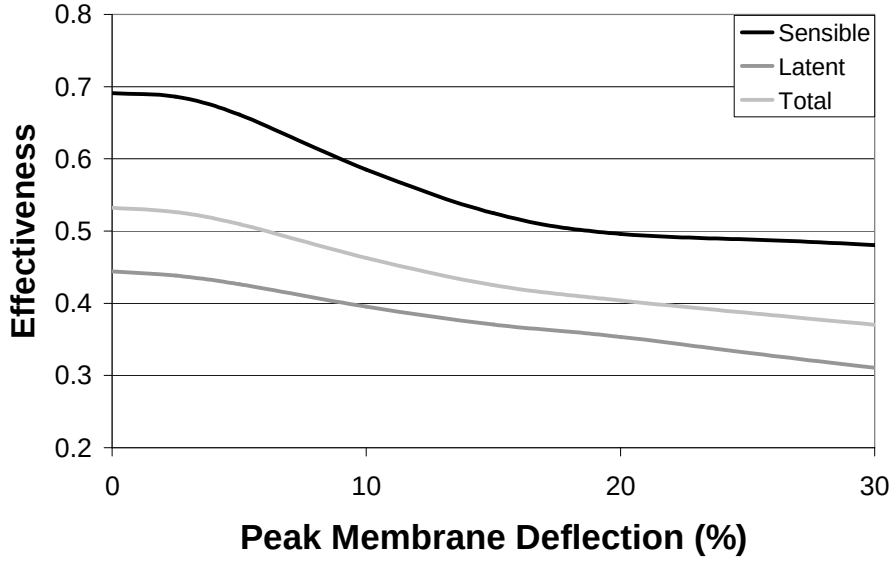

Figure 5.12: Effectiveness as a function of peak membrane deflection at NTU = 6.

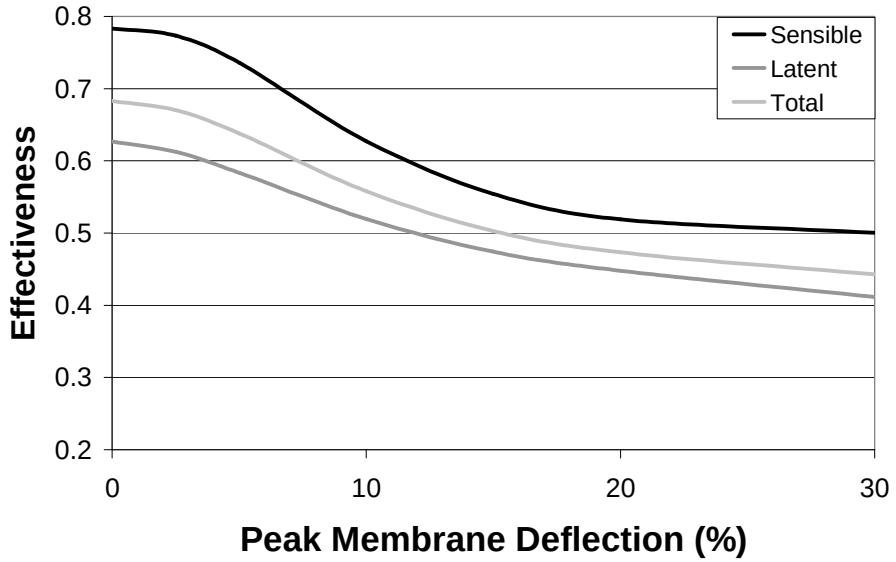

Figure 5.13: Effectiveness as a function of peak membrane deflection at NTU = 12.

Therefore, Figure 5.13 (i.e., a RAMEE operating at a NTU of 12) shows that if a counter-flow RAMEE with 4 mm and 2 mm air and solution channels operating with a NTU of 12 has a peak membrane deflection of 10% (which would have a maximum deflection of 0.4 mm), the sensible, latent, and total effectivenesses are reduced by

15.6%, 10.7%, and 12.5%, respectively, compared to the same system with no deflections.

The effects of the non-uniform channels on the RAMEE performance is further demonstrated by plotting the total effectiveness as a function of Cr* for different values of peak membrane deflections, which is shown in Figure 5.14 and Figure 5.15. The results reveal how the effectiveness decreases as the deflection size increases, which has the effectiveness decreasing at all Cr* values, but more significantly at lower Cr* values. As a result, the characteristic effectiveness peak becomes less distinct and becomes absent at deflections greater than 10%. Also, the operating Cr* that produces the maximum total effectiveness increases from the optimal Cr* to higher Cr* values as the deflection size increases. These trends are observed for both NTU values (i.e., 6 and 12) but they are more prominent at the higher NTU value.

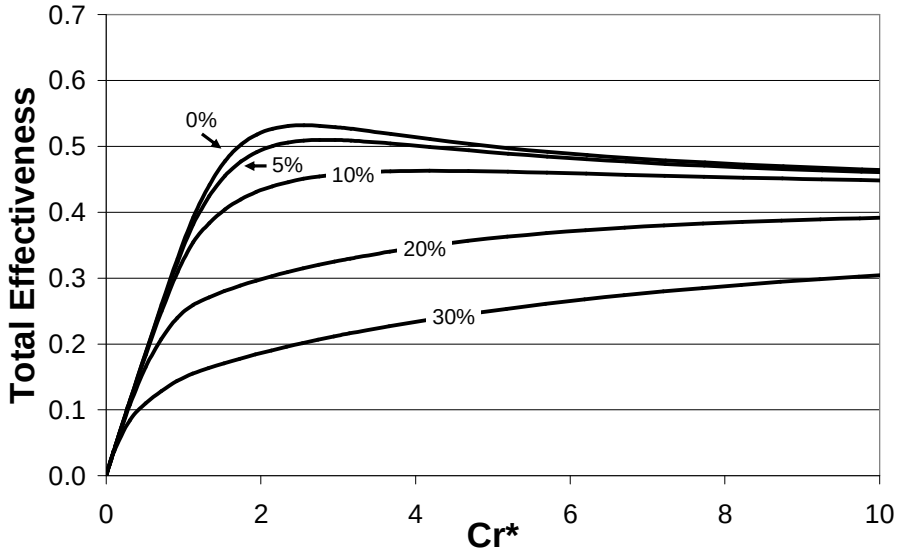

Figure 5.14: Total effectiveness as a function of Cr* at different values of peak membrane deflections at NTU = 6.

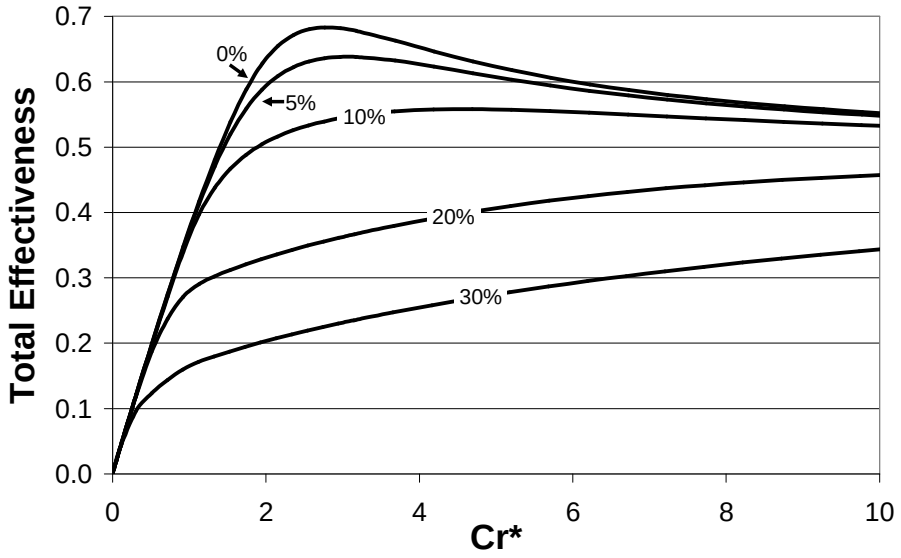

Figure 5.15: Total effectiveness as a function of Cr* at different values of peak membrane deflections at NTU = 12.

5.4.3 Comparison Between Algebraic and Numerical Methods

Two methods are used to describe the effects of the non-uniform channels on the RAMEE effectiveness. The algebraic method is simpler and determines the effectiveness without directly simulating a RAMEE with non-uniform channels, but it assumes the solution is not mixed when it travels between LAMEEs. The numerical method is more complex and directly simulates the non-uniform channel. Table 5.3 compares the results from the two methods and shows that both predict that the peak total effectiveness decreases as the deflection size increases. The results show that the simpler algebraic method is unable to exactly reproduce the results obtained by directly simulating the non-uniform channels. The results also show that the mixing of the solution between LAMEEs has a significant effect on the RAMEE performance. Therefore, the effects of the non-uniform channels on the RAMEE effectiveness have to

be determined by directly simulating the non-uniform channels. Nonetheless, using the algebraic method is reasonably accurate up to a peak deflection of 20%.

Table 5.3: Comparison peak total effectiveness for different deflections determined by algebraic and numerical methods when NTU = 6.

Deflection (%)	Peak Total Effectiveness (%)		Difference (%)
	Algebraic	Numerical	
5	52.8	51.0	1.8
10	49.4	46.3	3.1
20	37.9	40.4	-2.4
30	26.7	37.0	-10.3

5.5 Effects of Non-Uniform Channels on Experimental Prototypes

Comparisons between numerical and experimental results have demonstrated several discrepancies (Erb et. al 2010, Mahmud et. al 2010). The numerical results often have higher effectiveness values than higher than the experimental results and the experimental results do not demonstrate a peak in effectiveness that is present in the numerical results. Both of these discrepancies are present in the numerical and experimental results for Prototype #3 operating at a NTU of 12 as shown in Figure 5.16. This section numerically investigates if these discrepancies are due to the effects of non-uniform channels. The following analysis compares the experimental results of Prototype #3 (Mahmud et. al 2010) to numerical results with non-uniform channels with different peak membrane deflections.

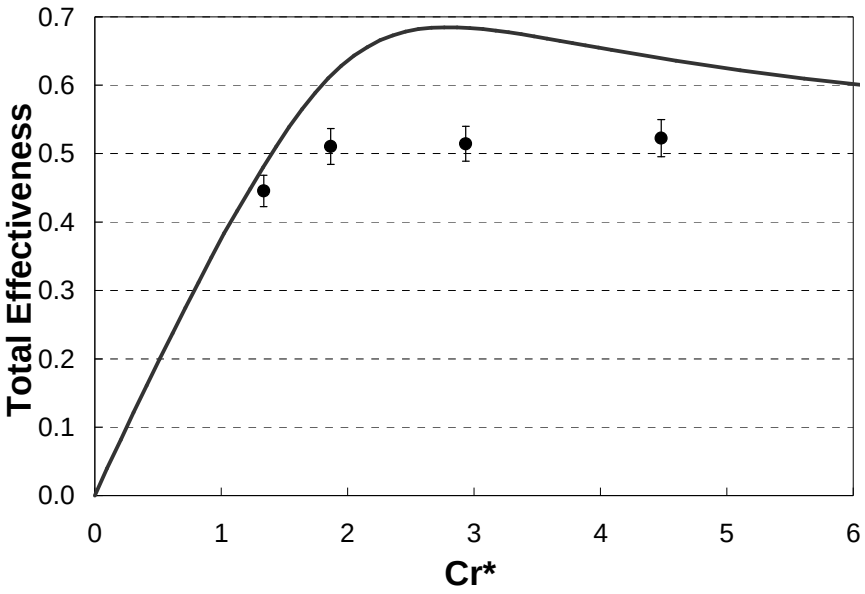

Figure 5.16: Experimental and numerical results of Prototype #3 (Mahmud et. al. 2010) operating at NTU = 12 and AHRI summer conditions.

Prototype #3 was built and tested by Mahmud et al. (2010) and utilizes a combination cross-counter flow configuration. The key dimensions and properties of Prototype #3 are shown in Table 5.4. Testing was conducted near AHRI summer conditions at NTU values of 4, 7, 8.5, and 12, with each NTU value tested at 4 Cr* values ranging between 1 and 5 for a total of 16 experimental data points. The ratio between NTU and NTUm for Prototype #3 is ~3.6 for all the data points.

Table 5.4: RAMEE Prototype #3 specifications.

Property	Value
Panel Dimensions	
Length	1 800 mm
Width	200 mm
Entrance Length	76 mm
Channel Thicknesses	
Air	4.2 mm
Solution	2.7 mm
Membrane Properties	
Thickness	0.2 mm
Thermal Conductivity	0.334 W/(m·K)
Water Vapour Permeability	1.66 x 10^{-6} kg/(m·s)

Numerical results for non-uniform channels with peak membrane deflections from 0% to 20% are simulated and are based on the specification of Prototype #3. These numerical results utilize a counter flow configuration while Prototype #3 uses a cross-counter flow configuration. However, Figure 5.17 shows that the numerical results for a counter flow and cross-counter flow configured RAMEE based on the specification for Prototype #3 are very similar. The differences between the two flow configurations are minimal and less than the differences between the counter flow RAMEE with uniform channels and non-uniform channels with peak membrane deflections of 5% (Figure 5.17). Therefore, the counter-flow numerical results can be used to compare the cross-counter combination experimental results.

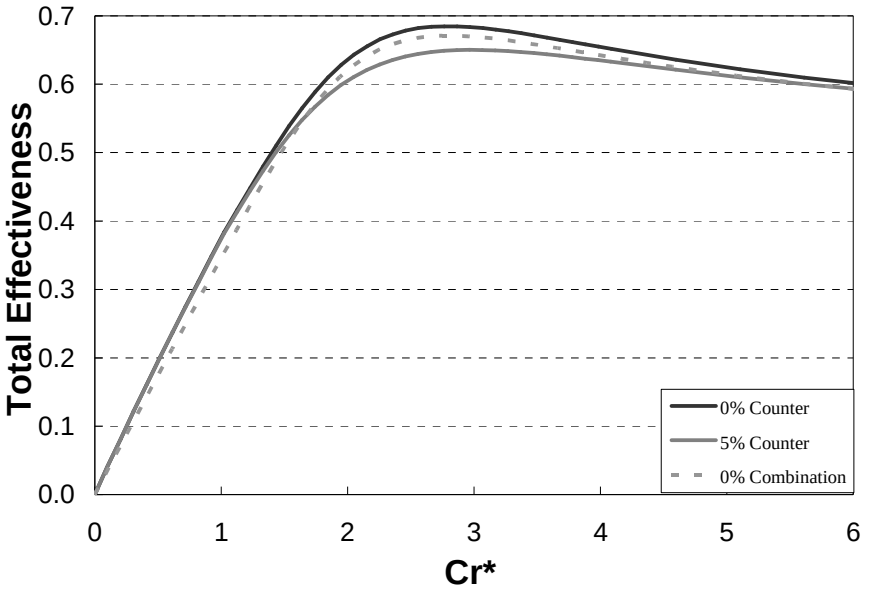

Figure 5.17: Numerical results based on Prototype #3 at NTU = 12 operating with either a counter flow or cross-counter combination flow configurations. Counter flow configurations for uniform channels and for non-uniform channels with a peak membrane deflection of 5% are used.

The total effectiveness numerical results with non-uniform channels are applied to the experimental results for Prototype #3 operating at NTU = 12, which is shown in Figure 5.18. The experimental results are bounded between the numerical results for

membrane deflections of 10% and 20%. The experimental results are very similar to the trend for the numerical results with a deflection of 10% in that their effectivenesses rapidly increase to a plateau as Cr* increases without achieving a peak value. From these results, the size of the peak membrane deflection in Prototype #3 is interpolated to approximately 12%. The size of the deflection also appears be relatively constant for the different Cr* results, which shows that the deflection size is not too dependent on the solution flow rate.

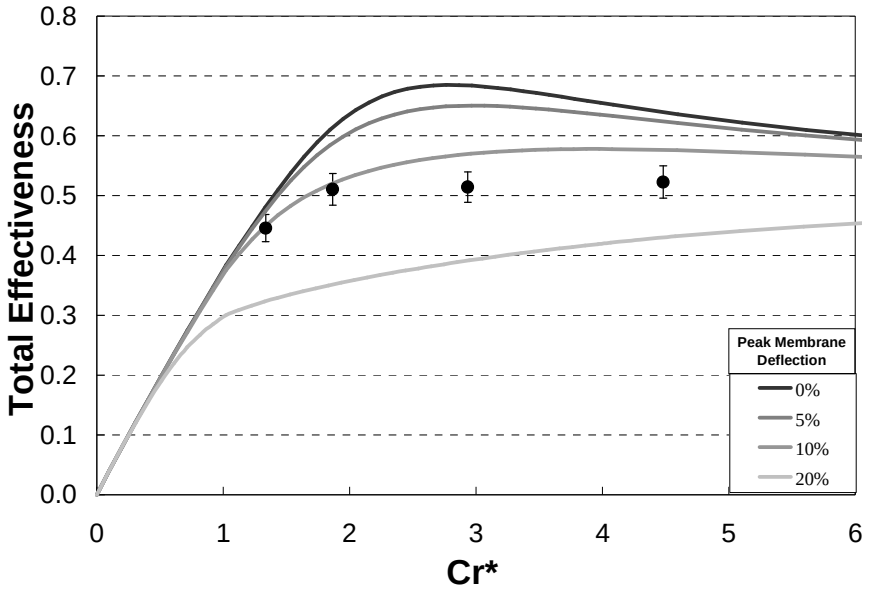

Figure 5.18: Prototype #3 experimental and numerical total effectiveness at NTU = 12. Numerical results are for non-uniform channels with peak membrane deflections between 0% and 20%.

The experimental and numerical results for the sensible and latent effectivenesses are shown in Figure 5.19 and Figure 5.20. Both figures show the same general trends as the total effectiveness results, with the results mostly being bounded by the numerical results for membrane deflections of 10% and 20%.

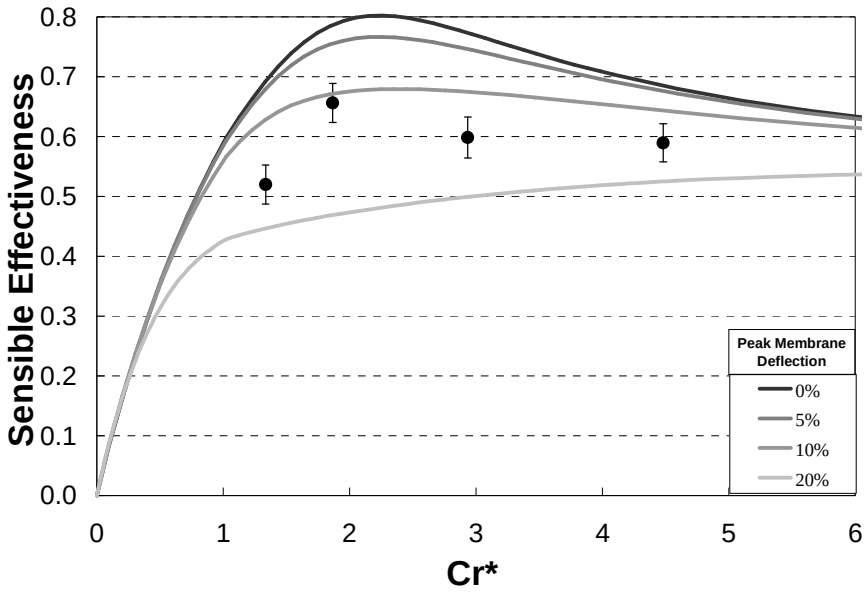

Figure 5.19: Prototype #3 experimental and numerical sensible effectiveness at NTU = 12. Numerical results are for non-uniform channels with peak membrane deflections between 0% and 20%.

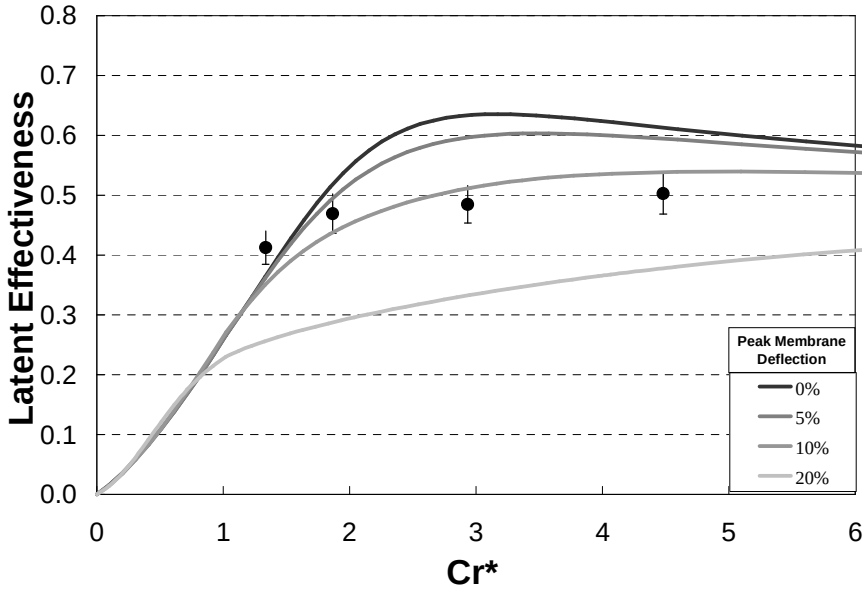

Figure 5.20: Prototype #3 experimental (Mahmud et al. 2010) and numerical latent effectiveness at NTU = 12. Numerical results are for non-uniform channels with peak membrane deflections between 0% and 20%.

There are additional experimental results from Prototype #3 for different NTU values of 4, 7, and 8.5 and their total effectiveness results are shown in Figure 5.21 to

Figure 5.23. The experimental results for the NTU values of 7 (Figure 5.22) and 8.5 (Figure 5.23) are still bounded between the numerical results for deflections of 10% and 20%, which was the case for when NTU is 12. The results for NTU of 4 are outside these bounds and are between deflection of 5% and 10%. These results show that the size of membrane deflection in Prototype #3 is relatively constant for different air flow rates (i.e., different NTU), except at low NTU (i.e., high air flow rate) where the deflection size is slightly decreased. This is a general statement due to the limited number of data points.

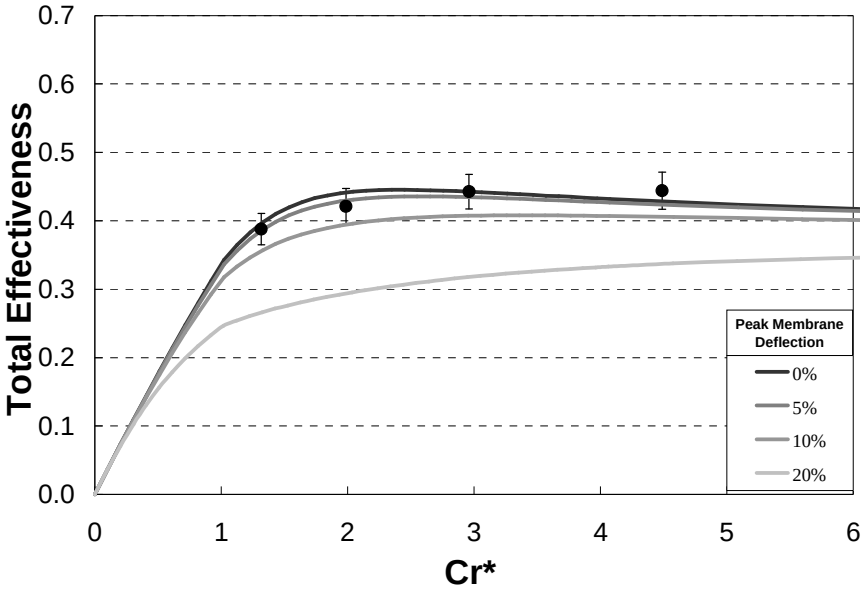

Figure 5.21: Prototype #3 experimental (Mahmud et al. 2010) and numerical total effectiveness at NTU = 4. Numerical results are for non-uniform channels with peak membrane deflections between 0% and 20%.

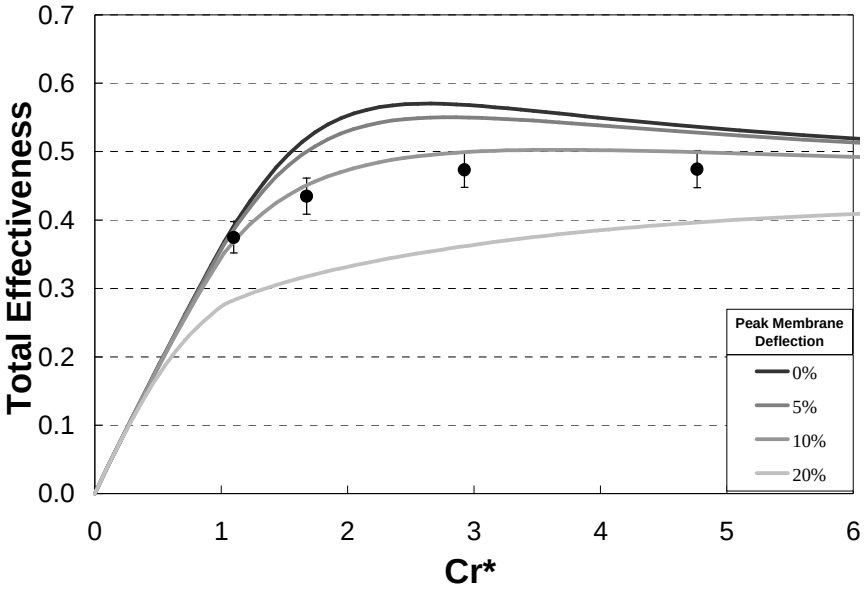

Figure 5.22: Prototype #3 experimental (Mahmud et al. 2010) and numerical total effectiveness at NTU = 7. Numerical results are for non-uniform channels with peak membrane deflections between 0% and 20%.

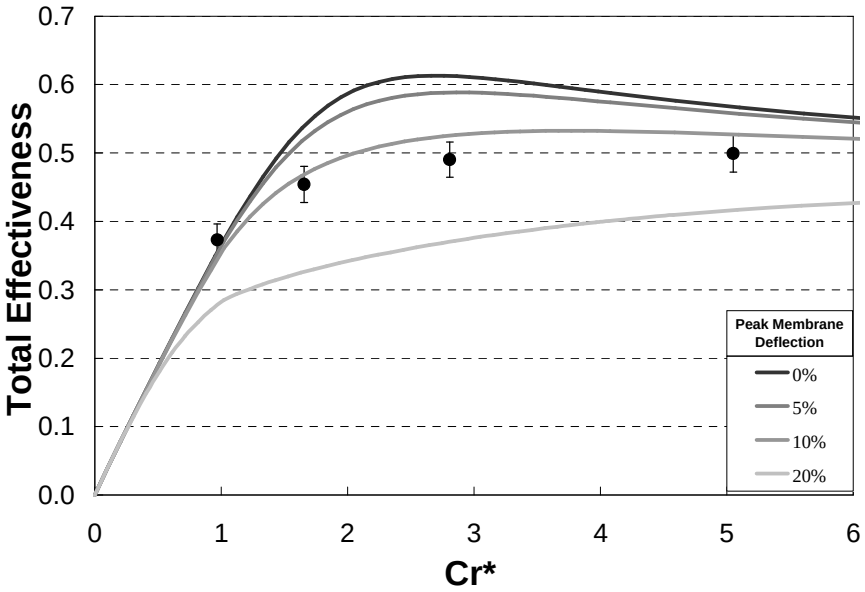

Figure 5.23: Prototype #3 experimental (Mahmud et al. 2010) and numerical total effectiveness at NTU = 8.5. Numerical results are for non-uniform channels with peak membrane deflections between 0% and 20%.

5.6 Limitations of Numerical Analysis of Non-Uniform Channel Thicknesses

The numerical analysis of a RAMEE with non-uniform channel thicknesses is able to successfully reproduce the experimental results by simulating peak membrane deflection around 12%. This shows that some of the discrepancy demonstrated by the previous RAMEE prototypes between the experimental and numerical results (uniform channels) can be attributed to the fluid flow maldistributions and variable overall heat and moisture transfer coefficients caused by non-uniform channels. However, the actual size of these predicted deflections is very small and seems impractical. In the case of Prototype #3, a 12% deflection represents a deflection of 0.5 mm. It was proposed by Mahmud et al. (2010) that the size of the deflections in Prototype #3 could easily exceed 1 mm.

The differences between the predicted and proposed channel thicknesses can be attributed to many things. The model assumed a simple channel deformation pattern which may not adequately describe the actual deflections. The effects on heat transfer and fluid flow by the air channel support structures were not considered and thus neglected. The fluid flows are also assumed to be laminar which is justified for non-deformed channels, but the flow may be transitional or turbulent in the deformed channels. A transitional/turbulent flow would increase the overall transfer coefficients and result in a smaller decrease in effectiveness for a given deflection compared to a laminar flow. Therefore, a more complex model that addresses these limitations might predict that Prototype #3 operates with a membrane deflection of about 1 mm.

Nevertheless, the numerical results with non-uniform channels show the same trend as the experimental results and demonstrate that the absence of the peak in total

effectiveness is due to the non-uniform channel. Further investigation into the effects of non-uniform channels is recommended and is best studied with a computational fluid dynamics (CFD) model. CFD will more accurately model the complex fluid flow pattern, especially if it is turbulent, in the exchanger and the heat and moisture transfer coefficients. The fluid flow and heat and moisture transfer resistances results from the CFD analysis could then be implemented into the numerical model to properly address the effects of non-uniform channels on the RAMEE performance. This analysis is beyond the scope of this study and is left for future study.

5.7 Chapter 5 Summary

The purpose of Chapter 5 was to consider the effects of exchangers with non-uniform channels on the RAMEE performance. It was shown that the direct effects of the non-uniform channels are that the fluid flow becomes maldistributed with more fluid flowing in the wider sections of the channel, and the overall heat and moisture transfer coefficients become variable. These variable fluid flow rates and overall transfer coefficients were then shown to reduce the RAMEE effectiveness and that this reduction increases as the size of the deflection increases. A characteristic of this decrease is that the peak in effectiveness is greatly reduced and eventually vanishes as the deflection size increases. This understanding of these effects of non-uniform channel thicknesses were then applied to the experimental results from Prototype #3, which showed that the numerical results with non-uniform channels were very similar to experimental results. Further analysis of these results implied that Prototype #3 is operating with membrane deflections of around 12%.

Chapter 6

SUMMARY, CONCLUSIONS, AND FUTURE WORK

6.1 Summary

Run-around membrane energy exchangers (RAMEE) allow heat and moisture transfer between isolated supply and exhaust ventilation air streams. Liquid to air membrane energy exchangers (LAMEEs) are placed in the supply and exhaust ducts and transfer heat and moisture between the air and a liquid desiccant that is circulated between the supply and exhaust LAMEEs. The ability of the RAMEE to transfer heat and moisture between isolated supply and exhaust ducts makes it suitable for several HVAC applications, such as hospitals and building energy retrofits.

The objective of this thesis was to expand on the understanding of the RAMEE operation and performance, which focused on the effects of outdoor air conditions and the effects of non-uniform exchanger channels on the RAMEE performance. This was achieved through numerical simulations and comparisons with experimental results where available. The numerical model used in this thesis was developed and validated by Vali (2009) and was introduced in Chapter 2. Slight modifications were made to the model to better describe the RAMEE and accomplish the objectives of the study.

The effects of outdoor air conditions on RAMEE performance were investigated in Chapter 3. Contour plots for the sensible, latent, and total performances at different outdoor air conditions were developed. These plots have contours of effectiveness and

supply air temperature, humidity ratio or enthalpy change superimposed on a psychometric chart and the values are for the case when the RAMEE is operating with peak total effectiveness. The contour plots showed that the RAMEE effectivenesses are very dependent on the outdoor conditions and may be less than 0% or exceed 100% for certain conditions. From these contour plots, the coupling of the heat and moisture transfers were discussed and elucidated. This coupling results in higher heat transfer when the difference between the indoor and outdoor air humidity ratios increase and higher moisture transfer when the difference between the indoor and outdoor air temperatures increase. A contour plot that describes the optimal Cr* for different outdoor conditions was also developed. Additional contour plots were created that describe the RAMEE when it is operating with peak sensible and latent effectivenesses. All of these contour plots aid in describing the relationship between the RAMEE performance and the outdoor air conditions and would facility RAMEE implementation studies.

Chapter 3 also contained a more detailed investigation into the performance of the RAMEE at outdoor air conditions that are cooler and moister or warmer and drier than the indoor air, which are referred to as -H* conditions. In many -H* conditions the RAMEE may be controlled (by controlling the solution flow rate) to selectively transfer either heat or moisture. This unique relationship between effectiveness and solution flow rate at –H* conditions was experimentally validated. This selective heat or moisture transfer was most pronounced at very low solution flow rates where the supply and exhaust LAMEEs are able to exchange sensible energy for latent energy and vice versa without exchanging a significant amount of energy between LAMEEs. These

behaviours at –H* conditions and very low solution flow rates could have energy saving potentials in climatic locations where many hours in a year have –H* conditions or in industrial applications that require selective heat or moisture transfers in –H* conditions.

The results in Chapter 3 on the relationships between the RAMEE performance and outdoor air conditions were used to develop correlations in Chapter 4. The correlations use NTU (RAMEE design parameter) and H* and ΔH (enthalpy difference between indoor and outdoor air) as input parameters. Sensible and latent effectiveness correlations for the case when the RAMEE is operating at its maximum total effectiveness were developed and are

$$\varepsilon_{Sen} = 0.0093 \cdot NTU \cdot H^* - 45 \cdot (NTU + 4)^{-3} + 8x10^{-5} \cdot (H^* + 0.4) \cdot NTU \cdot \Delta H + 0.678, \quad (6.1)$$

$$\varepsilon_{Lat} = 0.01 \cdot NTU \cdot H^{*-1} - 67 \cdot (NTU + 10)^{-2} - 3x10^{-5} \cdot (H^{*-1} + 2) \cdot NTU \cdot \Delta H + 0.671. \quad (6.2)$$

The total effectiveness is determined from these correlations by the relationship determined by Simonson and Besant (1999b), which is

$$\varepsilon_{Tot} = \frac{\varepsilon_{Sen} + H^* \varepsilon_{Lat}}{1 + H^*}. \quad (6.3)$$

Another correlation was determined to describe the Cr* (ratio of solution and air heat capacity rates) that results in the RAMEE operating at its maximum effectiveness. This Cr* is referred to as the optimal Cr* and its correlation is

$$Cr^*_{Optimal} = (LnNTU + 10) \cdot H^{*0.1} + \left[(H^* + 5)^{-2.4} - 0.023\right] \cdot \Delta H + 0.177 \cdot \quad (6.4)$$

The correlations are valid for +H* outdoor conditions from -6°C to 38°C and 0 to 24 g/kg and NTU values from 1 to 14. The maximum differences between the simulated and correlated changes in the supply air temperature, humidity ratio, and enthalpy are

minimal at 0.3°C, 0.1 g/kg, and 0.5 kJ/kg respectively. The maximum error between the simulated and correlated optimal Cr* is 0.3.

The effects of non-uniform exchanger channels on RAMEE effectiveness were investigated in Chapter 5. The channels were modeled with a sinusoidal pattern to represent the membrane deflection pattern observed in Prototypes #3. The deflection magnitude is the deflection size divided by the undeflected air channel thickness. The non-uniform channels create a maldistributed fluid flow and variable heat and moisture transfer coefficients. The non-uniform exchanger channels analysis shows that the RAMEE effectiveness reduced and that the reduction in effectiveness increases as the size of the deflection increases. For a RAMEE operating at a NTU of 12 with peak membrane deflections of 10%, the peak total effectiveness is reduced by 12.5% and the sensible and latent effectivenesses are reduced by 15.6% and 10.7% respectively. The non-uniform channels cause a greater decrease in effectiveness at lower Cr* values and result in a diminished effectiveness peak that is absent at higher deflection sizes. This decreased effectiveness and absent peak agrees with experimental findings from Prototype #3 and the numerical results imply that the prototype was operating with a peak membrane deflection of 12%

6.2 Conclusions

The investigations contained in this thesis produced the following conclusions.

1. The sensible, latent, and total effectivenesses of the RAMEE are variable and strongly influenced by the outdoor air conditions. The effectivenesses are strongly dependent on H* and mildly dependent on ΔH.

2. RAMEE effectivenesses can be less than 0% or exceed 100% for some outdoor conditions, which means that heat or moisture is transferred against or beyond its driving potentials at these conditions, which is a unique characteristic of the RAMEE.
3. The RAMEE optimal Cr* is highly variable with outdoor air condition and ranges between 1.5 and 3.5. Therefore, optimal RAMEE operations require controlling the solution flow rate based on the outdoor air conditions.
4. The performance of the RAMEE at –H* conditions allows heat and moisture to be selectively transferred depending on the operating Cr*. These performance characteristics at–H* conditions were validated experimentally.
5. The RAMEE effectiveness is reduced from the combined effects of fluid flow maldistribution and variable overall heat and moisture coefficients caused by non-uniform exchanger channels. The reduction in effectiveness increases as the size of the membrane deflection increases. The effectiveness peak decreases as the deflection size increases and becomes absent at higher deflections.
6. Exchangers with non-uniform channels have a decreased effectiveness, which results in the peak in total effectiveness being absent. These trends agree with the experimental findings from Prototype #3.

6.3 Recommendations for Future Work

The research in this thesis has shown the behaviour of the RAMEE at different outdoor air conditions and with non-uniform exchanger channels. The findings from this research have identified additional topics that require further study.

1. Frosting in the exchanger at low temperature conditions was neglected in producing the RAMEE performance contour plots. An investigation into the effects of frosting is required to determine if the RAMEE performance at these low temperature conditions shown in this study are accurate.
2. The underlying cause of the relationship between optimal Cr* and outdoor air conditions is not understood. Understanding this underlying cause would aid in operating the RAMEE during part-load conditions and controlling the transient response of the system.
3. The developed sensible and latent effectiveness correlations should be modified to include Cr* and –H* conditions as an input parameters. These modified effectiveness correlations would fully describe the RAMEE for all outdoor conditions and solution flow rates, which is required if the RAMEE is to be actively controlled during the year.
4. The analysis of the effects of non-uniform exchanger channels assumed the flow was laminar and neglected the effects of the air channel support structures. Both of these variables should be investigated further. It was proposed in Chapter 5 that this study should be conducted with a computational fluid dynamics (CFD) model because it can accurately model the complex channel flow and include the air channel support structures.

REFERENCES

Afshin, M. 2010. Modeling Selection of the Liquid Desiccant for a Run-Around Membrane Energy Exchanger, M.Sc. Thesis, Department of Mechanical Engineering, University of Saskatchewan

Ahmadi, M.S., 2008. Modeling the Transient Behavior of a Run-around Heat and Moisture Exchanger System. M.Sc. Thesis, Department of Mechanical Engineering, University of Saskatchewan.

Ahmadi, M.S., Erb, B., Simonson, C.J., Besant, R.W., 2009a, Transient Behavior of Run-Around Heat and Moisture Exchanger System. Part I: Model Formulation and Verification. International Journal of Heat and Mass Transfer 52, 6000–6011.

Ahmadi, M.S., Erb, B., Simonson, C.J., Besant, R.W., 2009b, Transient Behavior of Run-Around Heat and Moisture Exchanger System. Part II: Sensitivity Studies for a Range of Initial Conditions. International Journal of Heat and Mass Transfer 52, 6012–6020.

AHRI. 2005. ANSI/ARI Standard 1060, Standard for Rating Air-to-Air Exchangers for Energy Recovery Ventilation Equipment. Arlington, VA: Air-Conditioning & Refrigeration Institute.

ANSI/ASHRAE Standard 55-2004, Thermal Environmental Conditions for Human Occupancy. Atlanta: ASHRAE.

ANSI/ASHRAE STANDARD 62.1-2004, Ventilation for Acceptable Indoor Air Quality. Atlanta: ASHRAE.

ASHRAE, 2000, HVAC Systems and Equipment Handbook, Ch 44: Air-to-Air Energy Recovery. ASHRAE, Atlanta.

Beriault, D., 2010, Run-Around Membrane Energy Exchanger Prototype 4 design and Laboratory Testing, M.Sc. Thesis, Department of Mechanical Engineering, University of Saskatchewan, Saskatoon, Saskatchewan.

Cisternas, L.A., Lam, E.J., 1991, Analytic Correlation for the Vapour Pressure of Aqueous and Non-Aqueous Solutions of Single and Mixed Electrolytes. Part II. Application and Extension, Fluid Phase Equilibria, 62 (1), 11-27.

D & R International. 2009. 2008 Buildings Energy Data Book. The Buildings Technologies Program, Energy Efficiency and Renewable Energy, U.S. Department of Energy.

Environmental Protection Agency (EPA), Laboratories for the 21st Century: Best Practices, Laboratories for the 21st Century, U.S., <www.epa.gov/lab21gov/pdf/bp_rightsizing_508.pdf>, accessed January 26, 2010.

Erb, B., Simonson, C.J., Ahmadi, M.S., and Besant, R.W., 2010. Experimental Measurements of a Run-Around Membrane Energy Exchanger (RAMEE) with Comparison to a Numerical Model, ASHRAE Transactions, 115(2) 689-706

Fan, H., 2005. Modelling a Run-Around Heat And Moisture Recovery System, M.Sc. Thesis, Department of Mechanical Engineering, University of Saskatchewan, Saskatoon, Saskatchewan.

Fan, H., Simonson, C.J., Besant, R.W. and Shang, W., 2006. Performance of a Run-Around System for HVAC Heat and Moisture Transfer Applications Using Cross-Flow Plate Exchangers Coupled with Aqueous Lithium Bromide, International Journal of HVAC&R Research, 12 (2), 313-336.

Fang, L., Clausen, G. and Fanger, P.O., 2000. Temperature and Humidity: Important Factors for Perception of Air Quality and for Ventilation Requirements. ASHRAE Transactions, 106, 503-510.

Hemingson, H., 2005. Preliminary Testing for Run Around Heat and Moisture Exchanger, Summer Work Report, Department of Mechanical Engineering, University of Saskatchewan, Saskatoon, Saskatchewan.

Incropera, F., DeWitt, D., 2002. Fundamentals of Heat and Mass Transfer. 5th Ed. New York: John Wiley & Sons.

Iskra, C., 2007, Convective Mass Transfer between a Hydrodynamically Developed Airflow and Liquid Water with and without a Vapor Permeable Membrane, M.Sc. Thesis, Department of Mechanical Engineering, University of Saskatchewan.

Katahabar Systems, <www.kathabar.com>, accessed March 1, 2010.

Kays, W., London, A., 1998 Compact Heat Exchangers, 3rd Ed. Kreiger Publishing, Malabar, FL.

Kosonen, R. and Tan, F., 2004. The Effect of Perceived Indoor Air Quality on Productivity Loss. Energy and Buildings, 36(10), 981-986.

Larson, M.D., 2006. The Performance of Membrane in a Newly Proposed Run-Around Heat and Moisture Exchanger, Department of Mechanical Engineering, University of Saskatchewan.

Larson, M.D., Simonson, C.J., Besant, R.W., and Gibson, P., 2007, The Elastic and Moisture Transfer Properties of Polyethylene and Polypropylene Membranes for Use

in Liquid-to-Air Energy Exchangers, Journal of Membrane Science, 302(1), 136-149.

London, A., Kays, W., 1951, The Liquid-Coupled Indirect-Transfer Regenerator for Gas-Turbine Plants, Transaction. ASME, 73, 529-42.

Luo, X., Roetzel,W., 1998, Theoretical Investigation on Cross-Flow Heat Exchangers with Axial Dispersion in One Fluid, Revue Générale De Thermique, 37 (3), 223-233.

Mahmud, K., Mahmood, G.I., Simonson, C.J., 2010, Besant, R.W., Performance testing of a counter-cross-flow run-around membrane energy exchanger (RAMEE) system for HVAC applications, Energy and Buildings, 42 (7), 1139-1147.

Norback, D., Michel, I., Widstrom, J., 1990. Indoor Air Quality and Personal Factors Related to Sick Building Syndrome. Scandinavian Journal of Work, Environment, & Health, 16 (2), 121-128.

Rasouli, M., Simonson, C.J., Besant, R.W., 2010a Applicability and Optimum Control Strategy of Energy Recovery Ventilators in Different Climatic Condition. Energy and Buildings, 42 (9), 1376-1387.

Rasouli, M., Simonson, C.J., Besant, R.W., 2010b, Optimal Control of Energy Recovery Ventilators and their Impact on Energy and Comfort, Submitted to International Journal of Energy.

Shah, R.K., London, A.L., 1978, Laminar flow forced convection in ducts, Academic Press, New York, NY.

Shah, R.K., 1981, Thermal design theory for regenerators, in: Kakac, A., Bergles, A.E., Mayinger, F., (Eds.), Heat Exchangers: Thermal-Hydraulic Fundamentals and Design, Hemi-sphere, New York, pp. 721-763.

Shang, W., Besant, R.W., 2005, Effects of Pore Size Variations on Regenerative Wheel Performance. Journal of Engineering for Gas Turbines and Power, 127, 121-135.

Simonson, C.J., Besant, R.W., 1999a, Energy Wheel Effectiveness: part II – correlations, International Journal of Heat and Mass Transfer, 42, 2171-2185.

Simonson, C.J., Besant, R.W., 1999b, Energy Wheel Effectiveness: part I – Development of Dimensionless Groups, International Journal of Heat and Mass Transfer, 42, 2171-2185.

Vali, A. 2009. Modeling a Run-around Heat and Moisture Exchanger System Using Two Counter/Cross Flow Exchangers. University of Saskatchewan.

Vali, A., Simonson, C.J., Besant, R.W., Mahmood, G., 2009, Numerical Model and Effectiveness Correlations for a Run-Around Heat Recovery System with Combined Counter and Cross Flow Exchangers, Int. J. of Heat and Mass Transfer 52, 5827-5840.

Venmar CES Inc., <www.venmarces.com>, Accessed April 8, 2010.

Zaytsev, I.D. and Aseyev, G.G., 1992. Properties of Aqueous Solutions of Electrolytes. CRC Press, Inc., Boca Raton, FL.

PZhang, L.Z., 2009, Flow Maldistribution and Thermal Performance Deterioration in a Cross-Flow Air to Air Heat Exchanger with Plate-Fin Cores. International Journal of Heat and Mass Transfer, 52, 4500-4509.

Zhang, L.Z., Niu, J.L., 2002, Effectiveness Correlations for Heat and Moisture Transfer Processes in an Enthalpy Exchanger with Membrane Cores, ASME Journal of Heat Transfer, 124 (5) 922-929.

Zhang, L.Z., Niu, J.L., 2001, Energy Requirements for Conditioning Fresh Air and the Longterm Savings with a Membrane-Based Energy Recovery Ventilator in Hong Kong, Energy 26, 119–135.

Zhang, Y., Jiang, Y., Zhang, L., Yuchun, D., Zhaofen, J., 2000, Analysis of Thermal Performance and Energy Savings of Membrane Based Heat Recovery Ventilator, Energy, 25, 515-527.

Zhou, Y.P., Wu, J.Y., Wang, R.Z., 2007, Performance of Energy Recovery Ventilator with Various Weathers and Temperature Set-Points, Energy and Buildings 39, 1202–1210.

APPENDIX A

EFFECTS OF TEMPERATURE AND HUMIDITY RATIO ON RAMEE PERFORMANCE

A.1 Introduction

Section 3.2.2 introduced the primary and secondary potentials that drive heat and moisture transfer in the RAMEE. The section proposes that heat (moisture) transfer in the RAMEE is primarily driven by the difference in temperature (humidity ratio) between the indoor and outdoor air and to a lesser secondary extent by the humidity ratio (temperature) difference. In order to understand how these potentials drive heat and moisture transfer, the performances at a few select outdoor conditions are considered and compared with each other in this appendix. These outdoor conditions are warmer and moister than the indoor conditions and thus have a positive operating condition factor (i.e., $H^*>0$).

Case 1 serves as the reference outdoor air condition and it is shown on the psychometric chart in Figure A.1. Case 1 is compared to two other cases to demonstrate the effects of the outdoor air conditions (Numbered circles and diamonds are used to represent the air and solution conditions respectively while dashed lines connecting the inlet and outlet conditions of a fluid represent process lines. These lines do not represent the exact process the air or solution undergoes in the exchanger, which can be very complex and are also highly dependent on the outdoor air conditions.

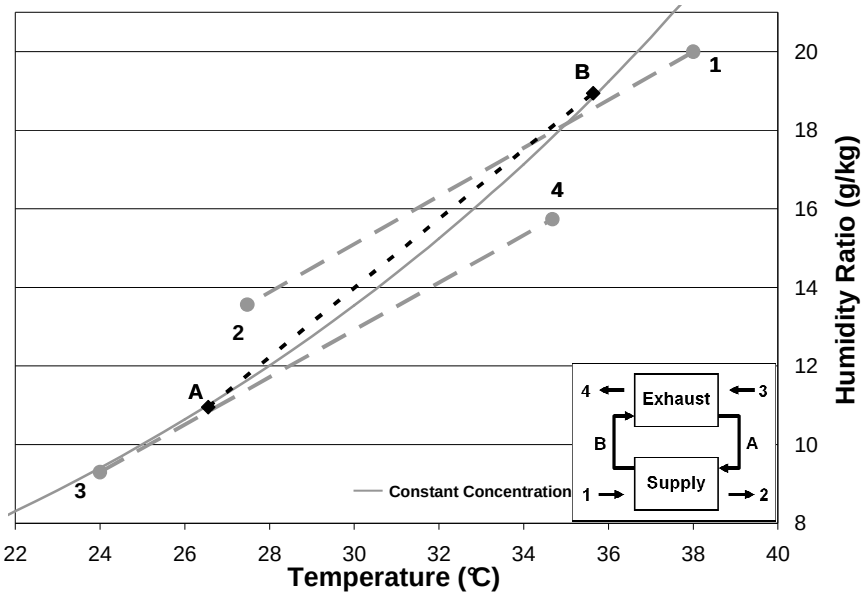

Figure A.1: Case 1 inlet and outlet bulk property conditions of the air and desiccant in the supply and exhaust exchangers.

Table A.1: Outdoor air condition and system effectiveness for the studied cases.

Case	Cr*	Outdoor Condition		System Effectiveness		
		T (℃)	W (g/kg)	Sensible (%)	Latent (%)	Total (%)
1	2.9	38	20	75.7	60.2	65.5
2	2.4	38	14	70.9	67.9	69.5
3	3.3	27	20	121.2	54.7	61.5

In Case 1, the air passing through the supply exchanger is cooled and dehumidified (process line 1-2), while the air passing through the exhaust exchanger is warmed and humidified (process line 3-4). The desiccant in the supply exchanger gains heat and moisture (process line A-B), while in the exhaust exchanger it loses heat and moisture (process line B-A). The two desiccant process lines have the same end points because it is assumed that no heat and mass transfer occurs in the desiccant as it is pumped between exchangers. The concentration of the desiccant changes slightly (less than 0.5%) as it passes through the exchanger which is indicated by the constant concentration line in Figure A.1. Also, the average temperature and humidity ratio of

the desiccant (based on inlet and outlet conditions) is almost equal to the average temperature and humidity ratio of the air between the indoor and outdoor air.

The effectiveness of the system can be determined from the air properties at the inlet and outlet of each LAMEE in Figure A.1. The primary driving potentials for transfer is the difference in the temperature, humidity ratio, and enthalpy between the outdoor and indoor air (points 1 & 3), which serve as the denominator for the sensible, latent, and total effectiveness calculations respectively. The actual energy transferred (numerator in the effectiveness calculations) is determined from the difference in the temperature, humidity, and enthalpy between the air stream inlet and outlet in either the supply or exhaust exchangers (points 1 & 2 or 3 & 4). The average of the supply and exhaust values are presented in this study.

A.2 Effects of Humidity Ratio

Case 2 represents an outdoor condition that is at the same air temperature but lower humidity ratio when compared to Case 1. Comparing these two cases allows the effects of the humidity ratio to be determined. Figure A.2 plots both Cases 1 and 2 on the psychometric chart with the inlet and outlet conditions in Case 2 denoted with the primed numbers. The comparison between Case 2 and Case 1 reveals that decreasing the outdoor air humidity ratio:

- decreases the amount the supply air outlet is cooled which decreases the sensible effectiveness,
- decreases the temperature change the desiccant undergoes in the exchanger,
- has no effect on the average desiccant temperature, and
- decreases the latent transfer but increases the latent effectiveness.

These trends can also be seen in Figure 3.3.

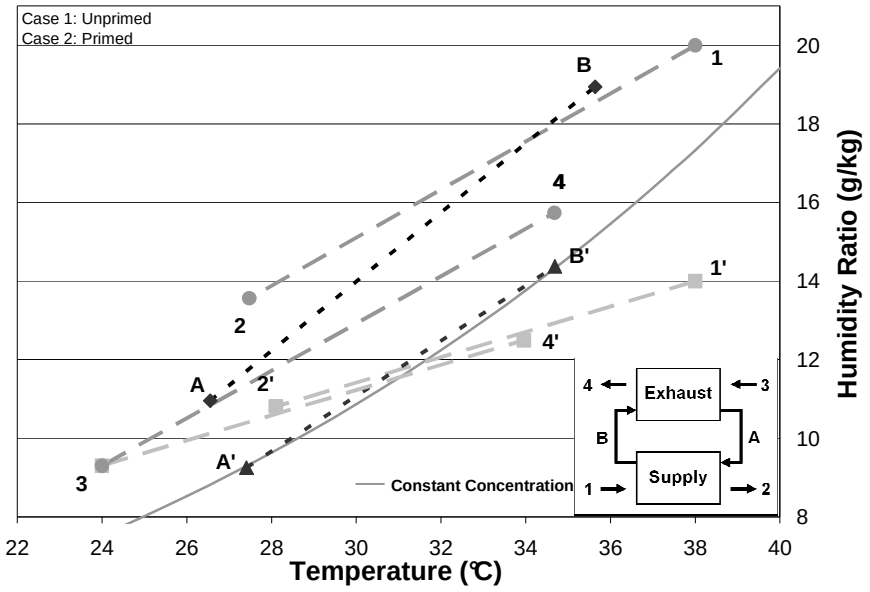

Figure A.2: Comparison between the inlet and outlet bulk property conditions of the air and desiccant in the supply and exhaust exchangers at Case 1 and Case 2 (primed numbers).

The above trends can be explained by considering the two effects that the moisture transfer has on the desiccant. The first effect of moisture transfer is that it changes the concentration of the desiccant. This concentration change is small and its effects are negligible. The other effect of moisture transfer on the desiccant is that the desiccant provides/absorbs the latent energy used/released during the phase change. The latent energy goes into or comes from the desiccant instead of the air because the convective heat transfer coefficient of the solution is more than an order of magnitude greater than the overall convective heat transfer coefficient of the air and membrane. The transfer of latent energy to/from the desiccant changes its temperature which alters the heat transfer potential between the air and desiccant solution. As a result, the moisture transfer influences the heat transfer in the system.

Applying the process described above to the comparison between Cases 1 & 2 (Figure A.2) allows the difference in their sensible performances to be elucidated. Case

1 has a higher moisture transfer potential (due to higher humidity ratio) than Case 2, which allows more moisture to be transferred into the desiccant solution in the supply exchanger. This additional moisture transfer and consequent latent energy release, increases the desiccant temperature in the supply exchanger. This warmer liquid desiccant exits the supply exchanger and enters the exhaust exchanger. The reverse process occurs in the exhaust exchanger, which results in a cooler liquid desiccant exiting it and entering the supply exchanger. In both exchangers, a greater heat transfer potential exists because the temperature difference between the desiccant and air at the inlets to the LAMEEs is larger in the case with the higher outdoor air humidity ratio (Case 1). This greater heat transfer potential in Case 1 causes Case 1 to have a higher sensible effectiveness than Case 2 even though both cases have the same air inlet temperatures.

A.3 Effects of Temperature

Case 3 is now introduced, which has the same humidity ratio as, but lower temperature than Case 1. Comparing these two cases can demonstrate the effects that the outdoor air temperature has on the system. This comparison is plotted in Figure A.3 and shows that decreasing the outdoor air temperature (Case 3 compared to Case 1):

- decreases the amount the supply air is dehumidified, which decreases the latent effectiveness,
- decreases the humidity ratio change the desiccant undergoes in the exchanger,
- has no effect on the average desiccant humidity ratio, and
- decreases the sensible transfer, but increases the sensible effectiveness.

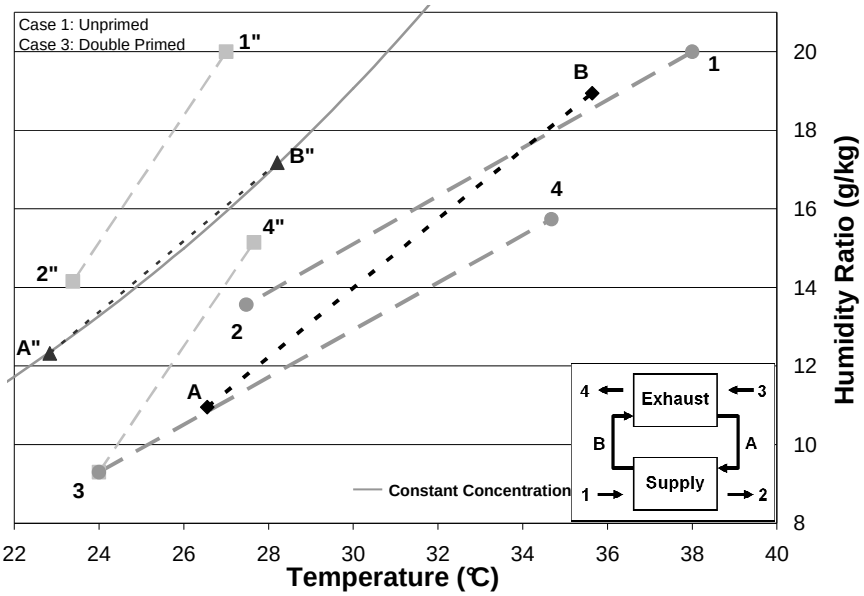

Figure A.3: Comparison between inlet and outlet bulk properties conditions of the air and desiccant in the supply and exhaust exchangers at Case 1 and Case 3 (double primed numbers).

Considering the moisture properties of the desiccant solution and their temperature dependencies allows the above noted trends to be explained. These properties (see Section 2.2.2) show that at a constant solution concentration, which can be assumed in the system, the humidity ratio of the air in equilibrium with the surface of the solution (referred to as the solution humidity ratio in this discussion) is exponentially related to the solution surface temperature. Because of this, the temperature of the desiccant influences its humidity ratio. Therefore the greater the temperature change of the desiccant as it flows through an exchanger, the greater the change in the humidity ratio of the solution. Changing the humidity ratio of the desiccant, changes the moisture transfer potential between the air and the desiccant, which affects the latent performance. And since heat transfer directly changes the desiccant temperature, which in turn changes the humidity ratio of the desiccant through the temperature-humidity

ratio relationship of the desiccant, the heat transfer in the RAMEE influences the latent performance.

Using the relationships outlined above, the comparison between Cases 1 & 3 (Figure A.3) can be explained thoroughly. The higher outdoor air temperature in Case 1 results in a higher heat transfer rate between the desiccant in the supply and exhaust exchangers. This higher heat transfer rate increases the temperature change that the desiccant undergoes in each exchanger. Based on the desiccant temperature-humidity ratio relationship, this greater heat transfer also increases the change in the humidity ratio of the desiccant in each exchanger (in addition to the small change due to the concentration change from moisture transfer). Therefore, Case 1, with its higher outdoor air temperature, has a greater change in the humidity ratio of the desiccant between the inlet and outlet of each exchanger compared to Case 3. This greater humidity ratio change increases the humidity ratio difference between the air and desiccant at the inlets of each exchanger, which increases the latent performance. This is why Case 1 has a higher latent effectiveness even though both cases have the same outdoor air humidity ratio.

A.4 Heat and Moisture Driving Potentials

The nature of the RAMEE allows the outdoor air temperature and humidity ratio to influence moisture and heat transfer respectively. The influence of the outdoor air conditions on heat and moisture transfer can be understood be considering them as primary and secondary driving potential. The driving potentials for heat transfer are the temperature (primary) and humidity ratio (secondary) differences between the indoor and outdoor air. Conversely, the driving potentials for moisture transfer are the

humidity ratio (primary) and temperature (secondary) differences between the air streams. The influence of the outdoor air conditions on both the heat and moisture transfers in the RAMEE is a unique characteristic of the system that does not occur in other energy recovery systems.